NUMERICAL AND EXPERIMENTAL INVESTIGATION OF FLOW THROUGH A CAVITATING VENTURI

A THESIS SUBMITTED TO
THE GRADUATE SCHOOL OF NATURAL AND APPLIED SCIENCES
OF
MIDDLE EAST TECHNICAL UNIVERSITY

BY

BORA YAZICI

IN PARTIAL FULFILLMENT OF THE REQUIREMENTS
FOR
THE DEGREE OF MASTER OF SCIENCE
IN
AEROSPACE ENGINEERING

DECEMBER 2006

Approval of the Graduate School of Natural and Applied Sciences

_____

Prof. Dr. Canan ÖZGEN

Director

I certify that this thesis satisfies all the requirements as a thesis for the degree of Master of Science.

_____

Prof. Dr. İsmail Hakkı TUNCER

Head of Department

This is to certify that we have read this thesis and that in our opinion it is fully adequate, in scope and quality, as a thesis for the degree of Master of Science.

_____

Prof. Dr. İsmail Hakkı TUNCER

Supervisor

Examining Committee Members

Prof. Dr. Sinan AKMANDOR (METU, AEE) _____

Prof. Dr. İsmail Hakkı TUNCER (METU, AEE) _____

Prof. Dr. Yusuf ÖZYÖRÜK (METU, AEE) _____

Assoc. Prof. Dr. Abdullah ULAŞ (METU, ME) _____

Dr. Mehmet Ali AK (TÜBİTAK, SAGE) _____

I hereby declare that all information in this document has been obtained and presented in accordance with academic rules and ethical conduct. I also declare that, as required by these rules and conduct, I have fully cited and referenced all material and results that are not original to this work.

Name, Last name:

Signature :

ABSTRACT

NUMERICAL AND EXPERIMENTAL INVESTIGATION OF FLOW THROUGH A CAVITATING VENTURI

Yazıcı, Bora
M.Sc., Department of Aerospace Engineering
Supervisor: Prof. Dr. İsmail Hakkı TUNCER

August 2006, 122 pages

Cavitating venturies are one of the simplest devices to use on a flow line to control the flow rate without using complex valve and measuring systems. It has no moving parts and complex electronic systems. This simplicity increases the reliability of the venturi and makes it a superior element for the military and critical industrial applications. Although cavitating venturis have many advantages and many areas of use, due to the complexity of the physics behind venturi flows, the characteristics of the venturies are mostly investigated experimentally. In addition, due to their military applications, resources on venturi flows are quite limited in the literature.

In this thesis, venturi flows are investigated numerically and experimentally. Two dimensional, two-dimensional axisymmetric and three dimensional cavitating venturi flows are computed using a commercial flow solver FLUENT. An experimental study is then performed to assess the numerical solutions. The effect of the inlet angle, outlet angle, ratio of throat length to inlet diameter and ratio of throat diameter to inlet diameter on the discharge coefficient, and the oscillation behavior of the cavitating bubble are investigated in details.

Keywords: Cavitation, Venturi, Multiphase Flow, Computational Fluid Dynamics, Experimental

ÖZ

KAVİTASYONLU VENTURİDEKİ AKIŞIN SAYISAL VE DENEYSEL İNCELENMESİ

Yazıcı, Bora
Y. Lisans, Havacılık ve Uzay Mühendisliği Bölümü
Tez Yöneticisi: Prof. Dr. İsmail Hakkı TUNCER

Ağustos 2006, 122 sayfa

Kavitasyonlu venturiler, komplex vana ve ölçüm sistemleri kullanılmadan akış hatlarında debi kontrolü yapmak için kullanılabilecek en basit elemanlardandır. Hiçbir karmaşık elektronik sistem ve hareketli parça ihtiva etmezler. Bu basitlik, kavitasyonlu venturileri güvenilirliğini arttırarak askeri ve kritik endüstriyel uygulamalarda üstünlük sağlamaktadır. Bu avantajlarına ve geniş uygulama alanlarına rağmen, arkalarındaki kompleks fizikten dolayı, venturilerin karakteristikleri genelde deneysel olarak yapılan çalışmalardan elde edilmiştir. Askeri uygulamalarda sıkça kullanıldıklarından dolayı literatürde az sayıda belgeye ulaşılabilmektedir.

Bu tez kapsamında, ticari akış çözücü olan FLUENT ile çeşitli kavitasyonlu venturi geometrileri iki boyutlu, iki boyutlu eksenel simetrik ve üç boyutlu olarak incelenmiştir. Akış çözümleyici programı doğrulamak için bir deneysel çalışma yapılmıştır. Böylece giriş açısı, çıkış açısı, boğaz uzunluğunun giriş çapına oranı ve boğaz çapının giriş çapına oranı gibi parametrelerin Çıkış sabiti ve salınım davranışları üzerindeki etkisi incelenmiştir.

Anahtar Kelimeler: Kavitasyon, Venturi, Çok Fazlı Akış, Hesaplamalı Akışkanlar Mekaniği, Deneysel

To My Parents

ACKNOWLEDGMENTS

I would like to express my deepest thanks and gratitude to Prof. Dr. İsmail Hakkı TUNCER for his supervision, encouragement, understanding and constant guidance.

Also I would like to express my gratitude to Dr. Mehmet Ali AK and Fatoş E. ORHAN for initializing and supporting this thesis.

I would like to express my sincere appreciation to Mr. Erhan KAPLAN, Mr. M. Cengizhan YILDIRIM and Mr. Bülent SÜMER for their crucial advices and invaluable efforts during the preparation of this thesis.

My gratitude is endless for my family, without whom this thesis would not have been possible.

TABLE OF CONTENTS

LIST OF TABLES

LIST OF FIGURES

LIST OF SYMBOLS

C_c	Core coefficient
C_d	Discharge coefficient
P_v	Vapor pressure
σ	Cavitation number
V_{th}	Throat velocity
ρ_l	Liquid density
ρ_m	Density of Mixture
μ_l	Liquid viscosity
μ_m	Viscosity of Mixture
D_{in}	Inlet Diameter
D_{th}	Throat Diameter
Re	Reynolds number
$\dot{m}$	Mass flow rate
$\dot{m}_{ideal}$	Ideal Mass flow rate
$\dot{m}_{real}$	Real Mass flow rate
St	Strouhal number
f	Frequency of oscillation
L_D	Length of the diffuser part of venturi
L_{th}	Throat length
A_c	Core area
Φ_1	Inlet angle (deg)
Φ_2	Outlet angle (deg)
α_k	Volume fraction of phase k
H_d	Hydraulic diameter
T_u	Turbulence intensity

CHAPTER 1

INTRODUCTION

Cavitating venturis are one of the simplest flow control devices and are widely used in a range of industries. Numerous industrial flow processes are controlled by such devices. They are commonly used to meter propellants in liquid rocket engine tests by controlling the mixture ratio of the fuel and the oxidizer. The fact that venturies may provide a constant flow rate under varying downstream pressure, they are particularly useful during the ignition transient when the downstream pressure in the combustion chamber rises rapidly.

A cavitating venturi typically consists of a converging section, a short straight throat section, and a diffuser as shown in Figure 1-1. When the downstream pressure P_2 is less than 85-90% of upstream pressure P_1, the flow may cavitate at the throat, and flow through the venturi orifice becomes “choked”. In general, a further decrease in the downstream pressure does not influence the mass flow rate.

Figure 1-1.Sample Drawing of a Cavitating Venturi, Cavitating Part is Illustrated as Black.

In spite of wide use of venturies, relatively little research data on its operating characteristics and on the mechanisms of operation are available in literature.

Moreover, there is almost no data in literature about the influence the geometric parameters on the performance of the cavitating venturies.

In this chapter, the general applications of the cavitating venturies are discussed in detail, and a literature survey on cavitating venturi flows is given. In addition, the previous studies on venturi flows conducted at TÜBİTAK-SAGE are summarized

1.1 Applications of Venturi

Cavitating venturies can be used in applications where a passive liquid flow control system is required. Venturies are widely utilized in

- Flow Limiters
- Mixture Ratio Controllers
- Injectors
- Actuator Movement Equalizers
- Fire Extinguishers

1.1.1 Flow Limiter

A cavitating venturi can be used in two modes; one is the “cavitating” mode and the other is “non-cavitating” mode. If the pressure drop is not sufficient enough to cause the cavitation at the throat of the venturi, the second mode prevails. A venturi in a flow system switching between these two modes can be used as a flow limiter. If the back pressure decreases suddenly, flow will be choked so that the flow rate will be limited to a certain value. In the “non-cavitating” mode, the venturi can also be used as a flow measurement device.

A primary application for this kind of usage is seen in combustion systems. At the start up of the combustion process, when the back pressure is low, the fuel flow rate may be limited with a cavitating venturi. As the transient back pressure in the

combustion chamber rises, the cavitation stops and the venturi switches to its second mode.

Flow limiting feature of cavitating venturi can also be used to limit the flow rate of a centrifugal pump system. In Figure 1-2, Head (H) vs. Flow rate (Q) curves of pump and venturi plotted on the same graph. The intersection point will be the maximum flow point and further increase in available energy will not increase the flow rate after this maximum value is reached.

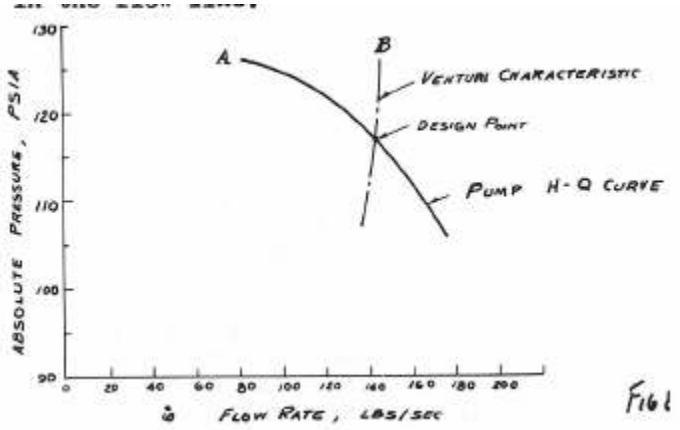

Figure 1-2. Simple Use of Cavitating Venturies with Pumps [1].

1.1.2 Mixture Ratio Controllers

Cavitating venturies will control the mixture ratio of any type of fluids and gasses. One of the best examples is the rocket engine's oxidizer to fuel ratio control application. As it is illustrated in Figure 1-3, where two fluids are fed through the combustion chamber from different lines. As long as the chamber pressure is below the pressure recovery limits of the venturies, the mixture ratio and flow rates may be kept constant. It should be noted that if venturies are not used, the flow in the feeding lines respond to the chamber pressure, and it will be impossible to keep the mixture ratios fixed.

In gas – fluid mixture cases venturies can similarly be used together with a sonic choke nozzle to control the mixture ratio.

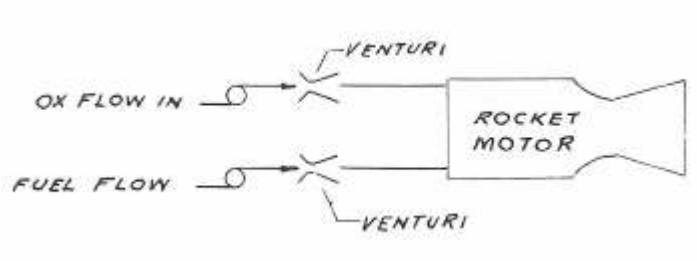

Figure 1-3. Mixture Ratios can be Controlled by Using Two Venturies for Each of the Fuel and Oxidizer Lines [1].

1.1.3 Injector

Through the throat of the cavitating venturi pressure will fall to the vapor pressure of the working fluid. Therefore, creation of such vacuum condition at the throat will be used to suck another fluid to mix with the working fluid. In Figure 1-4, a simple example is given for the mixture of detergent and water.

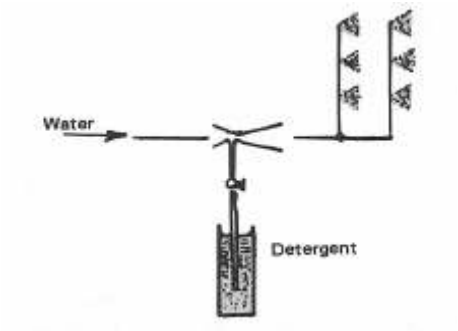

Figure 1-4. Cavitating Venturi was Used to Mix the Detergent and Water at a Constant Ratio [1].

1.1.4 Actuator Movement Equalizers

Cavitating venturies can be used in hydraulic motors and multiple actuators to provide uniform displacement. The displacement of actuators under varying loads can be equalized as long as the inlet pressure of the venturies is kept constant.

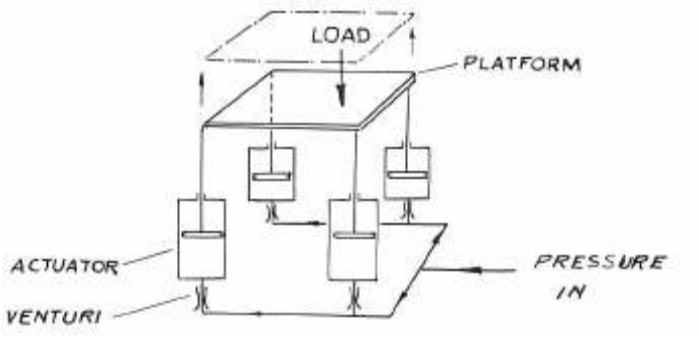

a)

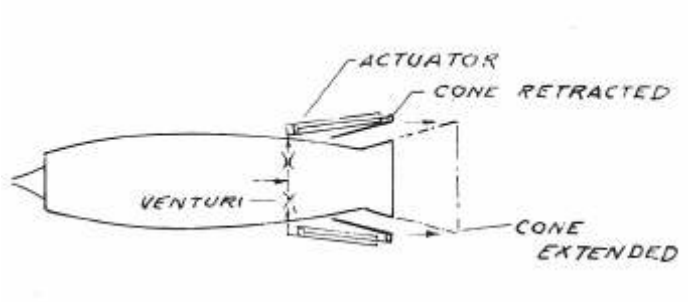

b)

Figure 1-5. Cavitating Venturies can be Used to Equalize the Actuator Movement, a), or to Equalize the Displacement System of a Trust Vector Control System [1].

An example for the actuator applications is the control of the displacement of a platform under non-uniform loading, which is given in Figure 1-5a. The cavitating venturi may provide a constant flow rate into the actuators, thus a uniform motion for the platform, independently from the loading on each actuator.

In Figure 1-5b the equalization of the actuators of a thrust vector control system is illustrated. With the use of a cavitating venturi, regardless of the loads acting on the nozzle plates, their displacements are equalized.

1.1.5 Fire or Disaster Control

For an extinguishing system one of the most critical problems is the difficulty of equalizing the flow rate between the branches of spray nozzles. Moreover, if one or several of them fail or damaged, a huge amount of extinguishing fluid will be directed to these lines rather than the other spray nozzles. So the whole system may fail in a short time. With the use of a cavitating venturi although some of the lines are damaged or burn-out, the flow rate through the other lines will not be affected. In Figure 1-6, a simple schematic view is illustrated.

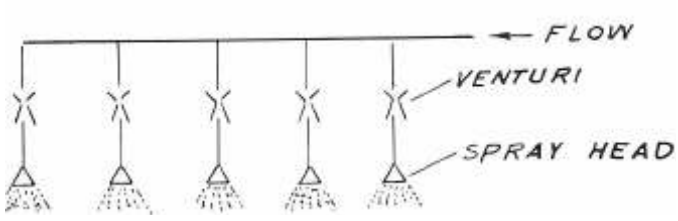

Figure 1-6. A Typical Illustration for Fire or Disaster Control Application. [1]

1.2 Literature Survey

Although cavitating venturies are widely used, publications on venturi flows are quite limited on literature. Early studies carried out by Fox Z. [1] are about the usage of a cavitating venturi to overcome the startup transient in rocket applications. Fox investigates the basic application of a venturi and its sizing features. Through seventies, the theoretical bases of cavitating flows are investigated by Boure, Fritte [2] and K.H. Ardron [3]. However the experimental studies on the effect of geometric properties of cavitating venturies are limited.

Several experiments are conducted by K.H. Ardron and D.W. Harvey at the NASA Lewis Research Center on the usage of cryogens in cavitating venturies [4]. These tests lead to the foundation of theoretical and numerical techniques to predict the behavior of flow through cavitating venturies. N.T. Thang and M.R.Davis in their theoretical work present the pressure distribution of a bubbly flow through the cavitating venturies and discuss the shockwaves created in cavitating venturies [5]. They later validate their theoretical findings through some experiments. But the main difference of this study is that the fluid is assumed to be a homogenous bubbly mixture of air and liquid water. This assumption allows them to simplify the equations governing the cavitating venturi flows.

At the beginning phases of Computational Fluid Dynamics, M. J. Gaston and J.A. Reizes tries to model bubble dynamics though a venturi with a potential flow solver[6]. Two years later J.D. Sherwood proposes a potential flow solution of a deforming bubble in a venturi [7]. Nevertheless, none of them is able to model the inception phases of cavitation and the collapse phase of the bubbles through a heterogeneous media.

Recently with the increasing power of the computers and the rising of commercial flow solvers through the this area several numerical simulations were performed with in-house and commercial flow solvers by G. P. Salvador and S. H. Grankel[8]. And one of the best works is proposed by Changhai Xu & Stephan D. Heister [9]. They describe the state of art of cavitating venturi flows with experimental studies and numerical calculations, and they point out the importance of the oscillatory features at the diffuser part of the venturi. They also comment on the effects of the Reynolds number on the oscillation behavior.

1.3 Research at TÜBİTAK – SAGE

In a research project carried out by TÜBİTAK–SAGE in 2003, Turkey's first operational liquid propellant rocket engine was designed, manufactured and tested. In this study the flow rate of the oxidizer and the fuel was mainly controlled by two

cavitating venturies. At the beginning phase of the project, due to the time and the financial limitations, instead of using an active flow control system, cavitating venturies were employed as a passive flow control system. Due to export license restriction on venturies in regard to military applications on rocket engines, purchasing of venturies from abroad wasn't successful. Therefore, a research project has started on developing and testing cavitating venturies. The performance of the cavitating venturies were calculated easily with the 1-D Bernoulli equations which is presented later in this thesis in detail [10], [11]. However, this simplified method can not predict the flow rate accurately. Since, these simplified equations do not account for the effect of the geometric properties like, the inlet angle, outlet angle and the throat length or inlet to throat diameter ratios.

To investigate the performance of the cavitating venturies, a simple test setup was designed and assembled. Several tests were conducted with several venturies but because of the restrictions on time of the on going project, the number of different venturies and the number of tests were limited. The working fluid in these tests was water due to the difficulty of using reactive oxidizers and fuels in the tests. In addition, a commercial flow solver FLUENT was also to predict the cavitating flows and the characteristics of the cavitating venturies.

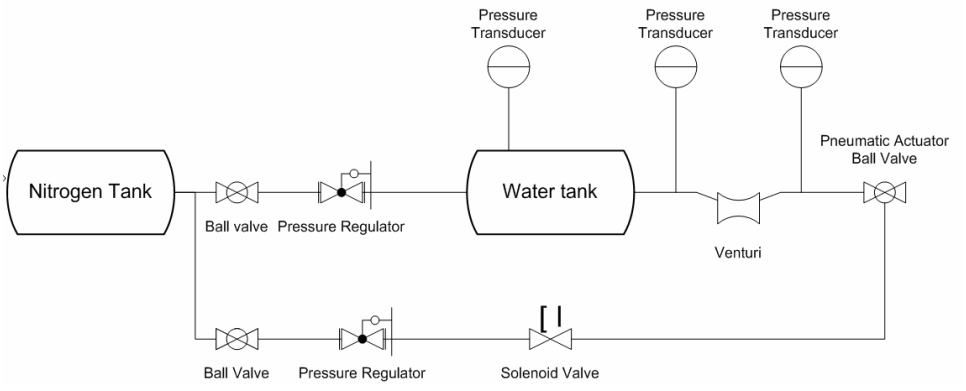

Figure 1-7. Sketch of Test Setup Developed in TÜBİTAK-SAGE

A simplified sketch of the test setup is given as figure 1-7. A high pressure gaseous nitrogen tank is used to pressurize the water tank and three pressure transducers are used to measure the tank pressure, inlet pressure and outlet pressure of the venturi. At this test setup, venturi exit is open to the atmosphere so the tests are performed with a constant cavitation number. The average flow rate through the venturi is measured through the remaining water in the tank.

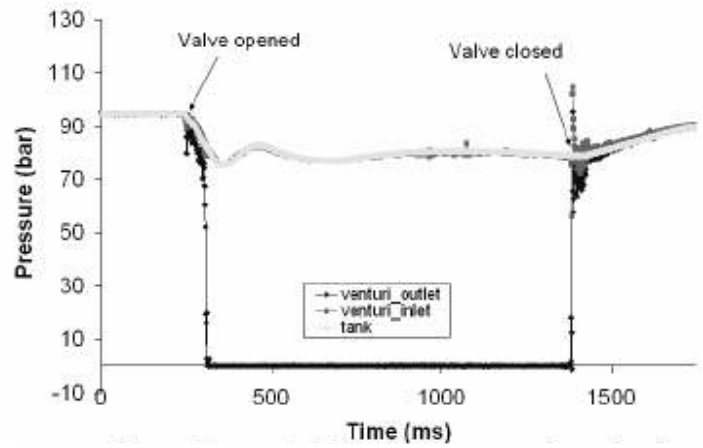

Figure 1-8. Data Obtained from the Pressure Transducers.

The dimensional data for the venturi are given in Figure 1-9. In Figure 1-8, pressure measurements taken from a typical venturi flow is given. Initially the pressure at the venturi inlet, outlet and in the tank are all the same. When the valve opened, the outlet pressure drops to vapor pressure and flow is choked in a few milliseconds. This measurement shows how a cavitating venturi responds quickly and restricts the flow rate.

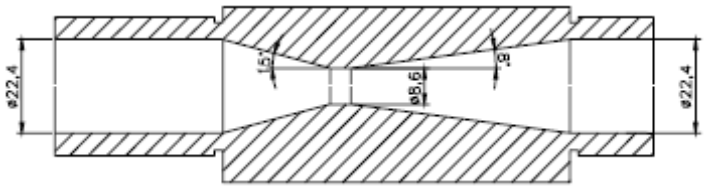

Figure 1-9. Technical Drawing of the Tested Venturi, All Dimensions in mm.

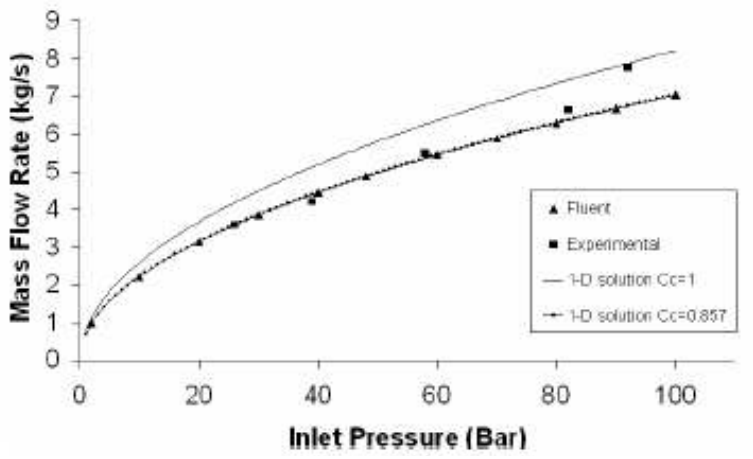

Figure 1-10. Comparison of the Result Obtained from 1-D Solutions, FLUENT and the Experiments.

In Figure 1-10, the mass flow rates which are calculated with 1-D flow solutions, FLUENT, and measured in the experimental study tests are given. In Figure 10, one can see the 1-D calculations made for two different C_c values. Where C_c is the effective liquid throat area ratio or "Core Coefficient", which can not be calculated with 1-D equations and is a constant value for every different geometries. Experiments were performed for four different inlet pressures while keeping the exit pressure equal to ambient pressure. Except the one in the 100 bars, FLUENT predictions compare well with the experimental data. 1-D solution with the C_c value equal to one predicts a mass flow rate 20% higher at very high pressures. In case of a rocket engine firing, this excess fuel or oxidizer may cause a failure or a performance loss which is not acceptable.

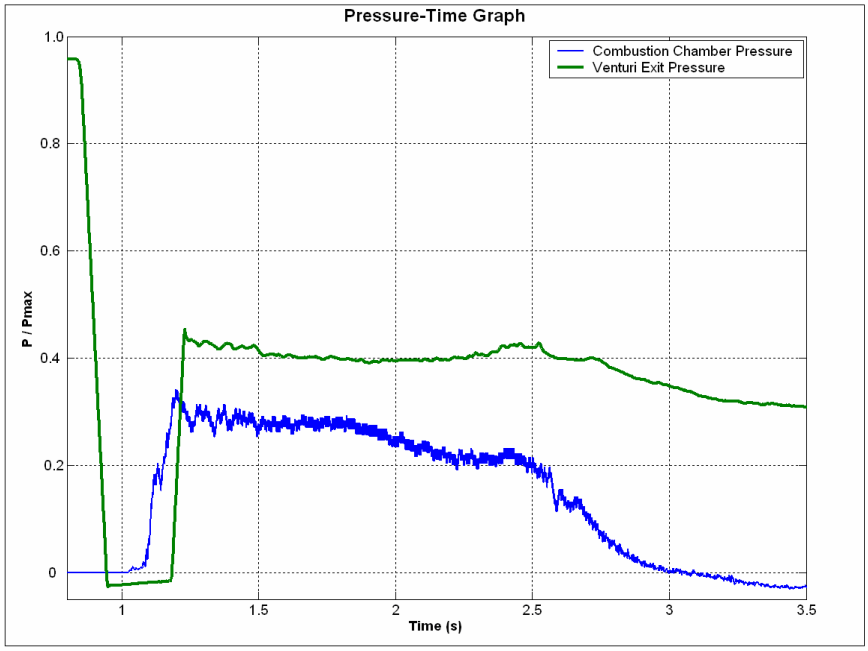

Figure 1-11. Pressure Measurement which Taken from Outlet of the Designed Venturi from a Liquid Propellant Rocket Engine Test

The time variation of pressure data acquired from an engine firing test is given in Figure 1-11 to describe how a cavitating venturi works in a real engine test environment. One of the pressure transducers is placed to the exit of the venturi and the other one is placed in the combustion chamber. At the beginning of the ignition, the venturi exit pressure is equal to the tank pressure. After the main fuel and the oxidizer valves are opened, the venturi exit pressure decreases to vapor pressure. Following the ignition process, the pressure wave goes through the feed lines, and the exit pressure of the venturi is seen to be kept almost constant at about a certain value.

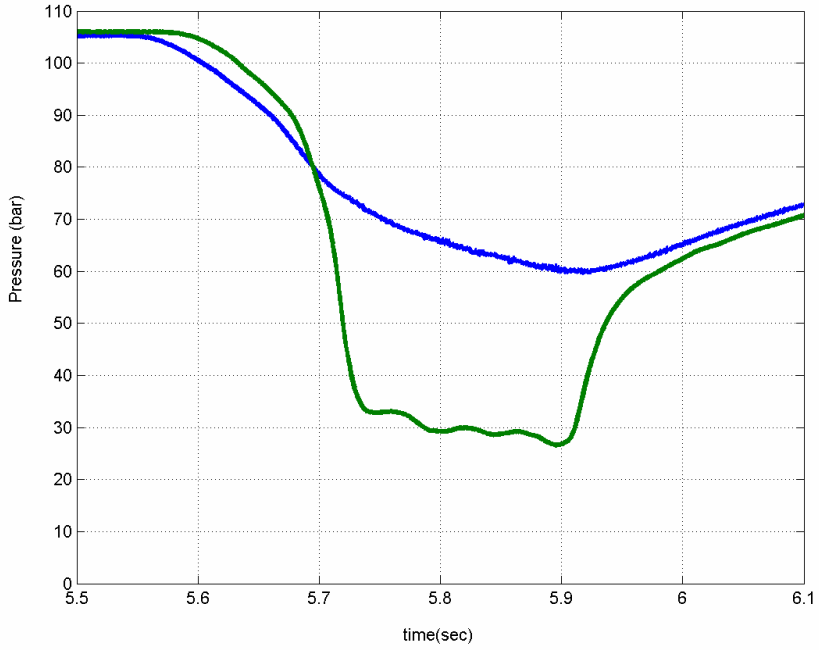

Figure 1-12. Pressure Data Acquired from the Cavitating Venturi Test. Blue line represents the inlet pressure and the Green line represents the exit pressure of the cavitating venturi.

The uncertainty of the effect of geometry on the performance of the cavitating venturi will cause delays on the time schedule of a project. In Figure 1-12, pressure measurements taken at the inlet and the exit of a cavitating venturi, which has the same inlet and outlet angles except the throat diameter increased two times than the venturi which the dimensions is given in Figure 1-9, is plotted. At this Figure, although the exit pressure was the ambient pressure, the exit pressure oscillates at 30 bar level, which is very different from the previous result given at Figure 1-8. Mass flow rate measurement also shows that the venturi is not choked properly. After further analyses performed with FLUENT, the venturi seems to be choked well due to the results which are given in Figure 1-13 and Figure 1-14. Therefore, doubts about the solver and the capabilities rise at this moment. And it is necessary to understand the limits of the solver for not to face with same problems in the

future. Also in future projects the design iterations have to be minimized to reduce the production and testing costs.

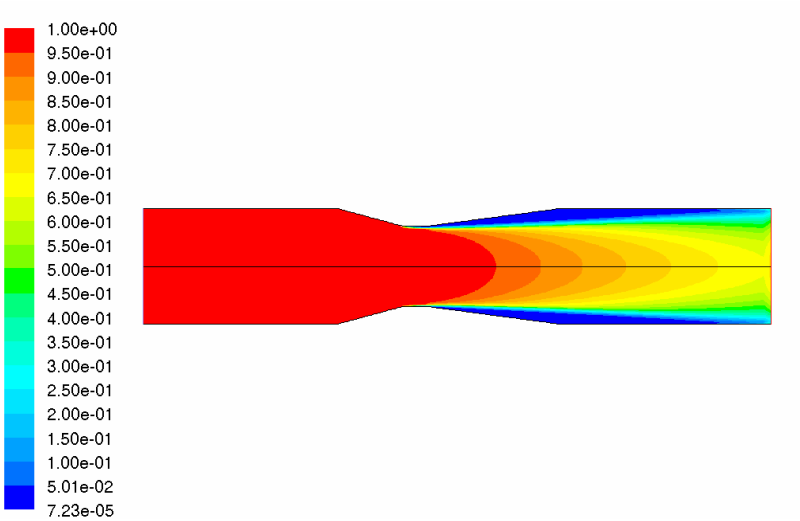

Figure 1-13. Volume Fraction of Liquid Water, red represents the fully liquid water zone and the blue represent the fully liquid vapor zone.

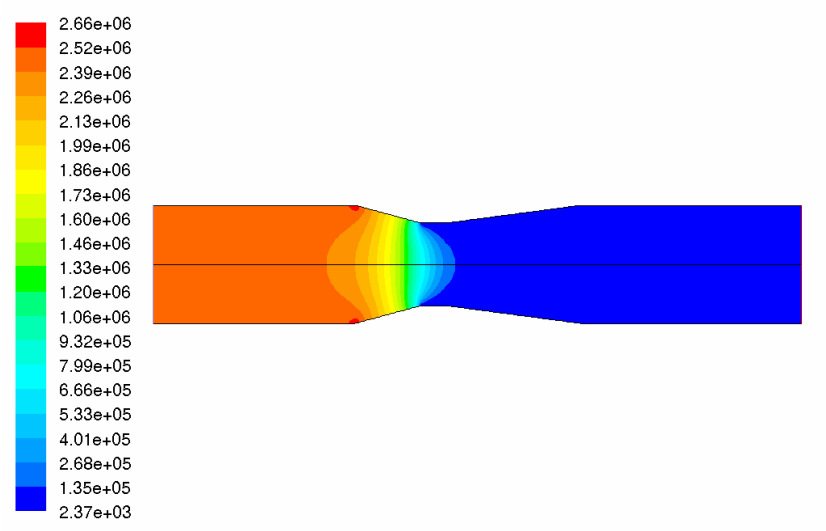

Figure 1-14. Pressure Through Venturi

Objective The Thesis

The aim of this thesis is to investigate the effect of geometry on the behavior of the cavitating venturi flows. This work mainly focuses on the effect of inlet, outlet angles and the dimensionless throat length on similar flows. The similarity parameters are chosen to be cavitation number which will be defined further and the Reynolds number, which has a characteristic length of the throat diameter. In addition, through the tests and numerical solution, the working fluid is water.

The effect of the geometry on the cavitating venturi flows is investigated with the commercial flow solver. But it is necessary to validate the solutions and tune the parameters of the solver. Although FLUENT has a validation case for cavitation through an orifice, due to the past experience, which is described in previous chapters, an experiment setup is designed and manufactured through this thesis. Validation case is also used to experiment on the mesh size dependency of the cavitating flows. And for a better visual observation, although all cavitating venturies are axis-symmetric, the test setup is designed to be 3-D Prismatic geometry. After obtaining the results of the 2-D axisymmetric cases, the cases which have interesting phenomenons like oscillations etc. These results are compared with the similar 2-D results and then will be tested experimentally to tune the flow solver. This methodology is seemed to be cumbersome but in order to obtain meaningful results it is necessary to do so.

In first two chapters, basics of cavitating flows and the areas of use of cavitating venturies are discussed in order to give background knowledge about the dimensionless parameters and the flow characteristics of venturi flows. The numerical methodology and Experimental setup are discussed in the third and the forth chapters. Also the experimental values that have to be measured and the experimental setup are discussed in the fourth chapter. In the fifth chapter the results of numerical solutions and the experiments were used to develop some engineering graphs. Also in this chapter the numerical and experimental matrixes are stated in details.

CHAPTER 2

VENTURI AND CAVITATING FLOWS

To understand cavitating venturi flows, it is better to give background information about the cavitation process. Also to understand the chocking phenomenon one has to investigate the speed of sound in multiphase flows and how the second phase affects the characteristics of the flow field. Moreover, to obtain more meaningful results it is necessary to define the geometry and the flow parameters with the non-dimensional numbers like Reynolds number which governs the viscosity effects and cavitation number which is a value to judge the strength of cavitation. Through this chapter also the basic calculation methods which depends on zero dimensional flow assumptions is also investigated in details.

2.1 Cavitation

A liquid at constant temperature could be subjected to decreasing pressure, P, which falls below the saturated vapor pressure, P_v. The value of (P_v-P) is called the tension, ΔP, and the magnitude at which rupture occurs is the tensile strength of the liquid, ΔP_c. The process of rupturing a liquid by decreasing in pressure at roughly constant liquid temperature is often called cavitation. If a liquid at constant pressure subjected to an increasing temperature above its critical temperature again the liquid will rupture by the increase in tension but in this time it is called 'boiling'. 'Cavitation' and 'boiling' are the names given to the way of rupturing of the liquid in constant temperature or constant pressure respectively. [13]

At the inlet of the cavitating venturi throat, the flow is accelerated such that the local static pressure decreases under the vapor pressure of the liquid. And the cavitation bubbles created at the wall of the throat separates from the leading edge

of the throat section. These bubbles move through the diffuser part of the cavitating venturi and collapse into smaller bubbles and disappear at a specific length due to the pressure recovery at the diffuser part. To the time that the bubbles created to the disappeared through the venturi at the locations where the bubbles exists the local pressure is set to the vapor pressure at that section of the venturi. In Figure 2-1, 2-2 and 2-3 the pressure distribution, the volume fraction of water and velocity distribution through a venturi can be seen.

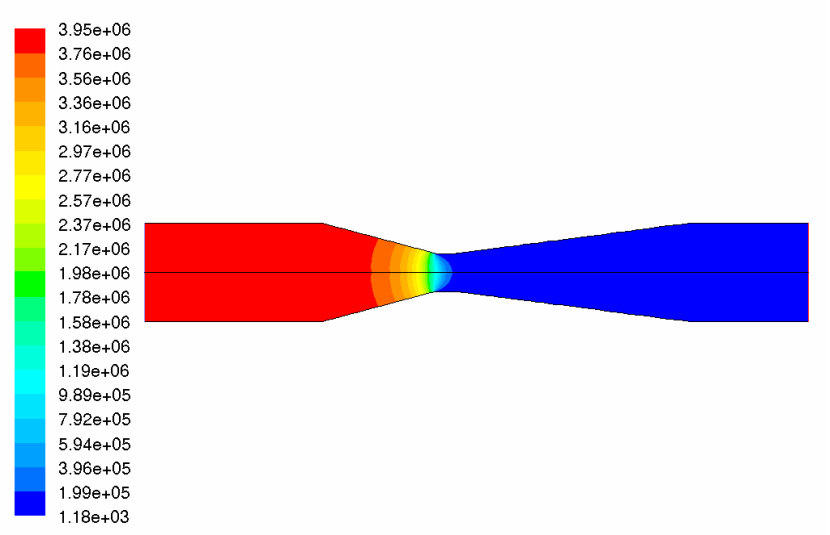

Figure 2-1. Pressure Distribution Through Venturi

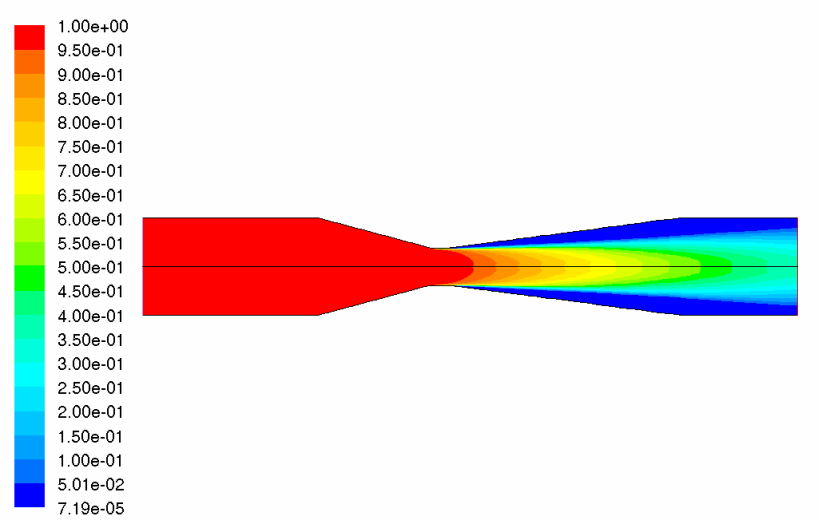

Figure 2-2. Volume Fraction of Liquid Phase Through Venturi

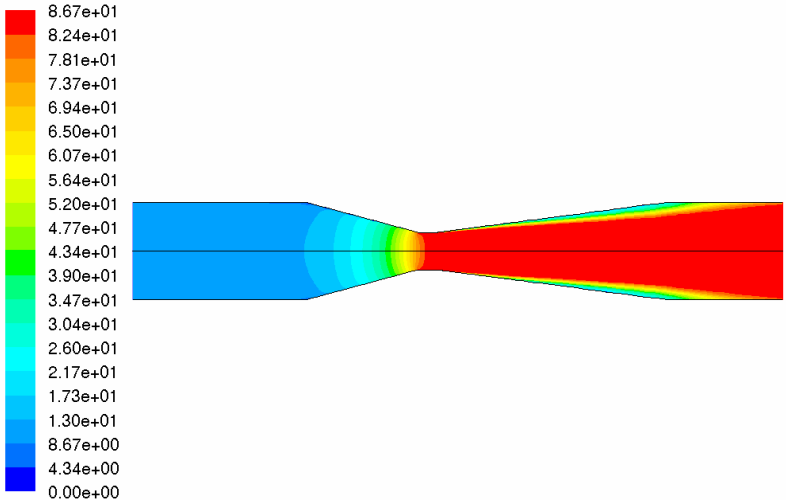

Figure 2-3. Velocity Field Through Venturi

2.2 Speed of Sound In Multiphase Flows And Choking Phenomenon

In sonic choked gas nozzles which are counterpart of cavitating venturies in gas flow, the flow at the throat is designed to attain Mach equal to `one` for the gas involved. For homogenous gases, the calculation of the speed of sound is not troublesome. In the case of liquid flow, choking phenomenon rather difficult to predict due to the fact that the difficulty of calculating speed of sound at the heterogeneous multiphase flow. In Figure 2-4, speed of sound is given as a function of void fraction of gas in water for two different k values 1.0 and 1.4. [13]

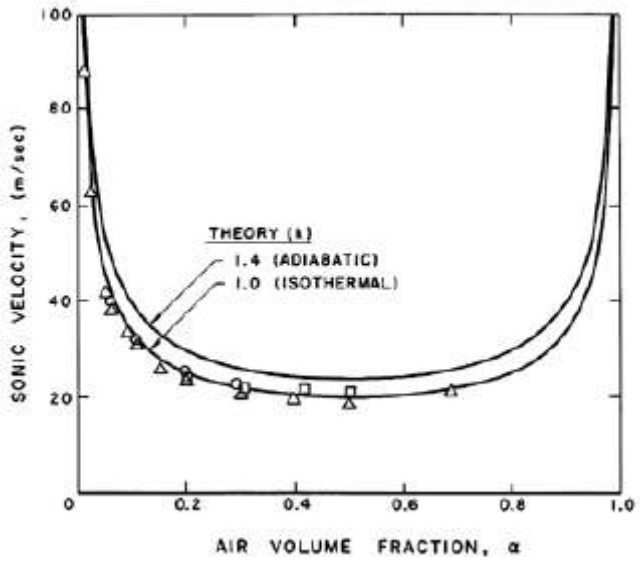

Figure 2-4. Sonic Velocity of Water / Bubble Mixture w.r.t. Air Volume Fraction.[13]

One have to keep in mind that Figure 2-4 is for homogenous bubble/liquid mixtures and not applicable for heterogeneous flows. In cavitating venturies the flow field is rather complex that to calculate the sonic velocity. Actually at the throat section there exist layers of several mixture ratios. Near the wall the cavitation starts so that the volume fraction ratio is close to 1. And a core of liquid remains at the

middle portion of the throat section of the venturi. Therefore, it is very difficult to judge the 'choking' condition on such heterogeneous media.

2.3 Dimensionless Parameters

Cavitating venturi flows are affected from several geometric parameters, flow parameters and liquid properties. Therefore, it is necessary to define dimensionless similarity parameters so as to decrease number of solutions and experiments. In cavitating venturi flows mainly there are two numbers which are important; one is Reynolds Number and the second one is the cavitation number, which was defined in detail below. Also there are two parameters which are used to analyze the flow or compare the performances of the venturies. One is the discharge coefficient, C_d, which defines the performance and the other is the Strouhal Number, S_t, which defines the unsteady bubble oscillations behaviors.

2.3.1 Cavitation number

The cavitation number σ is the most important parameter in the present work as it will set the overall extent of cavitation in the venturi. The cavitation number is defined in equation 2-1 as follows [9].

$$\sigma = \frac{P_1 - P_v}{P_1 - P_2} \tag{2-1}$$

Where the P_1 and P_2 are inlet and outlet pressure, respectively and P_v is the vapor pressure of the working fluid. If inlet pressure P_1 is relatively bigger compared to P_2 the cavitation number have a value higher than 1. And in the limit cavitation number has the value of 1 for the vacuum at the exit. Cavitation number is a measure to compare the strength of the cavitation when the value decreases to 1 the cavitation effect is strongest. After a certain value of the cavitation number

exceeded, cavitation process stops and the venturi lets the liquid flow with the mass flow rate affected from the exit pressure P_2.

2.3.2 Reynolds Number

The Reynolds Number "Re" measures viscous effects as in all Navies-Stokes solutions. We choose the Bernoulli velocity as the throat V_{th}, the venturi throat diameter D_{th}, liquid density ρ_l, and the dynamic viscosity μ_l as the dimensions of Reynolds number as in literature, [9].

$$\mathrm{Re} = \frac{\rho_l V_{th} D_{th}}{\mu_l} \tag{2-2}$$

With the increasing Reynolds number it is known that the oscillation exists in the flow field damps out [9].To increase the Reynolds number without changing the other parameters one has to increase the inlet pressure P_1 and also increase exit pressure such that the cavitation number stays constant.

2.3.3 Discharge Coefficient

For cavitating venturi flows discharge coefficient," C_d", can be defined in several ways but through this thesis the definition will be the ratio of the real mass flow rate to the ideal mass flow rate which is calculated with the Bernoulli velocity, V_{th}, at the throat. Through out numerical solution and the experiments the real mass flow rate is a known value and the ideal mass flow rate is calculated through the following equations. Ideal mass flow rate calculation assumes all the throat area is liquid and the core coefficient "C_c" is equal to one. To calculate the V_{th} one has to use the equation 2-8 for a known vapor pressure and inlet pressure value.

$$\dot{m}_{ideal} = \rho_l A_{th} V_{th} \tag{2-3}$$

$$\dot{m}_{real} = C_c \rho_l A_{th} V_{th} \tag{2-4}$$

$$C_d = \frac{\dot{m}_{real}}{\dot{m}_{ideal}} = \frac{C_c \rho_l A_{th} V_{th}}{\rho_l A_{th} V_{th}} = C_c \tag{2-5}$$

2.3.4 Strouhal Number

The oscillation of bubbles in the flow field is mainly due to the unsteady growth and collapse of the bubbles which are generated at the throat inlet of the cavitating venturi. In some applications like rocket engine flow control, these oscillations in the flow field gain importance. These unsteady flow fluctuations may couple with the combustion and induce instability on the flow field or can affect the performance of the injector atomizers. Although FLUENT does not govern the bubble formation and collapse, these effects can be seen on some high cavitation number values also which FLUENT can calculate. Here in equation 2-6, f, is the frequency of oscillations in Hz and V_{th} is the throat liquid velocity which is calculated with Bernoulli equation, and the L_D is the length of the diffuser part of the venturi, which is thought to be the main parameter which defines the oscillations.

$$St = f \frac{L_D}{V_{th}} \tag{2-6}$$

2.4 Preliminary Calculations With Bernoulli Equation

Flow domain can be modeled as a steady one-dimensional flow and one can easily derive the basic equations of the flow with some assumptions [12]. First we treat the cavitation region as a fixed, slip boundary which occupies a fixed fraction of the nozzle cross sectional area. The liquid passes through the remaining fraction of the nozzle area "A_c". ($A_c = A_{th}\ C_c$). The fraction "C_c" is a function of geometry. Also we can assume that the density of the liquid phase is constant and at that interphase mass transfer is negligible. Thus the mass flow through the nozzle can be expressed as:

$$\dot{m} = \rho_l C_c A_{th} V_{th} \tag{2-7}$$

An other assumption can be made as the flow through point 1 to point c in Figure 1-1 is lossless. Furthermore, due to the first assumption we can say that the pressure at point c is equal to the vapor pressure. With these assumptions and neglecting the dynamic pressure at inlet, we can write the momentum balance from point 1 to point c using Bernoulli's equation:

$$P_1 = P_v + \frac{1}{2}\rho_l V_{th}^2 \tag{2-8}$$

Where P_1 is inlet pressure, V_{th} is average velocity at point c, P_v is the vapor pressure. Combining the equation 2-7 and equation 2-8 one can easily calculate the mass flow rate

$$\dot{m} = C_c A_{th} \sqrt{2\rho(P_1 - P_v)} \tag{2-9}$$

To design cavitating venturi for a specified mass flow rate one can take the area 'A_{th}' from (2-9) and calculate the necessary diameter of the throat for a specified inlet pressure.

CHAPTER 3

NUMERICAL METHOD

Through the mid 70's the design of the cavitating venturies are performed with simple 1-D equations and huge numbers of experiments, due to the complexity of the flow field and to the absence of commercially available flow solvers which can handle cavitation phenomenon. However one can see the accuracy limits of 1-D equations in Figure 1-11. The 1-D solutions, for C_c equals to 1, depart almost 20% from the experimental measurements. Also it is very hard to experiment on every possible geometry for different working fluids and optimize their performance. Therefore, it is necessary to understand the limits of a commercial flow solver and to use it in preliminary design phases. Although cavitating venturies can be used for any fluid, through the numerical solutions, the working fluid is restricted for water.

Though this chapter, brief information will be given about the numerical methodology and the background of the flow solver. The additional equations to model the cavitation which are used by the flow solver will be investigated in details.

3.1 Numerical Methodology

Almost all cavitating venturies are axisymmetric but for our experiments for a better visual observation it is necessary to use 3-D prismatic sections rather than axisymmetric ones. Also production of the axisymmetric venturies is more expensive compared to 3-D Prismatic venturies. In addition, for each case a different venturi have to be manufactured for axisymmeric case. Therefore, the differences between axisymmetric and 2-D venturies are investigated through this

thesis. Also the effects of the wall boundaries are examined in details to decide the depth of the venturi in the experiments. And an optimization has to be performed on depth value of the experiment test section due to the limitation on test time which is restricted by the available tank volume. Therefore, to increase the test time the depth must be kept below a limited value. However, the effect of the wall increases with the decreasing depth also. Therefore both 2-D, 2-D axisymmetric and 3-D prismatic solution are performed through this thesis.

3.2 FLUENT Theory

FLUENT provides comprehensive modeling capabilities for a wide range of incompressible and compressible, laminar and turbulent fluid flow problems. Steady-state or transient analyses can be performed. In FLUENT, a broad range of mathematical models for transport phenomena (like heat transfer and chemical reactions) is combined with the ability to model complex geometries. Examples of FLUENT applications include laminar non-Newtonian flows in process equipment; conjugate heat transfer in turbo machinery and automotive engine components; pulverized coal combustion in utility boilers; external aerodynamics; flow through compressors, pumps, and fans; and multiphase flows in bubble columns and fluidized beds.

To permit modeling of fluid flow and related transport phenomena in industrial equipment and processes, various useful features are provided. These include porous media, lumped parameter (fan and heat exchanger), streamwise-periodic flow and heat transfer, swirl, and moving reference frame models. The moving reference frame family of models includes the ability to model single or multiple reference frames. A time-accurate sliding mesh method, useful for modeling multiple stages in turbo machinery applications, for example, is also provided, along with the mixing plane model for computing time-averaged flow fields.

Another very useful group of models in FLUENT is the set of free surface and multiphase flow models. These can be used for analysis of gas-liquid, gas-solid, liquid-solid, and gas-liquid-solid flows. For these types of problems, FLUENT

provides the volume-of-fluid (VOF), mixture, and Eulerian models, as well as the discrete phase model (DPM). The DPM performs Lagrangian trajectory calculations for dispersed phases (particles, droplets, or bubbles), including coupling with the continuous phase. Examples of multiphase flows include channel flows, sprays, sedimentation, separation, and cavitation. Robust and accurate turbulence models are a vital component of the FLUENT suite of models. The turbulence models provided have a broad range of applicability, and they include the effects of other physical phenomena, such as buoyancy and compressibility. Particular care has been devoted to addressing issues of near-wall accuracy via the use of extended wall functions and zonal models. Various modes of heat transfer can be modeled, including natural, forced, and mixed convection with or without conjugate heat transfer, porous media, etc. The set of radiation models and related sub models for modeling participating media are general and can take into account the complications of combustion. A particular strength of FLUENT is its ability to model combustion phenomena using a variety of models, including eddy dissipation and probability density function models. A host of other models that are very useful for reacting flow applications are also available, including coal and droplet combustion, surface reaction, and pollutant formation models [14].

3.3 FLUENT Cavitation Model

There are several methods exist in literature to model the cavitating flows.

Two Phase models (VOF):

This model threads the two fluids individually. The gas bubbles created and collapsed in the second fluid tracked through the control volume. The dynamics of the bubbles solved with additional equations. In this model also it is possible to apply the non-equilibrium dynamic effects because the creation, collapse and the collision of the bubbles does not happen immediately but it takes a certain time period. However none of the available commercial flow solvers have the capability

of treating the cavitation with this method. Fluent has the volume of fluid capability but this solver does not govern the creation of the second phase.

The Mixture models:

The Mixture model, like the VOF model, uses a single-fluid approach. It differs from the VOF model in two respects;

- The mixture model allows the phase to be interpenetrating. The volume fractions α_q and α_q for a control volume can therefore be equal to any value between 0 and 1, depending on the space occupied by the phase q and phase p.
- The mixture model allows the phase to move at different velocities, using the concept of slip velocities. (Note that the phases can also be assumed to move at the same velocity, and the mixture model is then reduced to a homogenous multiphase model.

The mixture model solves the continuity equation for the mixture, the momentum equation for the mixture, the energy equation for the mixture, and the volume fraction equation for the secondary phases, as well as algebraic expressions for the relative velocities if the phases are moving at different velocities.

3.3.1 Continuity Equation for the Mixture

The continuity equation for the mixture is

$$\frac{\partial}{\partial t}(\rho_m) + \nabla \cdot (\rho_m \vec{v}_m) = 0 \tag{3-1}$$

Where $\vec{v}_m$ is the mass-averaged velocity:

$$\vec{v}_m = \frac{\sum_{k=1}^{n} \alpha_k \rho_k \vec{v}_k}{\rho_m} \tag{3-2}$$

And ρ_m is the mixture density:

$$\rho_m = \sum_{k=1}^{n} \alpha_k \rho_k \tag{3-3}$$

α_k is the volume fraction of phase k.

3.3.2 Momentum Equation for the Mixture

The momentum equation for the mixture can be obtained by summing the individual momentum equations for all phases. It can be expressed as

$$\frac{\partial}{\partial t}(\rho_m \vec{v}_m) + \nabla \cdot (\rho_m \vec{v}_m \vec{v}_m) = -\nabla p + \nabla \cdot \left[\mu_m \left(\nabla \vec{v}_m + \nabla \vec{v}_m^{\mathrm{T}}\right)\right] + \rho_m \vec{g} + \vec{F} + \nabla \cdot \left(\sum_{k=1}^{n} \alpha_k \rho_k \vec{v}_{\mathrm{dr},k} \vec{v}_{\mathrm{dr},k}\right) \tag{3-4}$$

Where n is the number of phases, $\vec{F}$ is a body force, and μ_m is the viscosity of the mixture;

$$\mu_m = \sum_{k=1}^{n} \alpha_k \mu_k \tag{3-5}$$

$\vec{\upsilon}_{dr,k}$ is the drift velocity for secondary phase k:

$$\vec{v}_{\mathrm{dr},k} = \vec{v}_k - \vec{v}_m \tag{3-6}$$

3.3.3 Energy Equation for the Mixture

The energy equation for the mixture takes the following form:

$$\frac{\partial}{\partial t}\sum_{k=1}^{n}(\alpha_k \rho_k E_k) + \nabla \cdot \sum_{k=1}^{n}(\alpha_k \vec{v}_k(\rho_k E_k + p)) = \nabla \cdot (k_{\text{eff}} \nabla T) + S_E \tag{3-7}$$

Where k_{eff} is the effective conductivity $(\sum \alpha_k (k_k + k_t))$, where k_t is the turbulent thermal conductivity, defined according to the turbulence model being used. The first term on the right-hand side of above equation represent energy transfer due to conduction. S_E includes any other volumetric heat source.
In Equation (3-7),

$$E_k = h_k - \frac{p}{\rho_k} + \frac{v_k^2}{2} \tag{3-8}$$

For a compressible phase and $E_k = h_k$ for an incompressible phase, where h_k is the sensible enthalpy for phase k.

3.3.4 Volume Fraction Equation for the Secondary Phases

From the continuity equation for secondary phase p, the volume fraction equation for the secondary phase p can be obtained:

$$\frac{\partial}{\partial t}(\alpha_p \rho_p) + \nabla \cdot (\alpha_p \rho_p \vec{v}_m) = -\nabla \cdot (\alpha_p \rho_p \vec{v}_{\mathrm{dr},p}) + \sum_{q=1}^{n} (\dot{m}_{qp} - \dot{m}_{pq}) \tag{3-9}$$

3.3.5 FLUENT Cavitation Model Validation Case-Cavitation Over a Sharp-Edged Orifice

The purpose of this test is to validate the capability of the cavitation model when applied to a cavitating flow. The strength of the cavitation depends on the inlet pressure. When the inlet pressure is small, the cavitation number is large, and the flow is weakly cavitating. For larger inlet pressures, the cavitation number is smaller, which in turn results in a strong cavitating flow.

Fourteen test cases were solved for inlet pressures ranging from 1.9kPa to 4000000 kPa. The computed discharge coefficients were compared with the experimental correlation by Nurick. [5]

Problem description:

A 2D axisymmetric sharp-edged orifice is considered, as shown in Figure 3-1. Its geometric parameters are R/r=2.86 and L/r=7.94, where R, r, and L denote the inlet radius, orifice radius, and orifice length, respectively. The flow is assumed to be turbulent, and the standard k-epsilon model is employed. The specified boundary conditions are the total pressure Po at the inlet, which varies from 1.9kPa to 4000000 kPa, and the static pressure P_{exit} = 95 kPa at the exit.

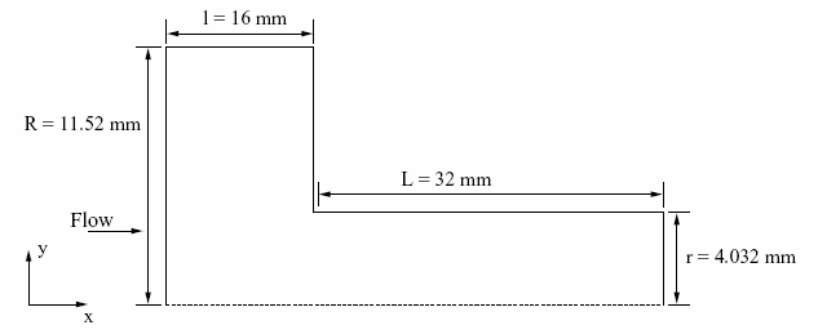

Figure 3-1. FLUENT Validation Case Geometry

Results:

Experimental data is available in the form of discharge coefficient versus cavitation number, where the discharge coefficient is defined as $\dot{m}/\dot{m}_{ideal}$, $\dot{m}$ is the computed mass flow rate, and $\dot{m}_{ideal}$ is the ideal mass flow rate through the orifice. The ideal mass flow rate through the orifice is computed as $\dot{m} = A_{th}\sqrt{2\rho(P_{in} - P_{exit})}$, where A_{th} is the cross-sectional area of the orifice, $A_{th}=\pi r^2$, ρ is the density, and P_{in} and P_{exit} are the inlet pressure and the exit pressure, respectively. At this solution the version of the FLUENT is 6.2.5 and 2D solver is used.

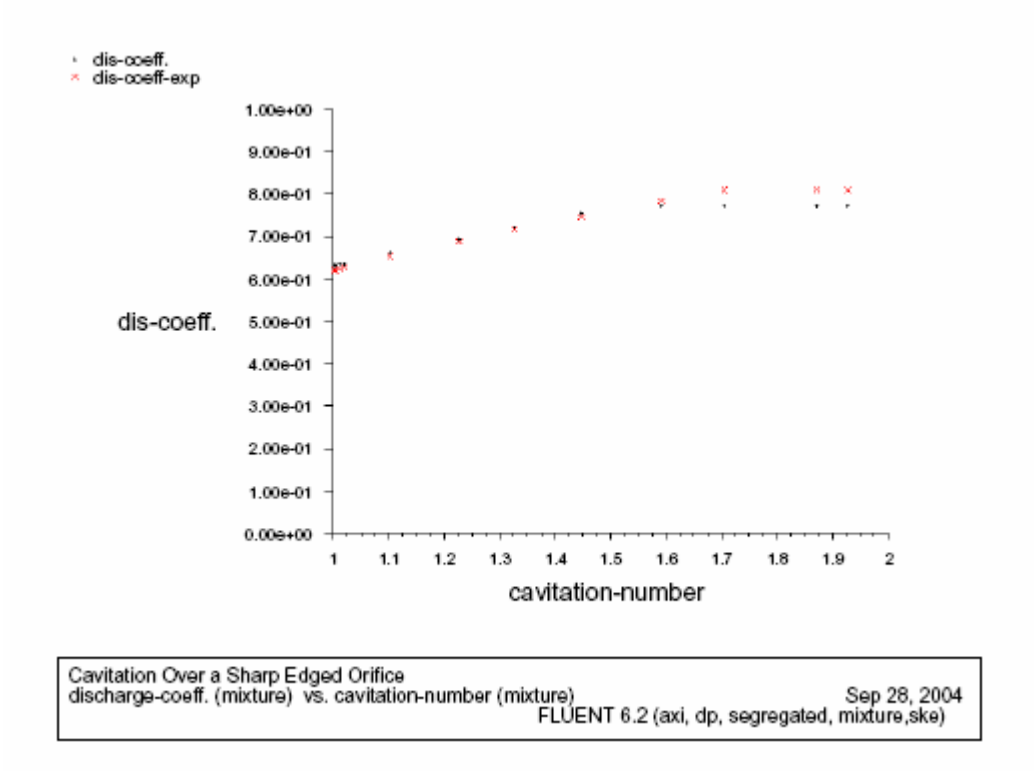

Figure 3-2. FLUENT Validation Case Results

In Figure 3-2, Fluent results are in great agreement with the experimental results. Also for the cavitating venturi case the previous test performed in TÜBİTAK-SAGE, in agreement with the Fluent results, which was shown in Figure 1-10.

In Figure 3-3, one of the results of the Fluent validation case was plotted. In this case the inlet pressure is 50 bars.

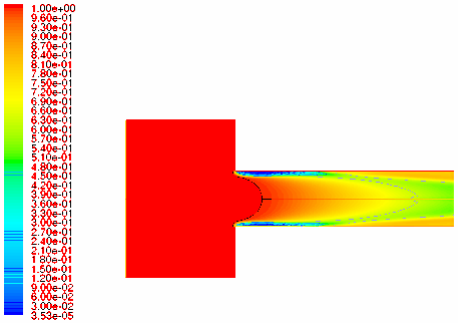

a) Volume fraction of liquid water

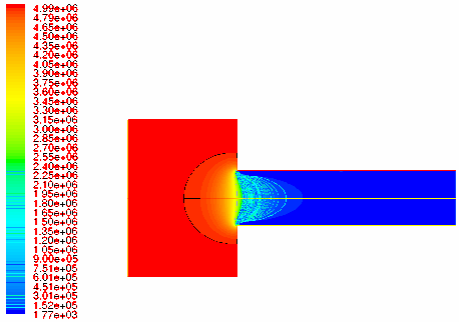

b) Pressure distribution in (Pa)

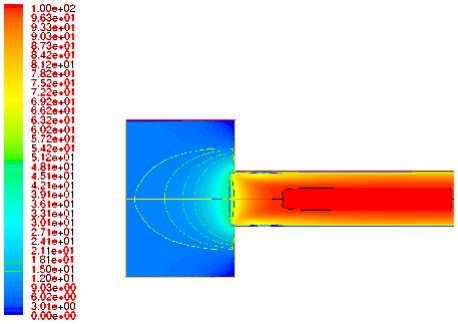

c)Velocity distribution (m/s)

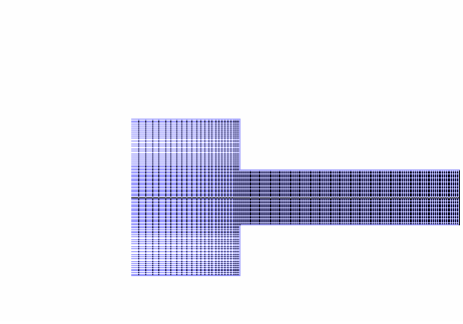

d) Grid resolution (7350 cells)

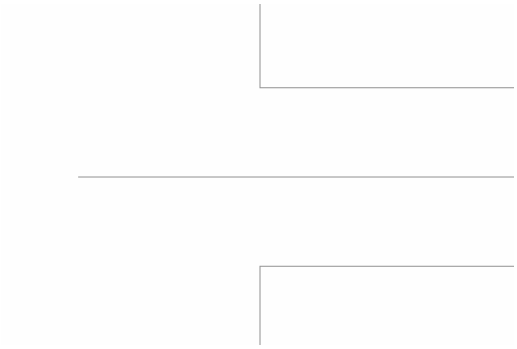

e) Grid at the throat section zoomed

Figure 3-3. Results for the FLUENT validation case at 50 bar inlet pressure.

Mesh dependency is also evaluated for the validation case. For 50 bar case the cavitation numbers for three different mesh sizes is given in Table 3-1. The percent difference between the solutions are calculated w.r.t. the results of the finest mesh which has 56400 cells. The difference is calculated by using equation 3-10.

$$\frac{ABS\left(C_{D\,mesh\_k} - C_{D\,mesh\_3}\right)}{C_{D\,mesh\_3}} 100 \quad . \qquad (3\text{-}10)$$

Table 3-1. Mesh Size Versus Cavitation Number for FLUENT Validation Case at 50 bars

Mesh Size (cells)	Discharge Coefficient	Percent Difference
3525 (original)	0.631	1.28 %
14100	0.626	0.48 %
56400	0.623	0.00 %

CHAPTER 4

EXPERIMENTAL STUDY

Although the experiments are difficult to perform it is necessary to validate the numerical simulation tools. Due to the complex flow behavior of cavitation it is very difficult to perform experiments. Most of the parameters to be measured like mass flow rate and pressure are the integral parameters that average the chaotic flow field behavior. To investigate the flow field in details, local parameters have to be measured but in such a chaotic environment it is difficult to do so. Therefore, visualization techniques have to be used in order to investigate the flow field without affecting the fluid flow. However in such a case, the test pressure and the design of the test section gain importance. Pressure can not exceed specific values due to stress limits in such visual materials. Although all cavitating venturies are axis-symmetric, for better visual observability, two-dimensional test sections can be used to understand the flow structure. Throughout this thesis several axisymmetric and 3-D prismatic venturi geometries are tested. And the effect of this difference is investigated in Chapter 5 in details.

4.1 Experimental Setup

In Figure 4-1, a simple sketch of the experimental setup is illustrated. Two high pressure nitrogen tanks are used to pressurize the water tanks. One is used to define the inlet pressure, P_1, and the other is used to set the outlet pressure, P_2. To regulate the pressure, two high pressure-high flow rate pressure regulators are used. Also two high pressure tanks are used to store the water. An additional needle valve is attached to the water tank at the exit of the test section because the pressure regulators work only one-way, therefore these regulators can not release the high pressure gas to reduce the pressure. To prevent the pressure rise in the outlet due to

the decrease in volume of the water tank at the exit a needle valve is attached and set to a value to get required pressure values. Also a solenoid valve operated ball valve is used to separate the two pressurized zones before the experiment starts. More over, two high pressure transducers attached to the proper locations like inlet of the test section and to the exit of the test section. Here an additional pressure sensor is not attached to the exit tank because the relief valve sets the outlet pressure to the required value. To measure the mass flow rate through the test section a turbine type flow meter is used. The pressure and the mass flow rate data is collected with a data acquisition system and send to the computer.

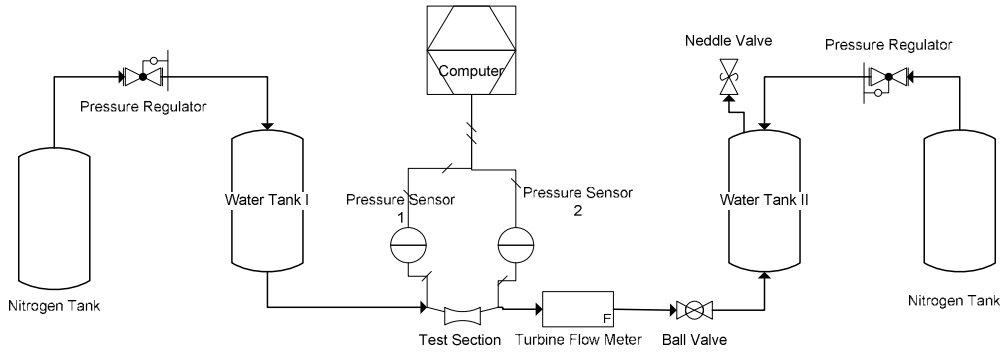

Figure 4-1. Test Setup Sketch

4.1.1 Test Section

There are two different set of test sections are designed and produced. For the preliminary tests four different axisymmetic venturi sections are used. These are the configurations which are more physically similar to the real venturies. However in these test the visibility of the bubble formation at the throat of the venturi is affected from the shape of the venturi. The other set of test sections is designed to be 3-D prismatic so that the core section of the venturi can be seen and this will be better for comparison with the numerical flow solutions.

4.1.1.1 Axisymmetric Test Sections

First set of test is done with axisymmetric venturi geometries. In total four different axisymmetric venturi geometries are manufactured. And the geometric properties are given in Table 4-1. Due to the manufacturing difficulties, a blur region at the throat section of the venturi remains in one of the venturies. Although wax is applied to the inside of the venturi the best visual quality which is achieved can be seen on Figure 4-2. The technical drawings of the cavitating venturies are given in Appendix A-1

Table 4-1. Geometric Properties of the Axisymmetric Venturies

	D_{in}	D_{th}	D_{in}/D_{th}	L_{th}	L_{th}/D_{in}	Φ_1	Φ_2
1	10 mm	5 mm	0.5	3 mm	0.3	30 deg	7 deg
2	10 mm	5 mm	0.5	3 mm	0.3	15 deg	15 deg
3	10 mm	5 mm	0.5	3 mm	0.3	15 deg	30 deg
4	10 mm	5 mm	0.5	3 mm	0.3	15 deg	60 deg

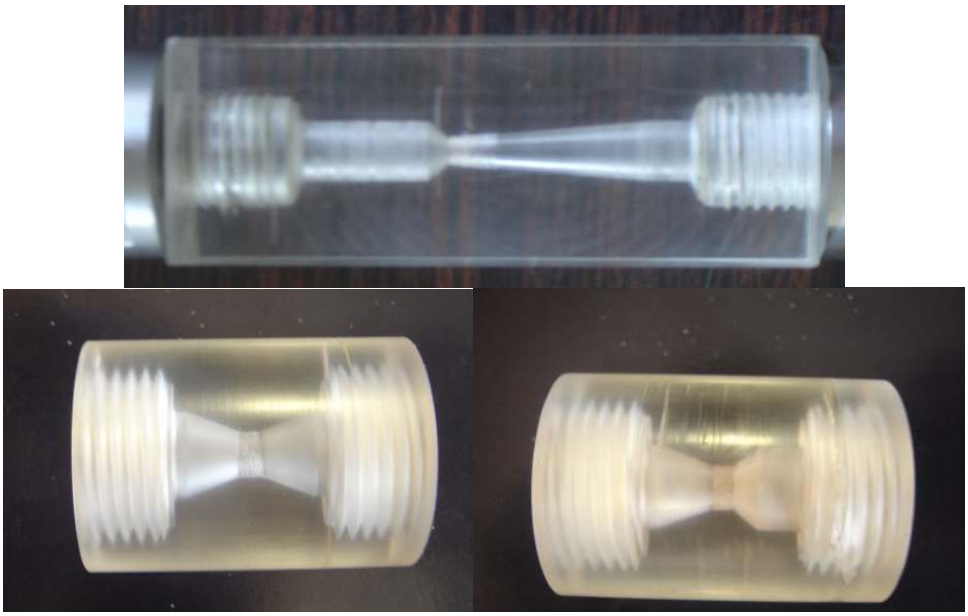

Figure 4-2. Pictures of the Tested Cavitating Venturies.

4.1.1.1 3-D Prismatic Test Section

To observe the cavitation process, venturi test section designed to be a 2-D cut of a common axisymmetric venturi. From the previous tests it is known that it is very hard to investigate the core flow and the fluctuations of the bubbles in an axisymmetric Plexiglas venturi because of the manufacturing errors. Therefore a 3-D prismatic test section designed to reduce the effect of these errors on visualization. But there exists some difficulties because of the shape. The pipelines connecting the test section with the pressurized tanks have circular cross-sections but the test section inlet and outlet have to be rectangular. To change the flow cross-section without disturbing the flow is done by additional adaptors, which the technical drawings and the pictures are given in Appendix A-1.

4.2 Measurements

4.2.1 Pressure Measurements

Pressure is one of the main parameter has to be measured to calculate the cavitation number. At least two high pressure transducers are necessary to investigate the flow field. One is in front of the venturi and the second one has to be placed after the venturi to calculate the P_2 in the cavitation number. An additional pressure transducer can be used to measure the throat pressure to ensure the cavitation. However, due to the sensitivity of cavitation at the throat this measurement will affect the characteristics of the cavitating venturi.

4.2.2 Mass Flow Rate Measurements

The main reason of the usage of the cavitating venturi is to limit or control the flow rate of the working fluid. Therefore, it is necessary to measure mass flow rate. In our experiments, to measure the flow rate a turbine type flow meter is used.

4.2.3 Visual Observations

A high speed camera is used to understand the bubble formation and dynamics of flow. The camera is capable of recording at 4000 fps in black & white.

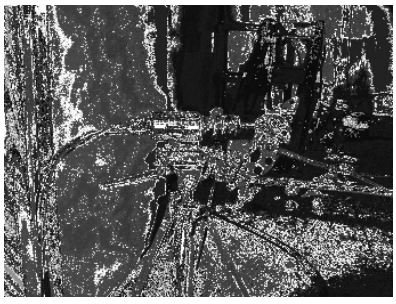

Figure 4-3. Picture of high speed camera

CHAPTER 5

RESULTS & DISCUSSIONS

The results obtained from numerical simulations and from the experiments are given in this chapter. Numerical simulations are performed for 2-D, 2-D Axisymmetric and 3-D prismatic cases. 2-D and 3-D prismatic venturi geometries, which are employed in the experiments, are used to investigate the differences from the 2-D axisymmetric venturi flows. The numerical solutions are also carried out to investigate the wall effects on the test section. The experimental results are also presented and compared with the numerical solutions.

5.1 Numerical Solutions

Numerical solutions are first aimed at investigating the effect of several parameters on the performance of venturi flows, and correlating them with a theoretical understanding. The correlations may then be used to further reduce the number of simulations. The venturi flows are investigated parametrically by forming a solution matrix based on the geometric variables of a venturi.

5.1.1 Numerical Solution Matrix

For a cavitation venturi, there are four basic geometric parameters: the inlet angle, outlet angle, D_{th}/D_{in} and L_{th}/D_{in}. Among them the inlet angle and the outlet angle are the most important parameters on cavitating venturi flows, and these two parameters are assigned five different values in the solution matrix (Table 5-1). In the literature [1] the optimum inlet and outlet angles are given as 15-18 degrees and 6-8 degrees, respectively. The inlet angles are taken as 7, 5, 30, 90 degrees. In addition, a smooth curved venturi inlet which is widely used in industry is also

added to the list. The exit angles vary from 7 to 15, 30, 60, 90 degrees. D_{th}/D_{in} ratio and L_{th}/D_{in} ratios are varied between two different values. D_{th}/D_{in} ratio value also defines the Reynolds number of the flow. Because, in most of the piping systems D_{in} is kept constant and the throat diameter is a restricted value to achieve the target mass flow rate for a specific inlet pressure and exit pressure. The last parameter is the cavitation number, "σ", which has three different values. Length of the throat and throat diameter is non-dimensionalized with the inlet diameter because of the similarity of the orifice flow with the cavitating venturi flow.

All these parameters are chosen such that the values are corresponding to meaningful dimensional numbers. Because fluent is a dimensional solver and in all solution the inlet diameter is chosen to be 22.4mm (1") which is a very common value for pipe engineers. And the throat values which are used in solutions are 8mm and 16 mm respectively. The length of the throat is chosen to be 5mm and 10 mm in dimensional domain, and also due to the pressure regulation on Plexiglas test section. The cavitation number values are chosen for 30 bar inlet pressure with 1 bar, 10 bar and 20 bar exit pressures, for the case which D_{th}/D_{in}=0.357 and 7.2 bar inlet pressure with 0.25 bar, 2.4 bar and 4.8 bar exit pressure, for the case which D_{th}/D_{in}=0.714. Also to investigate the effect of Reynolds number on the oscillation frequency of the cavitation bubble, inlet pressure increased to 60 bars for the case which D_{th}/D_{in}=0.357, but to keep the cavitation numbers fixed, backpressures for these cases are modified as 3 bars, 20 bars and 40 bars respectively for σ_1, σ_2 and σ_3. For the case which D_{th}/D_{in}=0.714, inlet pressure is increased to 30 bars and the exit pressures 1 bar, 10 bar and 20 bar respectively for σ_1, σ_2 and σ_3 to keep the cavitation number fixed. A summary of the solution matrix and a simple sketch of the venturi with the parameters shown are given in Figure 5-1 and Table 5-1 below.

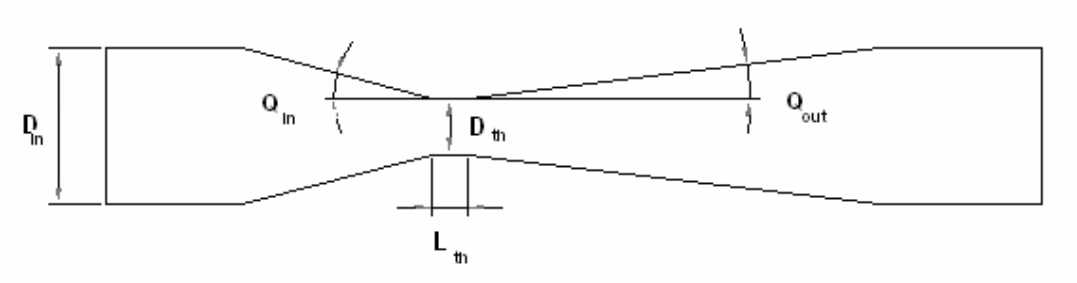

Figure 5-1. Geometric Parameters are Given on a Generic Venturi

Table 5-1. Solution Matrix for Numerical Solutions

Inlet Angle Φ_1 (deg)	Outlet Angle Φ_2 (deg)	D_{th}/D_{in}	L_{th}/D_{in}	σ
Curved	7	0.357	0.223	1.0336
7	15	0.714	0.446	1.4988
15	30			2.9979
30	60			
90	90			

Turbulence Effects:

Since FLUENT recommends k-e model for cavitation calculations, all calculations was made with this turbulence model. (To calculate the Turbulence intensity, hydraulic diameter values are used. H_d & $T_{u)}$

Turbulence intensity is assumed to be 5% through the solutions. And the hydraulic diameter value is taken to be the maximum diameter of the test section.

Sample Venturi Solution:

Numerical solutions obtained from a generic venturi are given in Figure 5-2, 5-3, 5-4, 5-5 and 5-6.

Pressure Contours:

In Figure 5-2, Static pressure distribution through a generic venturi solution is plotted. Through the throat section liquid is accelerated till the vapor pressure of water is reached. After that point although the flow is a mixture of the liquid and vapor phases, at the cross sections which has bubble the pressure is equal to vapor pressure.

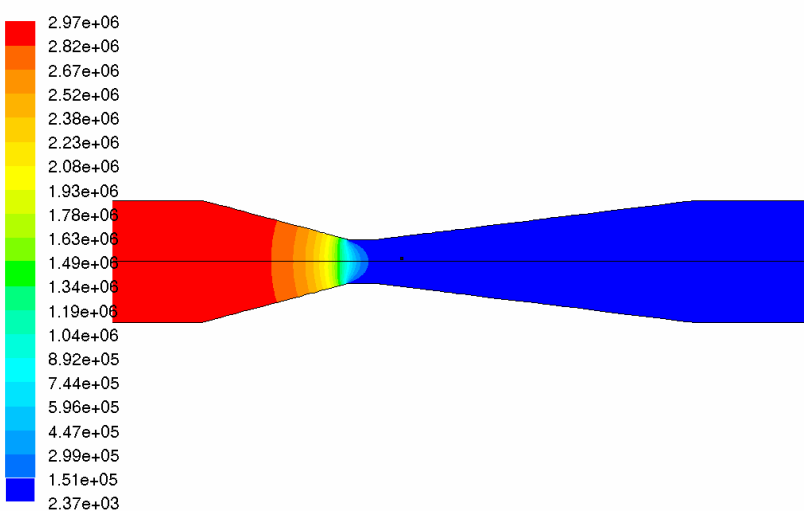

Figure 5-2. Pressure (Pa) Field Through a Generic Venturi

Velocity Contours:

Figure 5-3 shows how the velocity increases through the throat section of the venturi. This velocity can be calculated with simple 1-D equations.

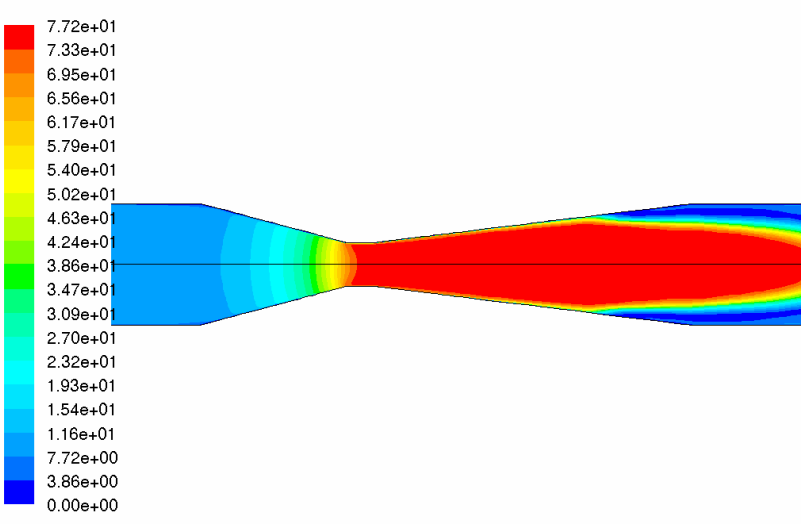

Figure 5-3. Velocity (m/s) Field Through a Generic Venturi

Phase Volume Fraction Contours:

Formation and diffusion of the gas phase at the throat section of the venturi is given in Figure 5-4. And in Figure 5-5 the vena contracta region can be seen. The thickness of the gas phase region at the throat defines the discharge coefficient of specific venturi geometry. The effect of boundary layer is reduced on the liquid core of the throat because of the formation of the gas phase at the walls through the throat section. This leads to a more uniform velocity profile through the throat section and allows us to use simple Bernoulli equation on such complex flow fields.

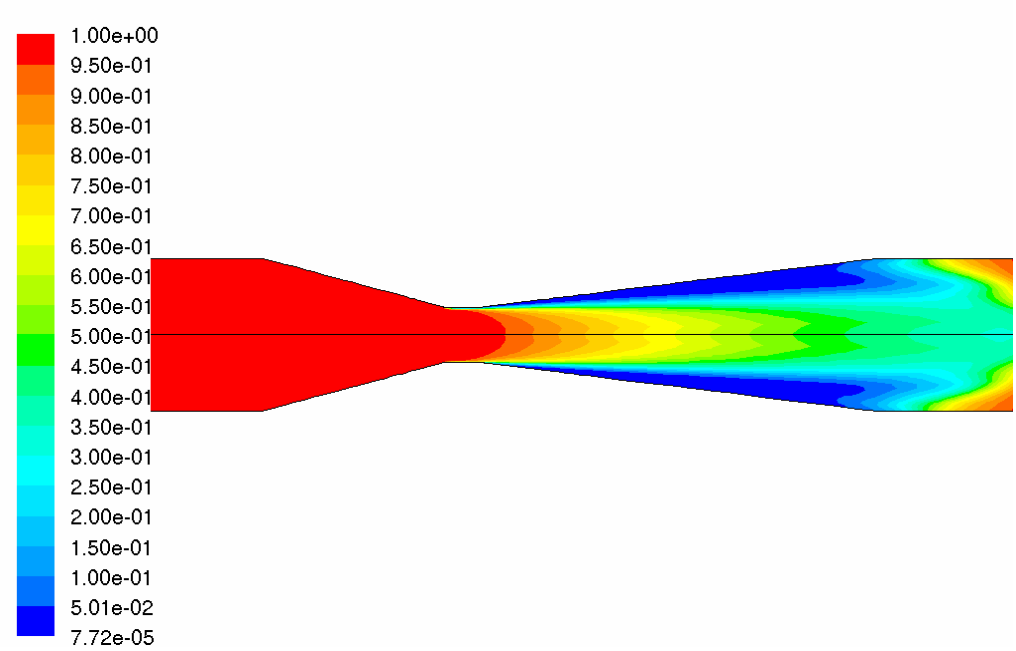

Figure 5-4. Liquid Phase Volume Fraction for a Generic Venturi

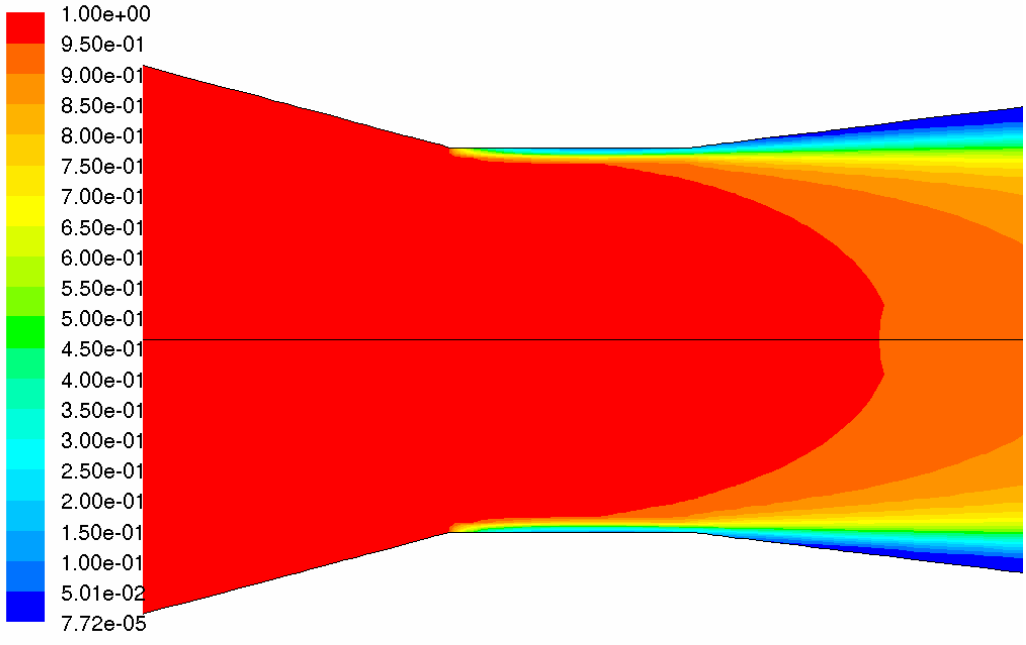

Figure 5-5. Liquid Phase Volume Fraction for a Generic Venturi Throat

Multiphase Mach Number Contours:

In Figure 5-6, Mach contours are plotted for a generic sample venturi flow solution. The speed of sound for multiphase flow is calculated with equation 5-1. It can be seen that at the throat section the Mach number is equal to 1 and the venturi is effectively chocked.

$$a = \sqrt{\frac{1}{\left((1-\alpha)\rho_g + \alpha\rho_l\right)\left(\frac{(1-\alpha)}{\rho_g a_g^2} + \frac{(\alpha)}{\rho_l a_l^2}\right)}} \tag{5-1}$$

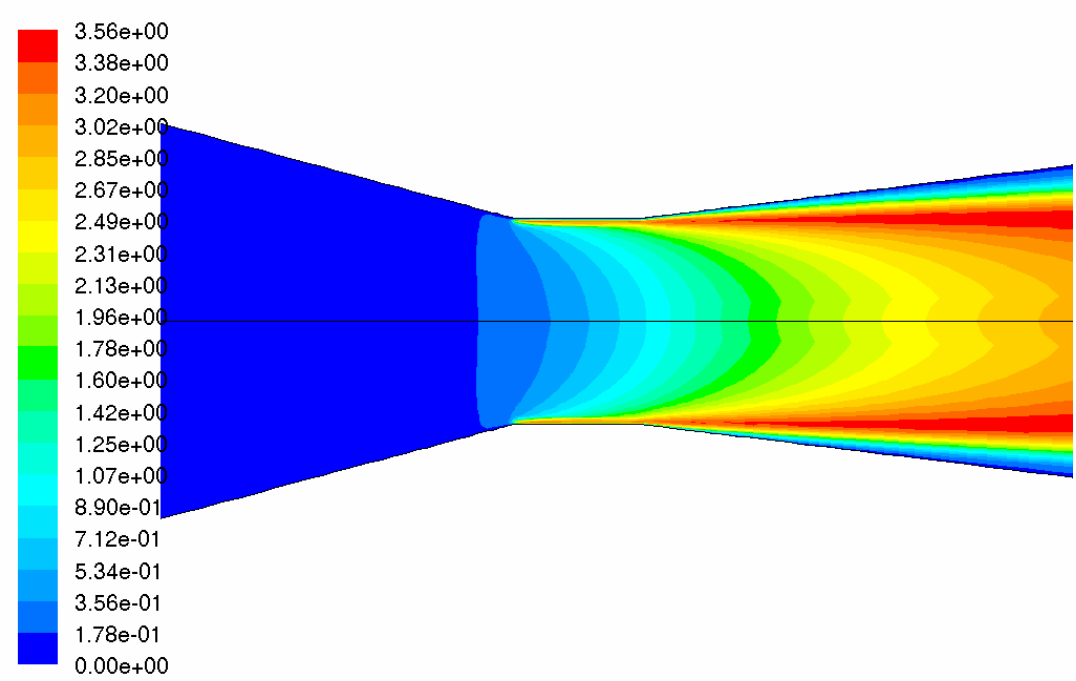

Figure 5-6. Mach Contour Plot for a Generic Venturi

5.1.2 2D-Axisymmetric Solutions

Through the numerical simulations effect of several parameters are investigated on the performance of the venturi. These parameters are inlet angle, outlet angle, ratio of length of throat to inlet diameter, ratio of throat diameter to inlet diameter, cavitation number and Reynolds number. Also there are two basics effect of these parameters exits. One is the on the discharge coefficient C_d and the other is the effect of Strouhal number on the oscillation frequency of the cavitating bubble. Each effect can be listed as follows

- Effect of Inlet Angle on Discharge Coefficient
- Effect of Outlet Angle on Discharge Coefficient
- Effect of L_{th}/D_{in} & D_{th}/D_{in} on Discharge Coefficient
- Effect of Reynolds Number on Discharge Coefficient
- Effect of Outlet Angle "Φ_2" on oscillation frequency of the Cavitation Bubble
- Effect of D_{th}/D_{in} & L_{th}/D_{in} ratio on oscillation frequency of the Cavitation Bubble
- Effect of Reynolds Number on oscillation frequency of the Cavitation Bubble

These effects will be discussed in details in the following sections.
For 2-D axisymmetric case the solution matrix will be same as in Table 5-1 except there are additional solutions for different Reynolds numbers are present. For solutions which performed for D_{th}/D_{in}=0.357 case, Re numbers are 6E5 and 9E5. And for D_{th}/D_{in}=0.714 Re numbers are 6E6 and 1.2E6.

5.1.2.1 Effect of Inlet Angle "Φ_1" on Discharge Coefficient "C_d"

The effect of inlet angle "Φ_1" on the discharge coefficient "C_d" is given in Figure 5-11 and 5-12. In these figures, through the rows the outlet angle"Φ_2"is constant and through the columns length of the throat is constant.

For a cavitating venturi if the flow is choked the discharge coefficient is not a function of the cavitation number. But for the cases which the cavitation does not occur the discharge coefficient is smaller than the cavitating ones. This is because the discharge coefficient is defined to be the ratio of ideal mass flow rate to the real one. The ideal mass flow rate is calculated by writing the Bernoulli equation between the throat and the inlet of the venturi. At the throat the limiting pressure is the vapor pressure of the working fluid. And for a smaller value of pressure the velocity at the throat is smaller than the cavitating one. Then the mass flow rate is going to be smaller than the cavitating case mass flow rate.

In the light of the discussions in the previous paragraph from Figure 5-11 and Figure 5-12 it can be seen than with the increasing inlet angle the discharge coefficient is decreasing for all three σ values. And for small Φ_1 (7 deg < Φ_1) values due to small bubble formation at the throat section, cavitation is affected more when the outlet angle Φ_2 is higher than 15 degrees for σ_3. Even for 60 and 90 degrees of exit angle, the cavitation is affected at σ_2 also. This is because the cavitating region does not find a place to stay on high exit angles and if this couples with the small bubble formation at the throat, the cavitation stops. (Figure 5-7). This phenomenon does not account for the case with a higher throat diameter ratio. This can be due to the high momentum of the flow at throat which pushes the back pressure further downstream and keeps the flow cavitating.

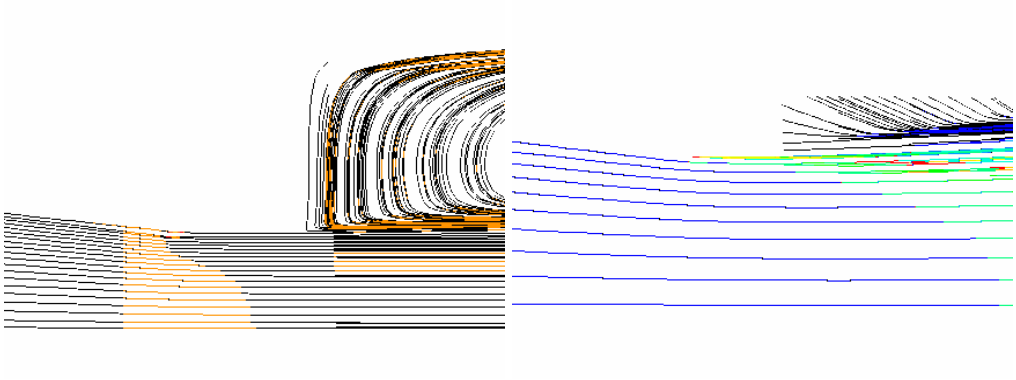

Figure 5-7. Flow Path Lines Colored with Phase Volume Fractions for Case σ_2.

5.1.2.2 Effect of Outlet Angle "Φ_2" on Discharge Coefficient "C_d"

If the flow is cavitating the discharge coefficient is not a function of the outlet angle "Φ_2". In Figure 5-13 & 5-14, it can be seen that for all cases with different throat lengths and different throat diameters if the flow cavitates at the throat, with the increasing exit angle the discharge coefficient is constant. But the exit angle defines if the cavitation exists for high cavitation numbers or not, because the exit angle defines the position of the cavitation bubble for a specific exit pressure. If the outlet angle is not sufficiently small to give space to bubble to hold on a section in the diffuser, the pressure wave at the exit moves back in to the throat of the venturi and stops cavitation. That's why only the venturies with outlet angle less than 15 degrees are cavitated for σ_3 values, which means small differential pressures. Also this angle defines the oscillation frequency of the cavitation bubble but this will be discussed on the following sections.

5.1.2.3 Effect of L_{th}/D_{in} & D_{th}/D_{in} on Discharge Coefficient "C_d"

It is very interesting to see in Figure 5-19 & 5-20, that the ratio of throat length to inlet diameter and the ratio of throat diameter to inlet diameter do not affect the discharge coefficient at all. Just for the case with inlet angle 90 degrees, the effect

of throat diameter ratio is interesting. The difference is also stated in orifice flow equations in the literature. But for lower inlet angles this effect disappears rapidly.

5.1.2.4 Effect of Reynolds Number on Discharge Coefficient "C_d"

It is known that for a cavitating venturi, if the venturi cavitates the discharge coefficient is a fixed value for all inlet pressures for a prescribed geometry. But in Figure 5-25 & 5-26 one can see that for all cases with the increasing Reynolds Number for small inlet angles (Curved and 7 degree) the discharge coefficient is increasing. This effect disappears with the increasing inlet angle. This phenomenon can be caused by the effect of momentum which pushes the vapor part at the throat to the wall of the throat. This will increase the effective core area and as a consequence of this the discharge coefficient increase. Also the Reynolds number has an effect on the unstable oscillating bubble frequency value but this will be discussed further.

5.1.2.5 Effect of Outlet Angle "Φ_2" on oscillation frequency of the cavitation bubble

When a cavitation bubble created at the throat of the venturi it diffuses to the downstream of the venturi and diffusion stops at a specific length. With the increasing cavitation number, the position of the bubble moves to upstream. This position is not always a stable point but oscillates between two arbitrary points on the diffuser of the venturi. These oscillations seen only for the venturies which has outlet angle less than 30 degrees. Over this value the diffuser length is getting smaller and the bubble is not able to stay on a stable position.

The oscillations of the bubble on a venturi can be seen in Figure 5-8. In this figure one period of the fluctuations are plotted. Also the variations on the exit mass flow rate caused by these fluctuations are given in Figure 5-9. Figure 5-10 is rather interesting; it is believed that when the cavitation occurs at the throat of the venturi than the flow is chocked so that the pressure waves at the exit can not be

transmitted to the upstream of the throat section. However, in Figure 5-10 the fluctuations on the inlet mass flow rate can be seen. Although these fluctuations are very small for this venturi, in some cases the magnitude of these fluctuations may rise as 50 % of the inlet mass flow rate. In Figure 5-8 at time 0.140s the core of the flow at the throat exit has the values of 0.85 to 0.9 phase volume fraction. The velocity of sound in such heterogeneous medium at some regions will increased so that at these points the Mach number is not equal to 1 anymore.

In Table B-2, it can be seen that the Strouhal number for a venturi, which has same D_{th}/D_{in} and the L_{th}/D_{in}, is a function of the outlet angle.

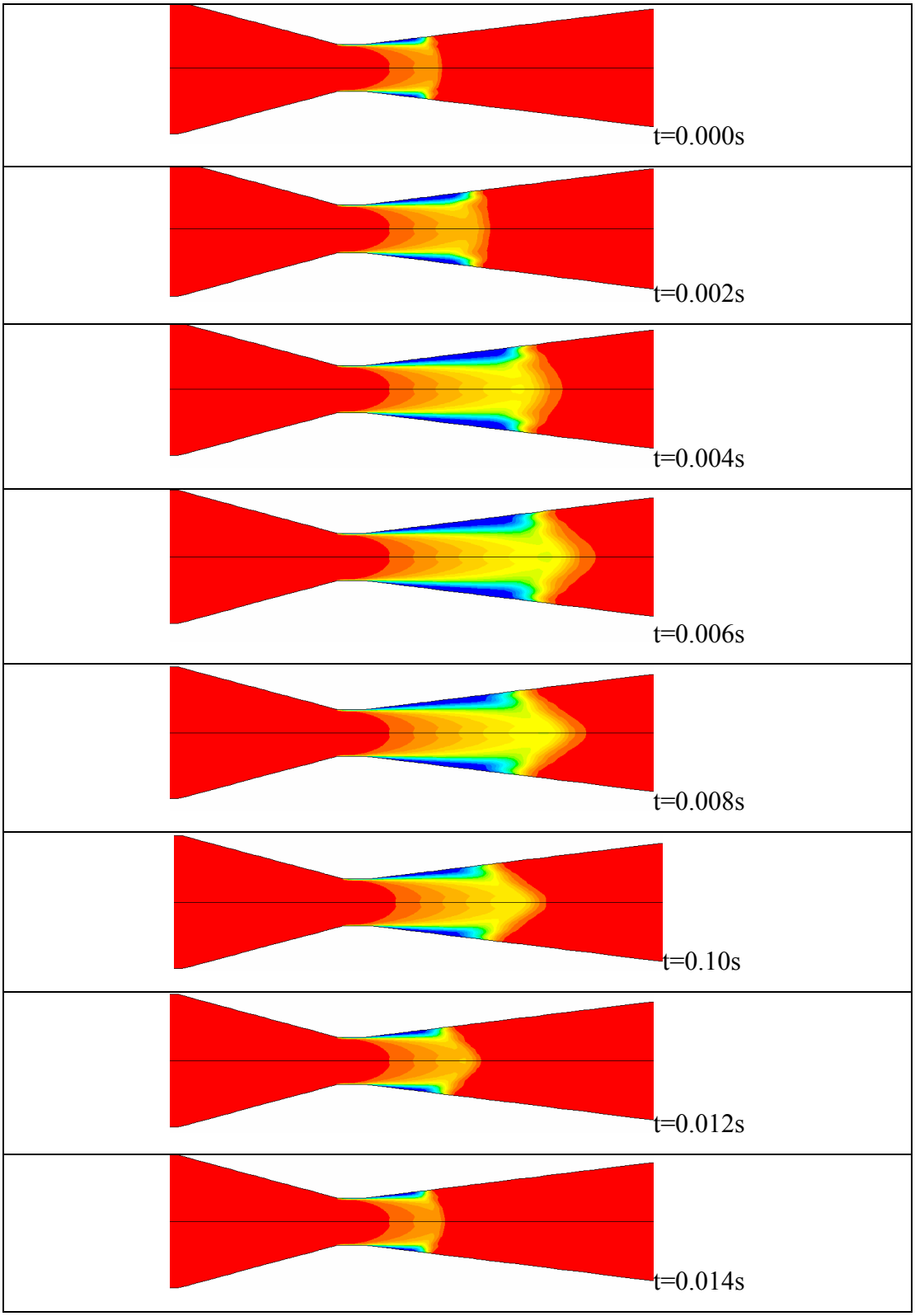

Figure 5-8. Variation of the Volume Fraction of Vapor Phase for Sample Venturi Geometry at σ_2.

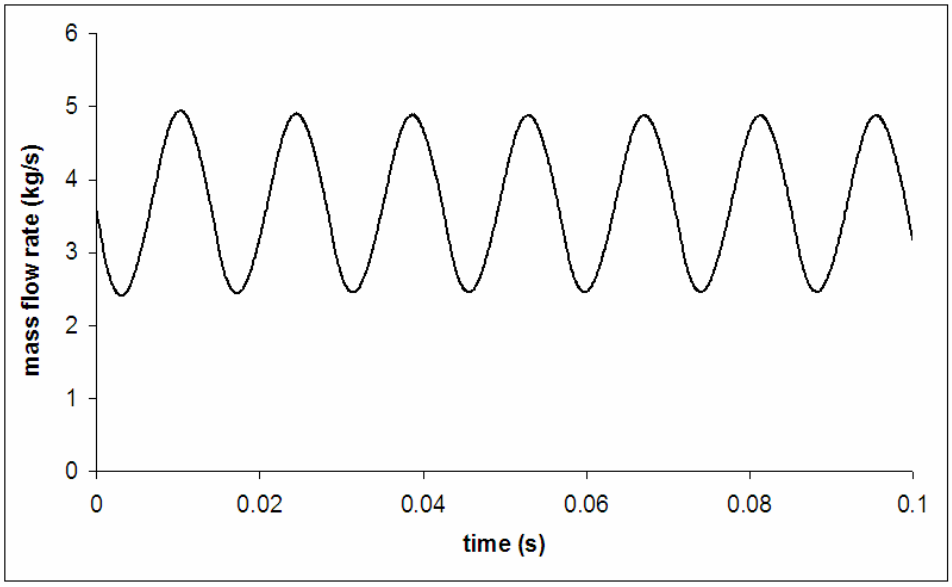

Figure 5-9. Unsteady Oscillation at the Exit Plane of the Venturi.

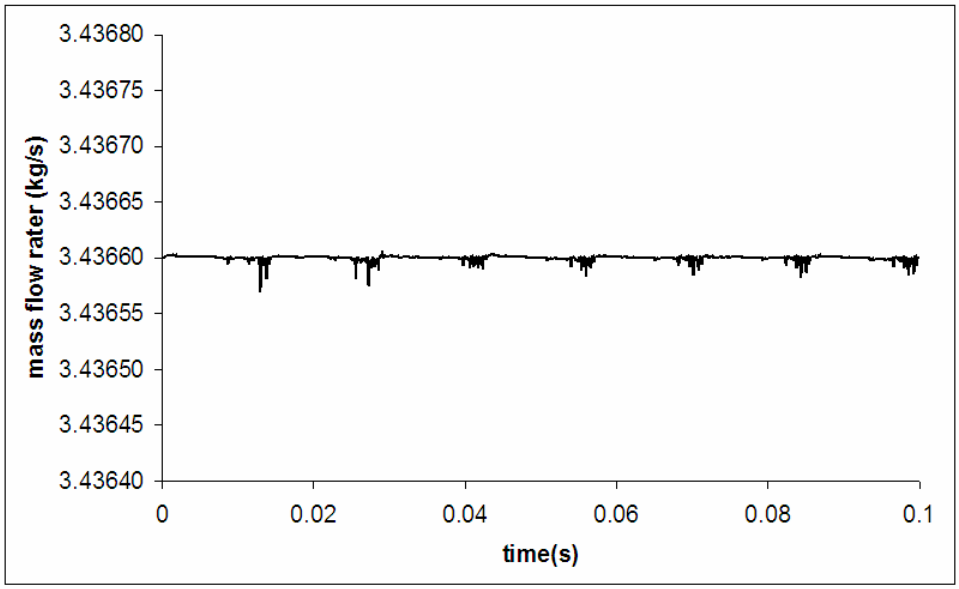

Figure 5-10. The Effect of Oscillating Cavitation Bubble on the Inlet Mass Flow Rate.

5.1.2.6 Effect of D_{th}/D_{in} & L_{th}/D_{in} ratio on oscillation frequency of the cavitation bubble

Although the Reynolds Number and the Cavitation number are similar for venturies, the oscillation behavior can be different. The cases where $D_{th}/D_{in} = 0.714$ the flow do not oscillates for any of the venturies. Which can be a consequence of the effect of different diffuser lengths of the venturies for the same geometric parameters. With the decreasing diffuser length the bubble can not be stay at the diffuser section.

The throat length has a different effect on the oscillation behavior, it does not affect the value of oscillation frequency but it reduces the oscillation magnitude at the inlet section. With the increasing throat length the bubbles which are produced at the throat inlet wall can cover the core of the throat at a smaller distance. This effect increases the volume fraction of vapor phase and reduces the fluctuations at the inlet mass flow.

5.1.2.7 Effect of Reynolds Number on oscillation frequency of the cavitation bubble

For relatively low Reynolds number flows the effect of viscous terms and the Reynolds stress terms become more significant. These terms tends to damp the unsteady oscillation in the cavitation bubble [9]. In table B.2, the Strouhal numbers calculated for several oscillation cases are given. Although the Strouhal number is decreasing the frequency of the oscillations are increasing in the solutions.

5.1.2.8 Summary of 2-D Axisymmetric Solutions

Through the axisymmetric solutions, parameters which thought to be effective on the performance of the cavitating venturi are given in previous sections. These can divided in to two main parts. One is the effects on the discharge coefficient and the

other is effects on the oscillation frequency. From the discussions it can be seen that the discharge coefficient is only a function of inlet angle and Reynolds number. But the effect of Reynolds number is almost negligible. And the exit angle defines the cavitation performance of the venturi and the oscillation frequency of the cavitation bubble. The effect of L_{th}/D_{in} is only seen on the inlet oscillations of the cavitating venturies. A longer throat gives a sufficient length to mixture to be homogenous through the throat of the venturi. But this does not change the frequency of the oscillation at the diffuser part. D_{th}/D_{in} ratio is one of the important parameter like in orifice flow, with the increasing throat diameter; the diffuser length is getting smaller compared to the one which has a smaller throat diameter for the same exit angle. And these effects the oscillation and cavitation behavior of the venturi due to the effect describes in related section in details.

5.1.3 2-D Solutions

During the experiments a 3-D prismatic section of the cavitating venturi is used. Therefore, the effect of this selection has to be investigated before the experiments. Because of time limitations, 2-D solutions are performed instead of 3-D solutions. These 2-D solutions are performed on the test matrix given in Table 5-1, but for a fixed Reynolds number, Re=6E6. The effect of several parameters are investigated such that;

- Effect of inlet angle on Discharge Coefficient
- Effect of outlet angle on Discharge coefficient
- Effect of L_{th}/D_{in} & D_{th}/D_{in} on Discharge Coefficient "C_d"
- Effect of Outlet Angle "Φ_2" on oscillation frequency of the cavitation bubble

, and given in the following sections.

For 2-D solutions the solution matrix given in Table 5-1 and the solutions are performed for Reynolds number equal to 6E5.

5.1.3.1 Effect of Inlet Angle "Φ_1" on Discharge Coefficient "C_d"

The effect of the inlet angle on discharge coefficient is not different from the 2-D - Axisymmetric and 2-D cases accept for the case which have a higher D_{th}/D_{in} diameter value. For the axisymmetric case for these D_{th}/D_{in} ratios and for σ_3 the cavitation occurred for the outlet angle values below 15 degrees. This is because of the difference between the volume expansions of these two cases. For the axisymmetric case the expansion area increases with the square of the radius but for the 2D case area increases just linearly. Also for the exit angles 60 & 90 degrees at σ_2 condition for D_{th}/D_{in}=0.357, the effect of back pressure on cavitation is not seen as in axisymmetric case. This can be a consequence of the volume expansion difference also.

5.1.3.2 Effect of Outlet Angle "Φ_2" on Discharge Coefficient "C_d"

For 2D case the effect of outlet angle "Φ_2" on the discharge coefficient is smaller. The cavitation will continue till the outlet angle increased to 30 degrees at σ_3 for D_{th}/D_{in} = 0.357. But for the case which has a larger throat diameter, small area expansion can not be able to hold the back pressure at the diffuser part. The effect can be seen in Figure 5-12.

5.1.3.3 Effect of L_{th}/D_{in} & D_{th}/D_{in} on Discharge Coefficient "C_d"

The effects are same as in axisymmetric solutions.

5.1.3.4 Effect of Outlet Angle "Φ_2" on oscillation frequency of the cavitation bubble

Two dimensional solutions show quite different oscillation behavior from 2-D axisymmetric case. For all 2-D solutions the oscillation is damped out. This damping may caused by the effect of volume ratio or the definition of the Reynolds number. For both 2-D and 2-D axisymmetric cases the characteristic length is

defined as D_{th} therefore the Reynolds number is same for both cases. But the volume extension at the diffuser part is not same. So this may lead such a different behavior on the oscillation charteristics of 2-D solutions.

5.1.3.5 Summary for 2-D results

In discharge coefficient point of view, 2-D and 2-D axisymmetric results have almost same values for every possible venturi geometry but the oscillation charteristics are very different from each other. This yields to the result that 2-D venturi sections can be used to obtain discharge coefficient but the limiting cavitation value, where the cavitation stops, and oscillation frequencies can not be simulated with 2-D sections.

	L_{th}/D_{in}=0.223	L_{th}/D_{in} =0.446
Φ_2=90	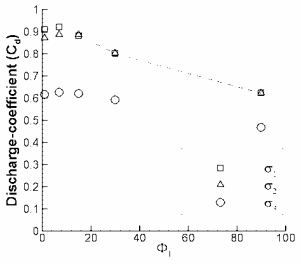	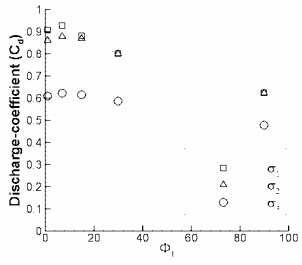
Φ_2=60	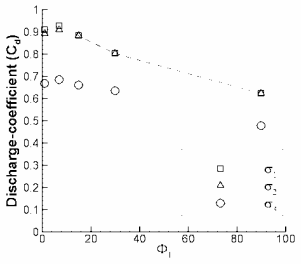	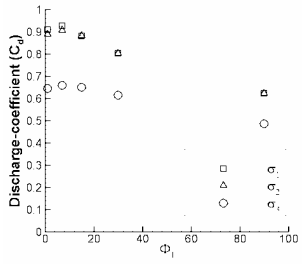
Φ_2=30	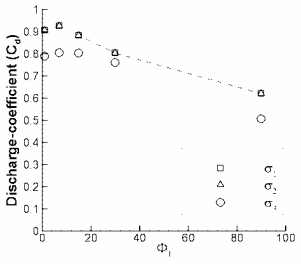	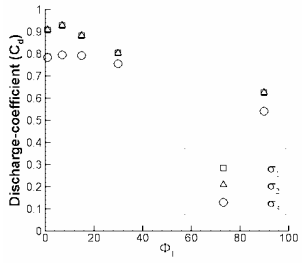
Φ_2=15	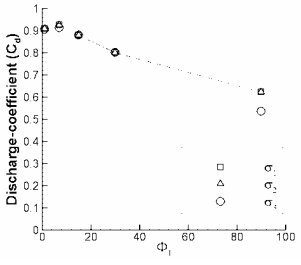	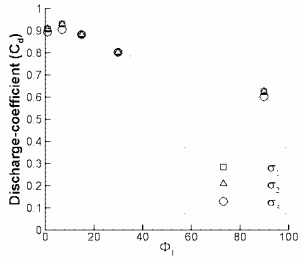
Φ_2=7	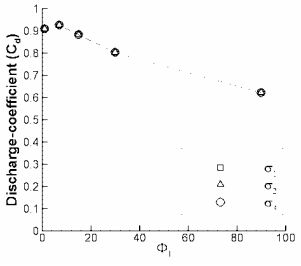	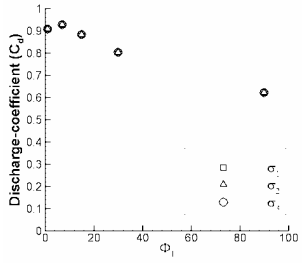

Figure 5-11. Discharge-Coefficient (C_d) vs. Φ_1 for 2D –Axisymmetric Solutions at Re=6E5 for D_{th}/D_{in}=0.357

	L_{th}/D_{in}=0.223	L_{th}/D_{in} =0.446
Φ_2=90	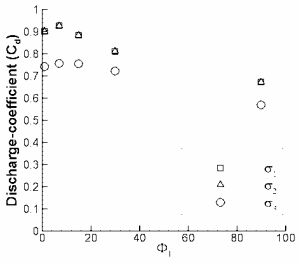	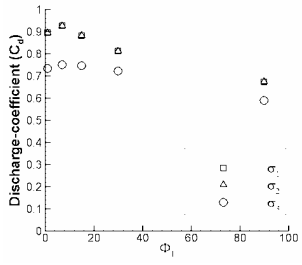
Φ_2=60	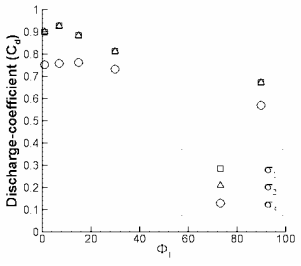	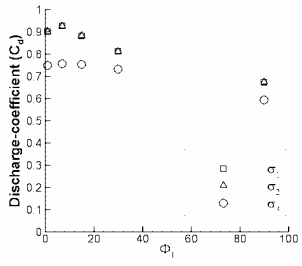
Φ_2=30	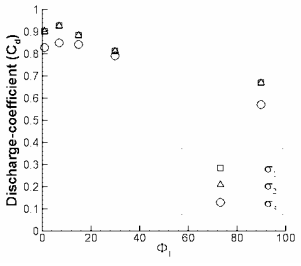	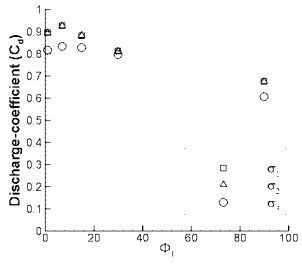
Φ_2=15	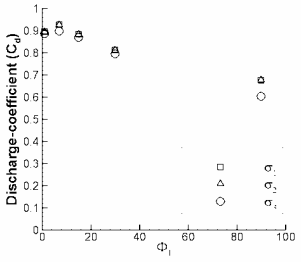	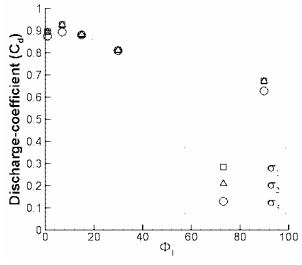
Φ_2=7	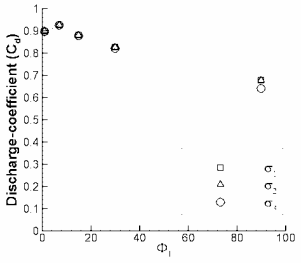	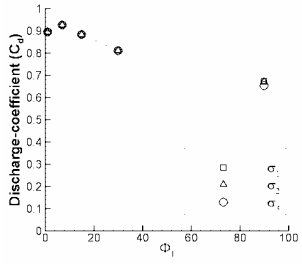

Figure 5-12. Discharge-Coefficient (C_d) vs. Φ_1 for 2D –Axisymmetric Solutions at Re=6E5 for D_{th}/D_{in} =0.714

	L_{th}/D_{in}=0.223	L_{th}/D_{in} =0.446
Φ_1=90	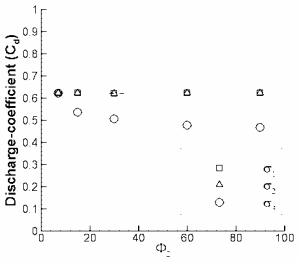	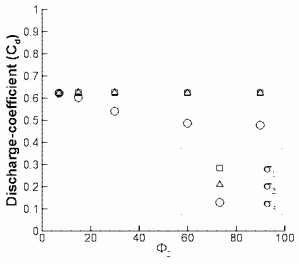
Φ_1=30	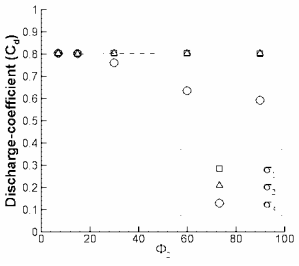	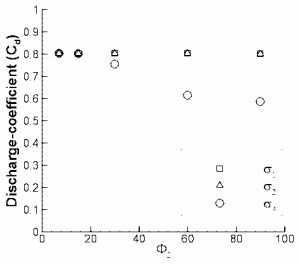
Φ_1=15	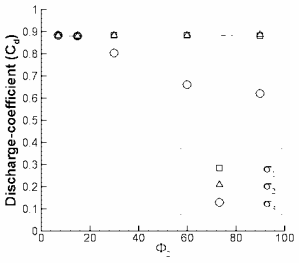	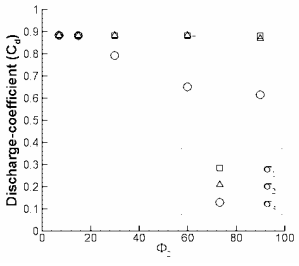
Φ_1=7	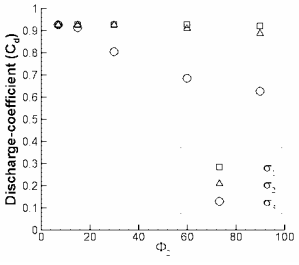	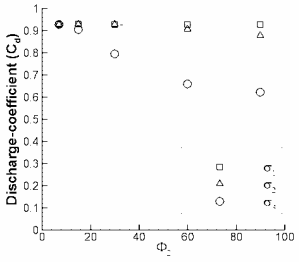
Φ_1=Curved	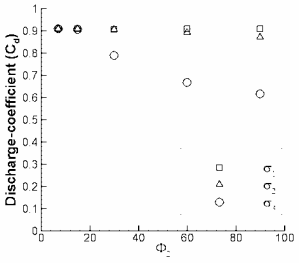	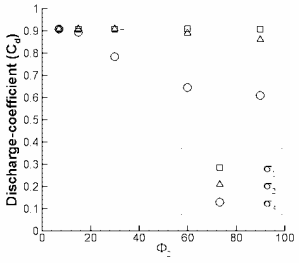

Figure 5-13. Discharge-Coefficient (C_d) vs. Φ_2 for 2D –Axisymmetric Solutions at Re= 6E5 for D_{th}/D_{in}=0.357

	L_{th}/D_{in}=0.223	L_{th}/D_{in} =0.446
Φ_1=90	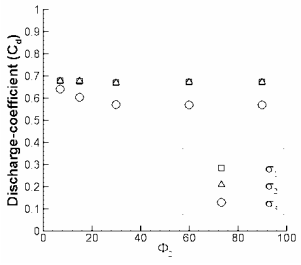	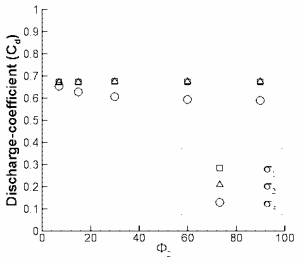
Φ_1=30	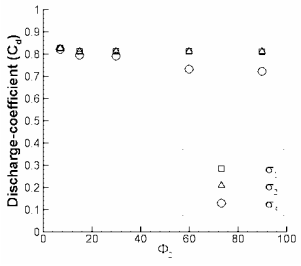	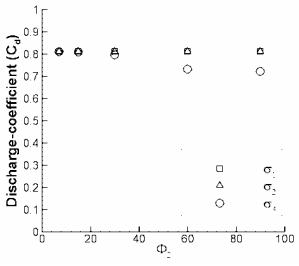
Φ_1=15	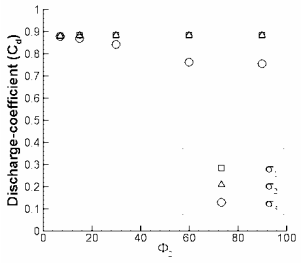	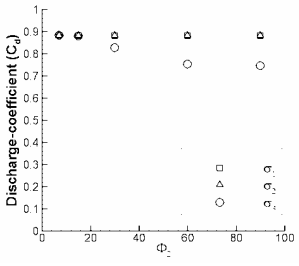
Φ_1=7	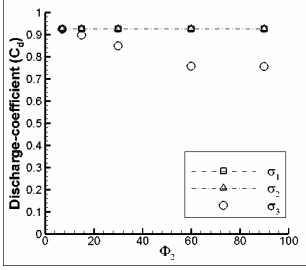	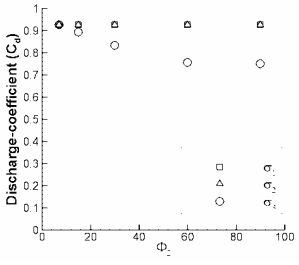
Φ_1=Curved	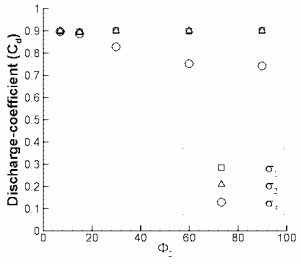	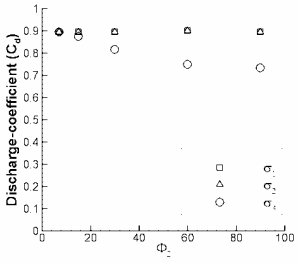

Figure 5-14. Discharge-Coefficient (C_d) vs. Φ_2 for 2D –Axisymmetric Solutions at Re= 6E5 for D_{th}/D_{in}=0.714

	L_{th}/D_{in}=0.223	L_{th}/D_{in} =0.446
Φ_2=90	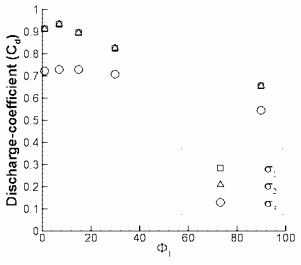	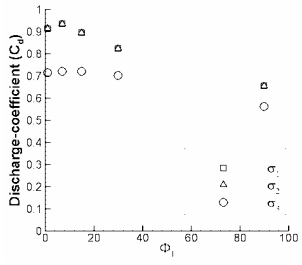
Φ_2=60	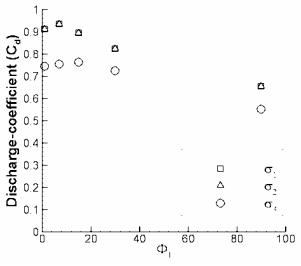	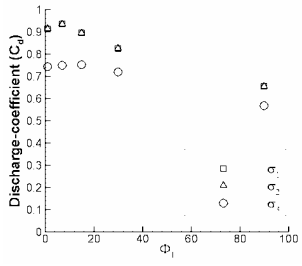
Φ_2=30	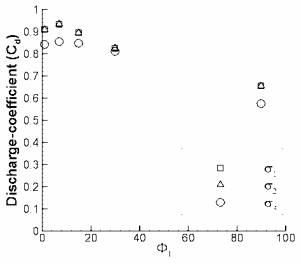	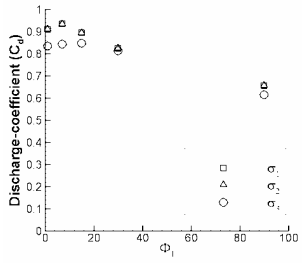
Φ_2=15	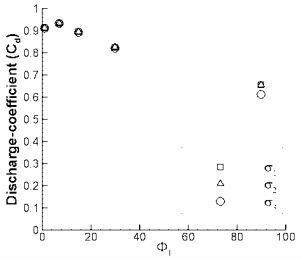	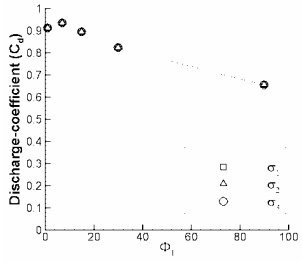
Φ_2=7	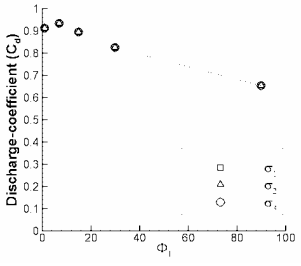	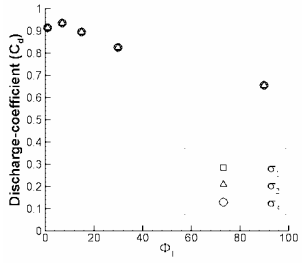

Figure 5-15. Discharge-Coefficient (C_d) vs. Φ_1 for 2D Solutions at Re=6E5 for D_{th}/D_{in}=0.357

	L_{th}/D_{in}=0.223	L_{th}/D_{in} =0.446
Φ_2=90	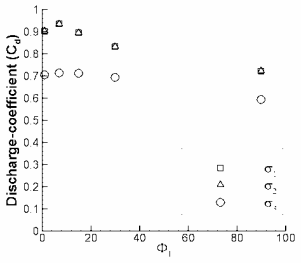	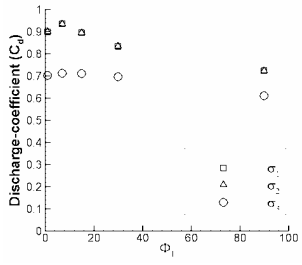
Φ_2=60	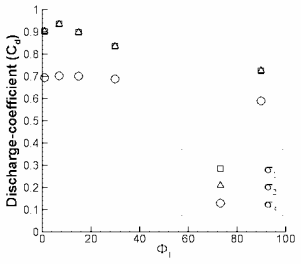	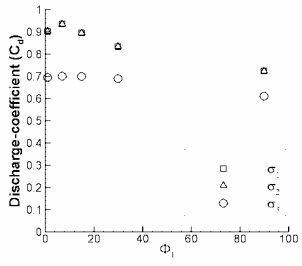
Φ_2=30	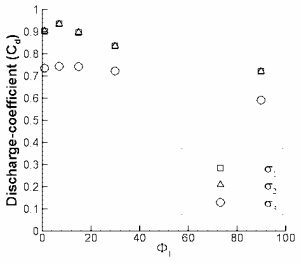	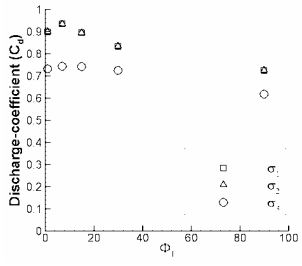
Φ_2=15	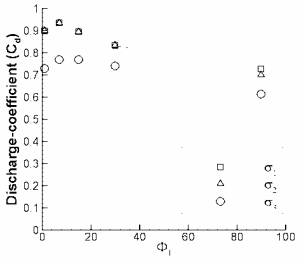	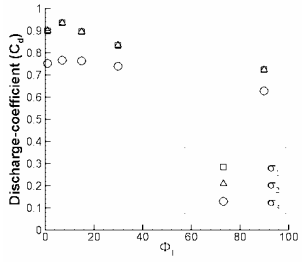
Φ_2=7	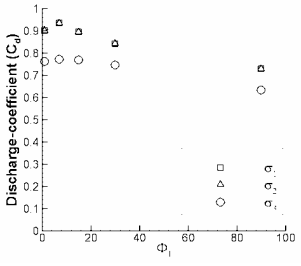	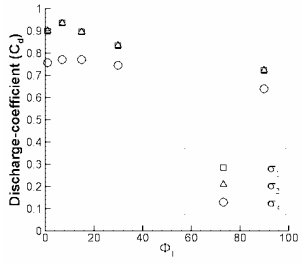

Figure 5-16. Discharge-Coefficient (C_d) vs. Φ_1 for 2D Solutions at Re=6E5 for D_{th}/D_{in}=0.714

	L_{th}/D_{in}=0.223	L_{th}/D_{in} =0.446
Φ_1=90	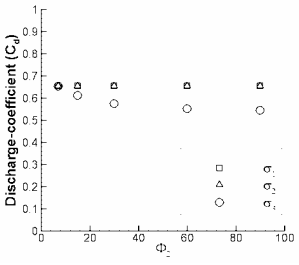	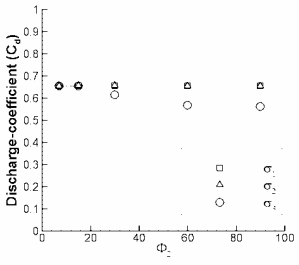
Φ_1=30	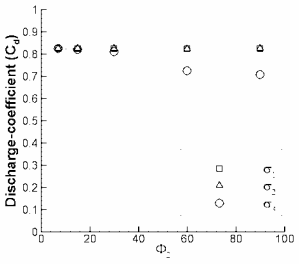	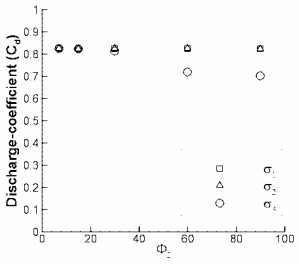
Φ_1=15	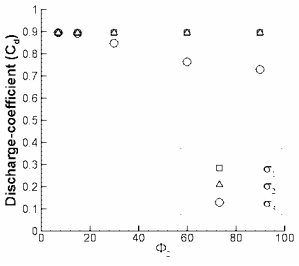	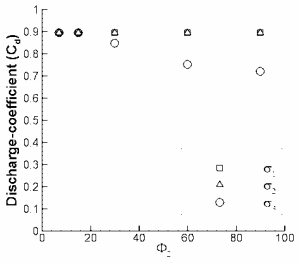
Φ_1=7	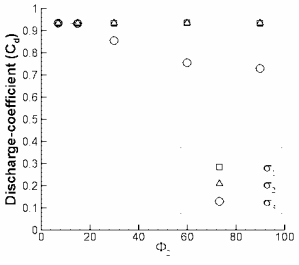	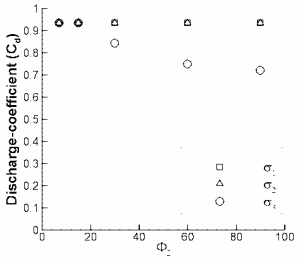
Φ_1=Curved	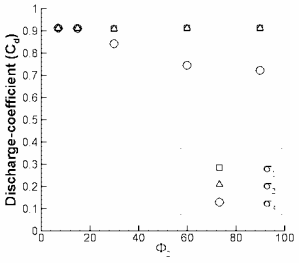	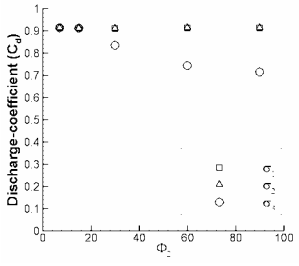

Figure 5-17. Discharge-Coefficient (C_d) vs. Φ_2 for 2D Solutions at Re=6E5 for D_{th}/D_{in}=0.357

	L_{th}/D_{in}=0.223	L_{th}/D_{in} =0.446
Φ_1=90	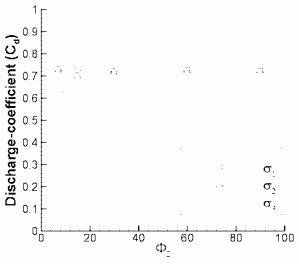	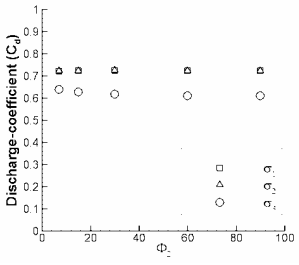
Φ_1=30	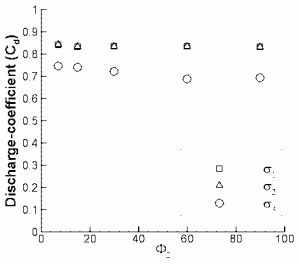	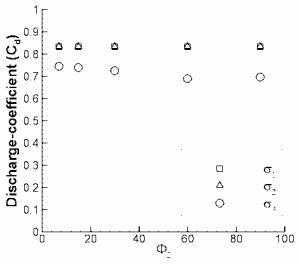
Φ_1=15	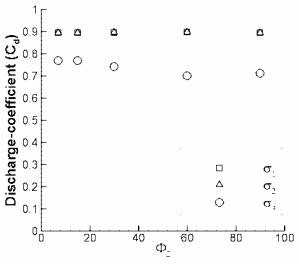	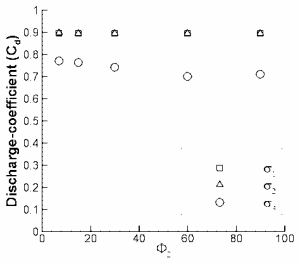
Φ_1=7	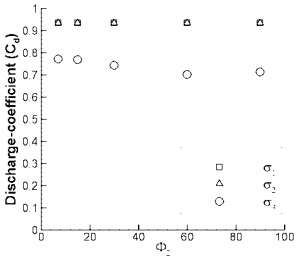	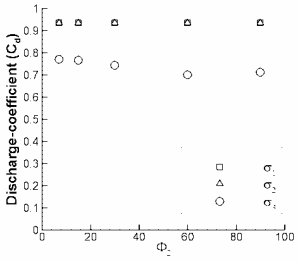
Φ_1=Curved	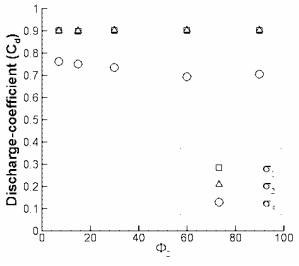	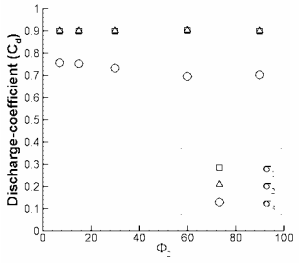

Figure 5-18. Discharge-Coefficient (C_d) vs. Φ_2 for 2D Solutions at Re=6E5 for D_{th}/D_{in}=0.714

	D_{th}/D_{in}=0.357	D_{th}/D_{in} =0.714
Φ_1=90	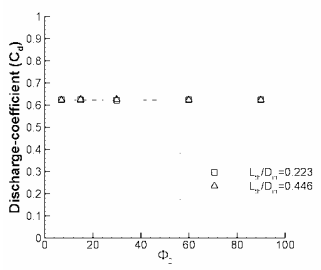	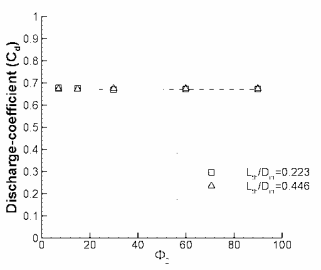
Φ_1=30	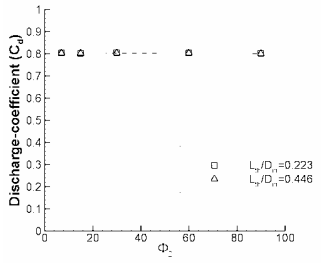	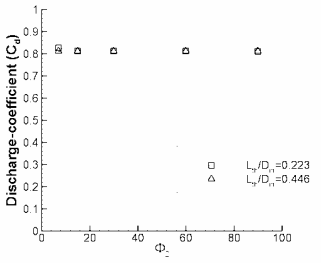
Φ_1=15	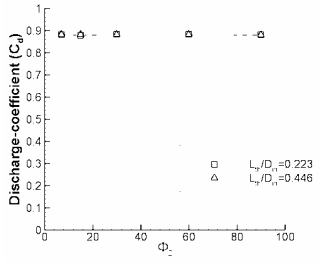	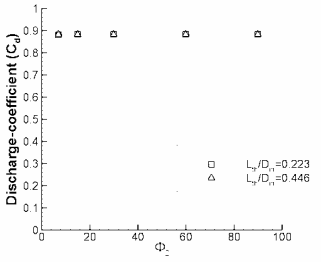
Φ_1=7	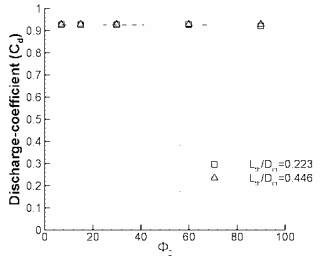	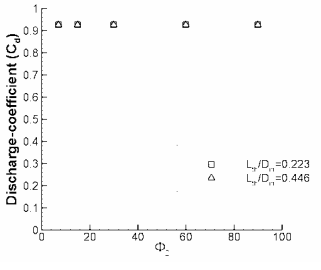
Φ_1=Curved	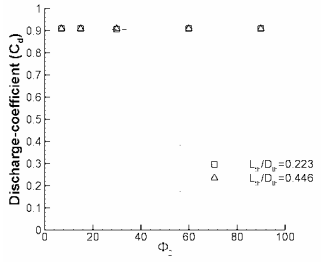	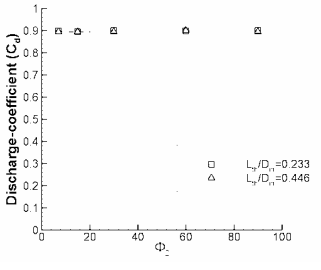

Figure 5-19. Effect L_{th}/D_{in} on Discharge-Coefficient (C_d) vs. Φ_2 for 2D-Axisymmetric Solutions at σ_1

	L_{th}/D_{in}=0.223	L_{th}/D_{in} =0.446
Φ_1=90	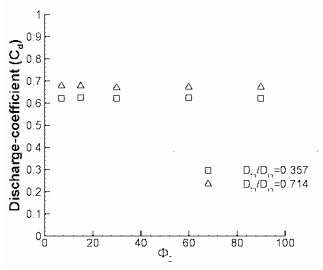	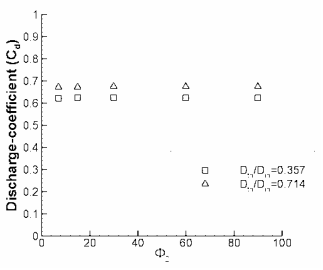
Φ_1=30	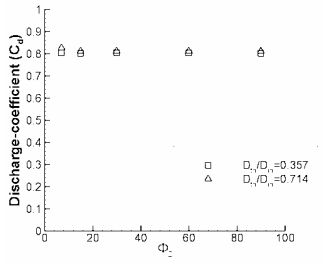	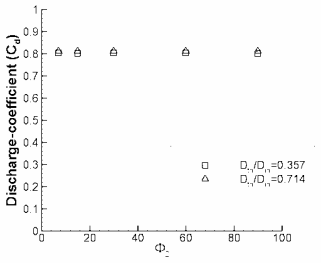
Φ_1=15	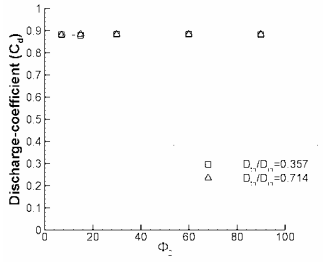	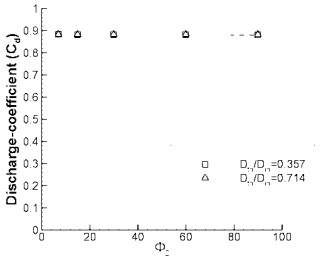
Φ_1=7	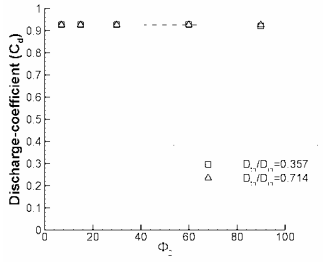	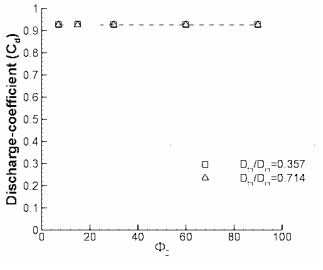
Φ_1=Curved	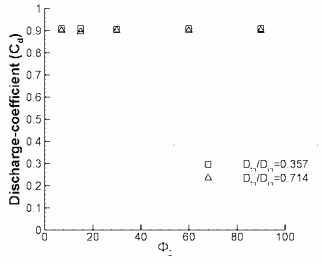	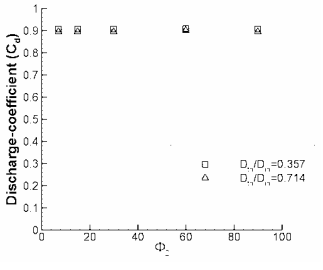

Figure 5-20. Effect D_{th}/D_{in} on Discharge-Coefficient (C_d) vs. Φ_2 for 2D-Axisymmetric Solutions at σ_1

	D_{th}/D_{in}=0.357	D_{th}/D_{in} =0.714
Φ_1=90	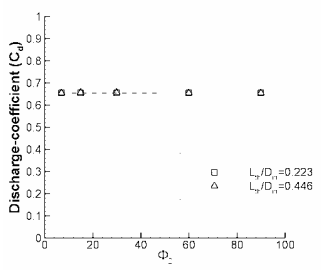	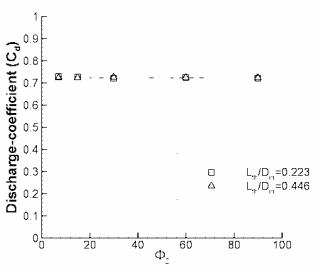
Φ_1=30	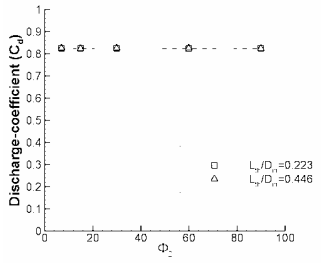	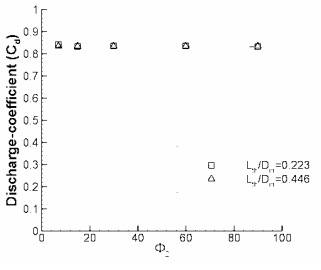
Φ_1=15	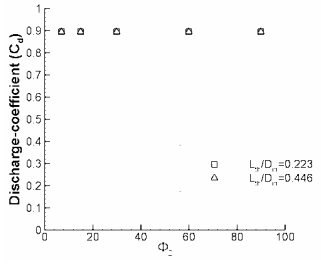	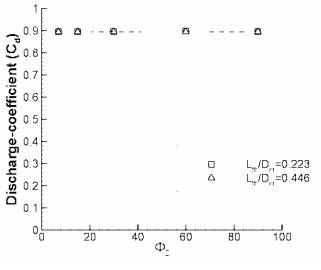
Φ_1=7	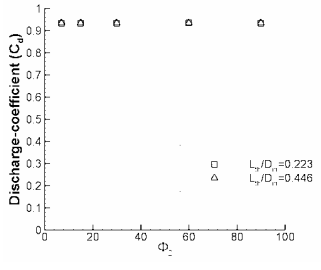	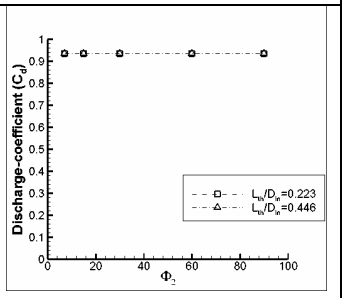
Φ_1=Curved	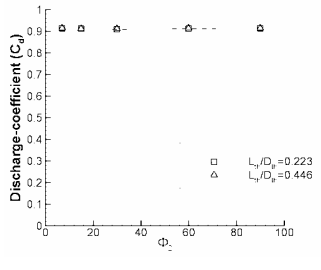	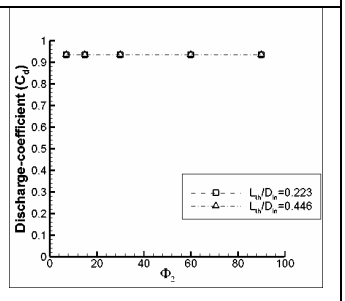

Figure 5-21. Effect L_{th}/D_{in} on Discharge-Coefficient (C_d) vs. Φ_2 for 2D Solutions at σ_1

	L_{th}/D_{in}=0.223	L_{th}/D_{in} =0.446
Φ_1=90	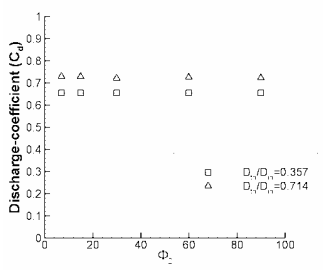	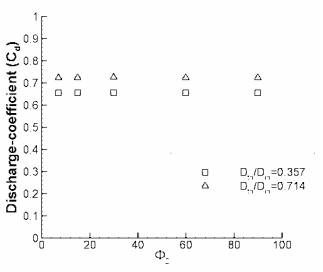
Φ_1=30	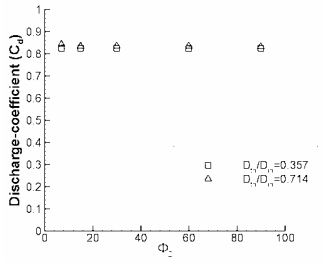	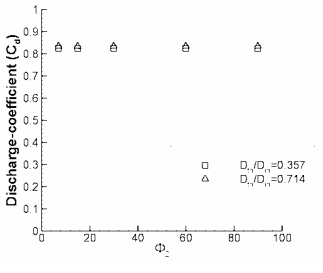
Φ_1=15	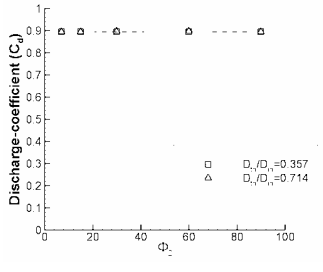	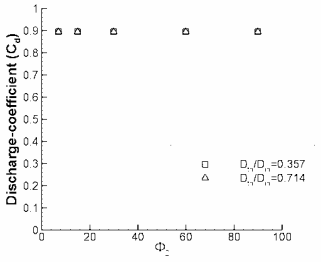
Φ_1=7	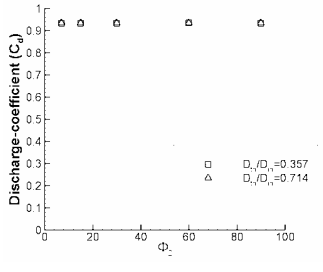	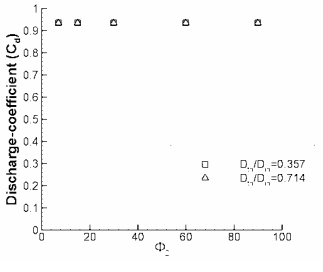
Φ_1=Curved	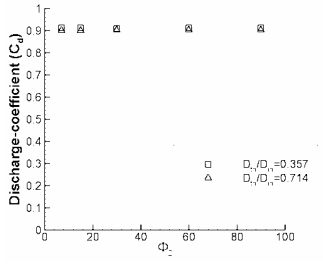	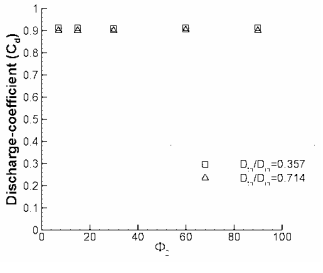

Figure 5-22. Effect D_{th}/D_{in} on Discharge-Coefficient (C_d) vs. Φ_2 for 2D Solutions at σ_1

	L_{th}/D_{in}=0.223	L_{th}/D_{in} =0.446
Φ_2=90	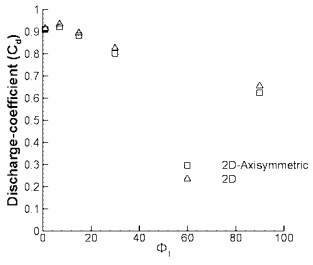	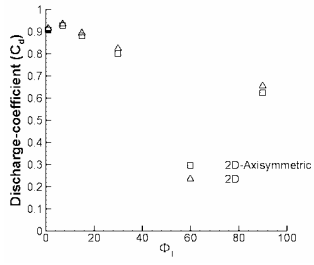
Φ_2=60	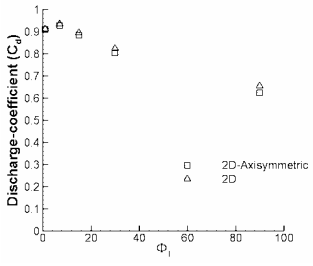	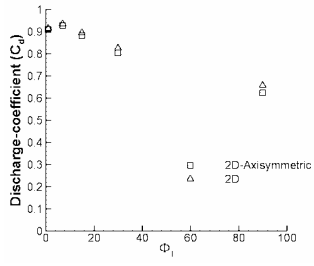
Φ_2=30	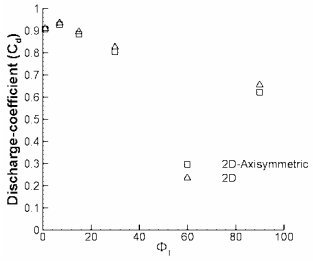	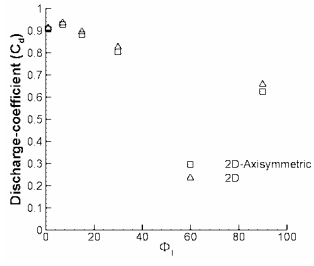
Φ_2=15	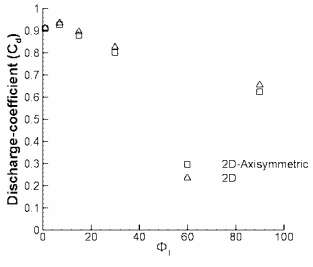	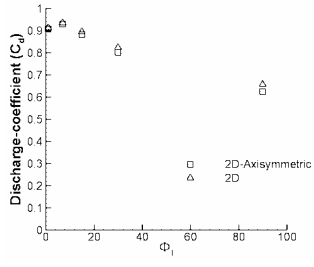
Φ_2=7	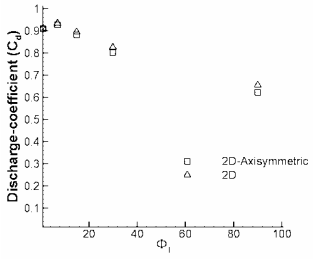	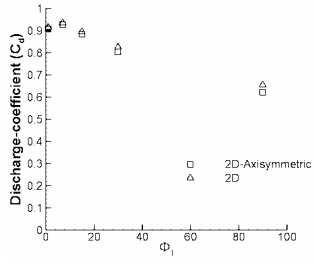

Figure 5-23. 2D- Axisymmetric Solutions vs. 2D Solutions for D_{th}/D_{in}=0.357 at σ_1

	L_{th}/D_{in}=0.223	L_{th}/D_{in} =0.446
Φ_2=90	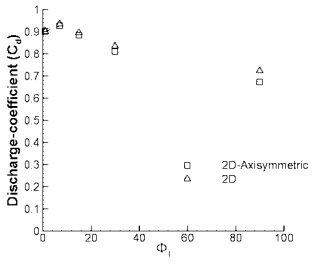	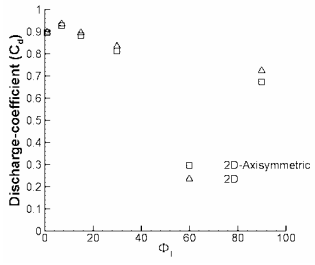
Φ_2=60	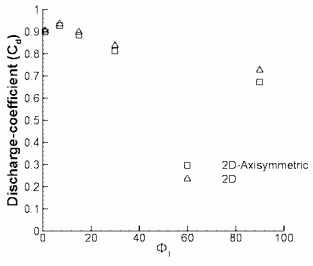	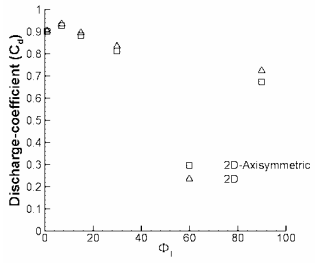
Φ_2=30	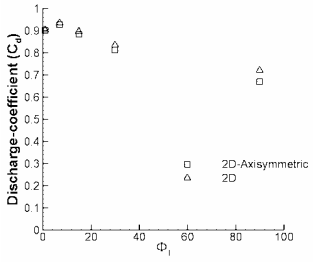	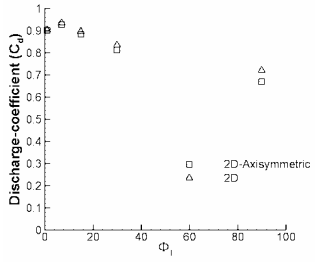
Φ_2=15	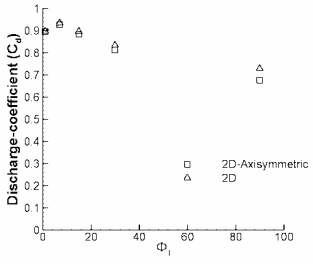	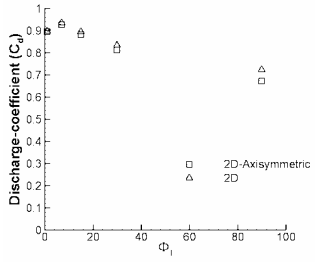
Φ_2=7	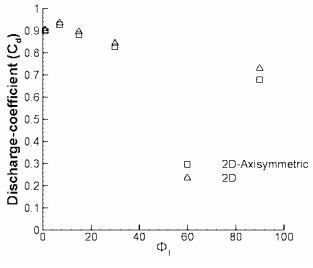	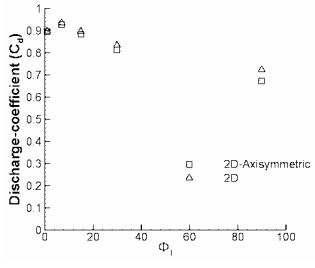

Figure 5-24. 2D- Axisymmetric Solutions vs. 2D Solutions for D_{th}/D_{in}=0. 0.714 at σ_1

	L_{th}/D_{in}=0.223	L_{th}/D_{in} =0.446
Φ_2=90	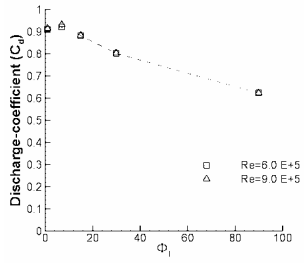	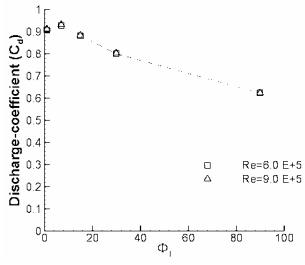
Φ_2=60	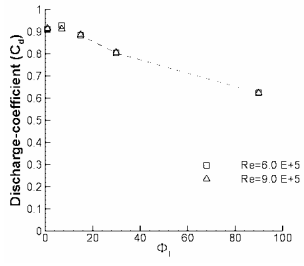	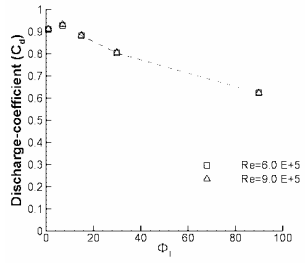
Φ_2=30	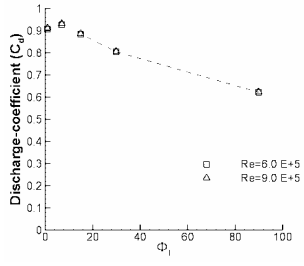	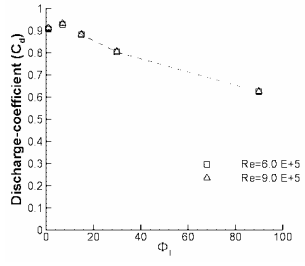
Φ_2=15	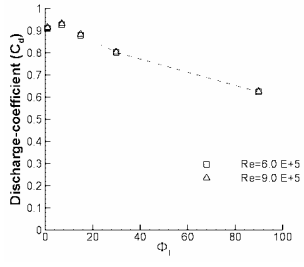	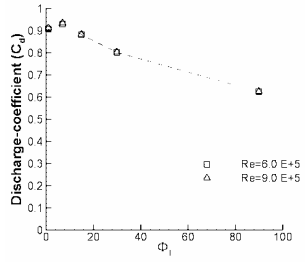
Φ_2=7	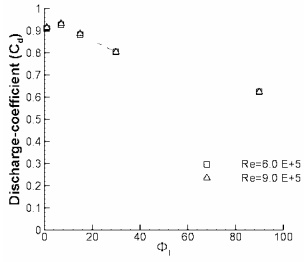	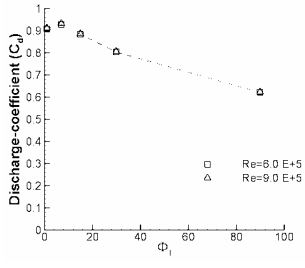

Figure 5-25. Reynolds Number Effect on Discharge Coefficient on Axisymmetric Venturi Flows for D_{th}/D_{in}=0.357 at σ_1

	L_{th}/D_{in}=0.223	L_{th}/D_{in} =0.446
Φ_2=90	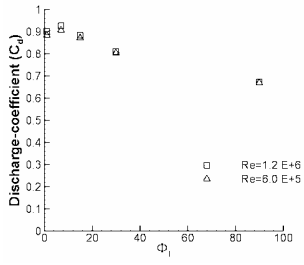	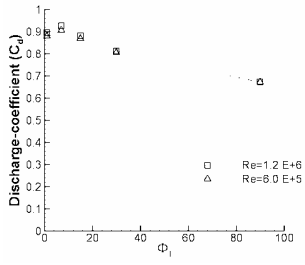
Φ_2=60	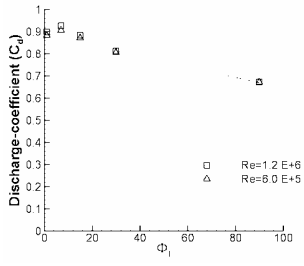	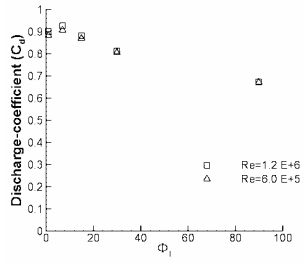
Φ_2=30	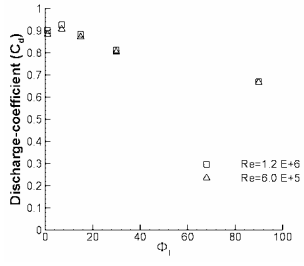	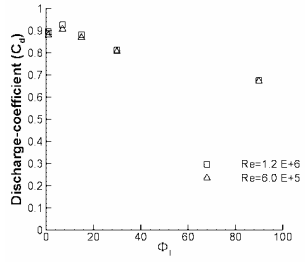
Φ_2=15	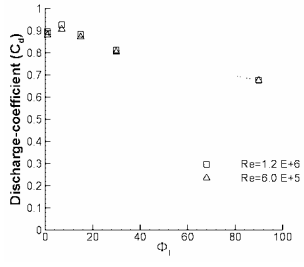	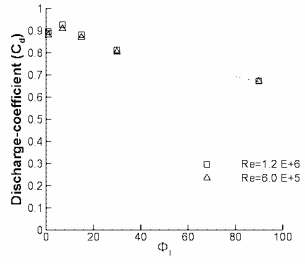
Φ_2=7	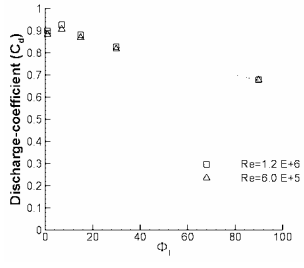	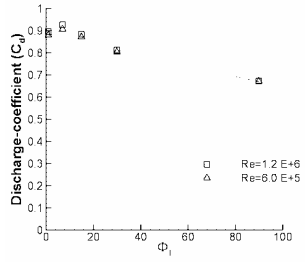

Figure 5-26. Reynolds Number Effect on Discharge Coefficient on Axisymmetric Venturi Flows for D_{th}/D_{in}=0. 0.714 at σ_1

5.1.4 Effect of the Wall Depth

Because the 3-D prismatic test section is used in the experiments, the wall has a certain effect on the flow and bubble dynamics because of the boundary layer formation on the walls. This effect is investigated with FLUENT in order to see the effect on the discharge coefficient and oscillation behavior. To reduce the effect, it is better to use a very deep test section but due to limitation on the pipe size and the difficulty of changing the pipe circular section to rectangular section the depth have to be optimized. Also the high pressure tank which is used in the experiments has a limited volume and with the increasing depth, the flow rate can be much higher than expected and this will reduce the experiment time.

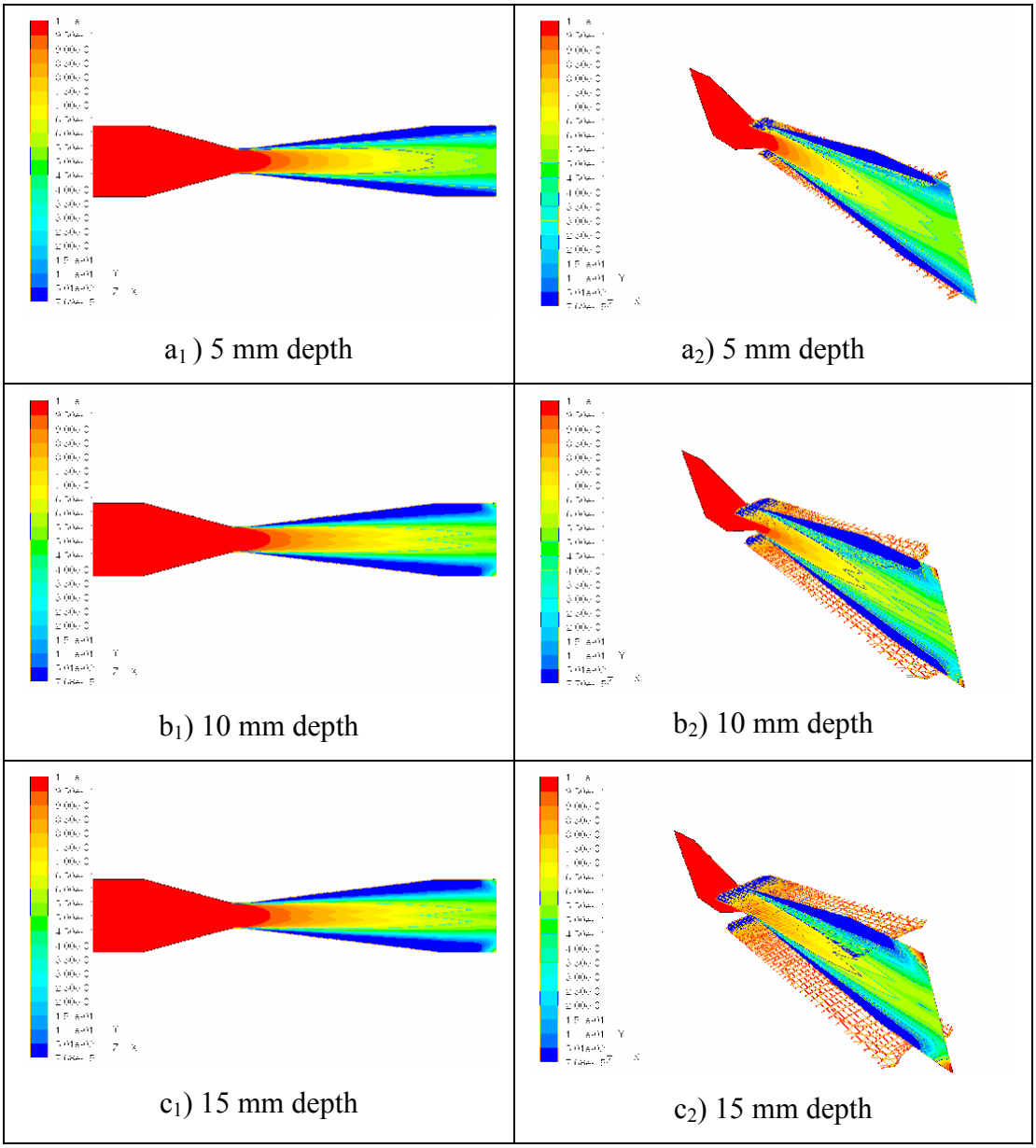

Figure 5-27. Effect of Wall for 3-D Prismatic Solutions at σ_1.

In Figure 5-27, the 3-D Prismatic solution obtained for three different depth values is plotted. And in Figure 5-28 the discharge coefficient obtained from 2-D, 2-D axisymmetric and 3-D prismatic solutions plotted for three different cavitation number. And it can be seen that the discharge coefficient does not affected too much from the walls and the difference does not exceeds 1 - 2 % from each other.

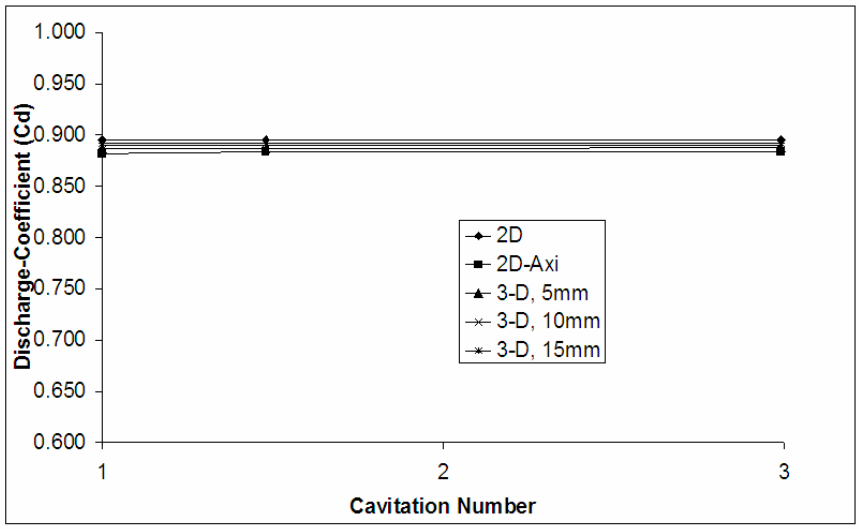

Figure 5-28, Discharge Coefficient vs. 2-D, 2-D Axisymmetric and 3-D Prismatic Solutions.

Table 5-2. Oscillation Frequency for 2-D, 2-D Axisymmetric and 3-D Prismatic Solutions

	f (Hz) σ_1	f (Hz) σ_2	f (Hz) σ_3
2-D	-	-	-
2-D Axisymmetric	-	80	92
3-D Prismatic(5 mm)	-	-	61.7
3-D Prismatic(10 mm)	-	-	62.1
3-D Prismatic(15 mm)	-	-	62.8

Also the oscillation charcteristics are compared. In Table 5-2 the oscillation frequencies are given for the same venturi geometry for three different cavitation numbers. And it is very interesting to see that the oscillation occurs at 3-D prizmatic and 2-D axisymmetric case but not in 2-D solutions. Also the oscillation frequency of 3-D and 2-D axisymmetric solution is different but this frequency value is consistent with in 3-D prismatic solutions.

5.1.5 Summary for Numerical Simulations

Through out the numerical simulations 100 different venturi geometries solved for three cavitation number values at two different Reynolds number for both 2-D axisymmetric and 2-D cases. Test number reduction techniques could not be applied to the numerical simulation due to the lack of empirical equations which correlates the geometric features of the venturi with the flow variables. The output of the simulations is the discharge coefficient "C_d", which defines the efficiency, and the oscillation frequency of the exit mass flow rate.

From the simulations it can be seen that exit angle "Φ_2", L_{th}/D_{in} ratio and Cavitation number "σ" do not have any effect on the discharge coefficient "C_d". Although D_{th}/D_{in} value affects the discharge coefficient for high inlet angles the sole effect is due to the inlet angle value, which is correlated as in equation (5-2).

$$C_d = 0.00003\Phi_1^2 + \left[0.0006\left(\frac{D_{th}}{D_{in}}\right) - 0.0066 \right]\Phi_1 - 0.0064\left(\frac{D_{th}}{D_{in}}\right) + 0.9726 \qquad (5\text{-}2)$$

In case of oscillations at the exit mass flow rate and the critical cavitation number, the exit angle "Φ_2" and the D_{th}/D_{in} ratio are the main parameters because of the fact that they are directly define the diffuser length of the venturi.

In the plots of several venturi simulations an arc is present in the phase volume fraction contours on the axis of the venturi. (Figure 5-5 & Figure 5-26). This may caused by a numerical error while defining the axis boundary condition at the axis of venturi.

5.2 Experimental Results

5.2.1 Experiment Matrix

For the experiments four different axisymmetric venturi geometries and a 3-D prismatic venturi test section is designed and manufactured. Through the axisymmetic venturi tests the objective is to see the effect of outlet angle on the critical cavitation number and on the frequency of the fluctuations at the exit pressure. Therefore several experiments are performed for different cavitation numbers.

5.2.2 Experiments with Axisymmetric Venturi Flows

In the experiments, a total of 8 flow cases with 3 different venturies were studied. In the first 3 cases, the inlet and exit angles are set at Φ_1 = 30deg, Φ_2 = 7deg, respectively, and the back pressure was varied for cavitation numbers in the range of 1-4. Similarly in Cases 4 and 5, where Φ_1 = 15deg, Φ_2 = 15 deg, and in Cases 6-8, where Φ_1 = 15 deg, Φ_2 = 60 deg, the backpressure was varied to assess the cavitating flows. The flow features through the venture was captured by a high-speed camera at 500 frames per second, and the pressure variations at the inlet and exit sections were measured using pressure transducers at a sampling rate of 5000Hz. The flow rate in the experiments could not be measured due the low response time of the flow meter used in the setup.

5.2.2.1 Case 1: Φ_1 = 30 deg, Φ2 = 7 deg, σ=1

In this case the inlet pressure is set to P_{in}=22bars (gage) and the exit pressure is set to P_{out}=0bars. As seen in Figure 5-30(a), as soon as the valve is opened, the exit pressure drops to -1 bar and remains constant. At t=2500 ms, the valve is closed, and the exit pressure recovers the inlet pressure. The fluctuations observed after the valve is closed are attributed to the water hammer effect produced as a result of rapid closing of the valve. The drop in the inlet pressure, which is about 10 bars, is due to the poor regulation of the gas pressure in the water tank. The variation of the cavitation number during the experiment is given in Figure 5-30(b). Since the exit pressure is 0 bars, the cavitation number remains constant.

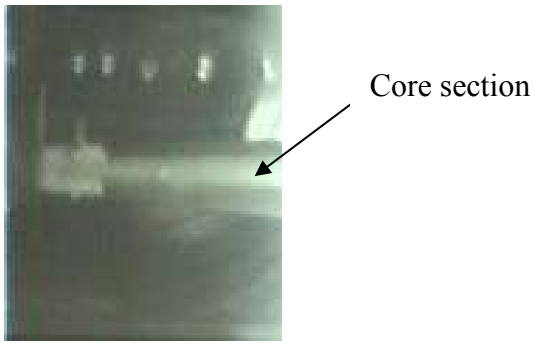

Figure 5-29. High Speed Camera Plot

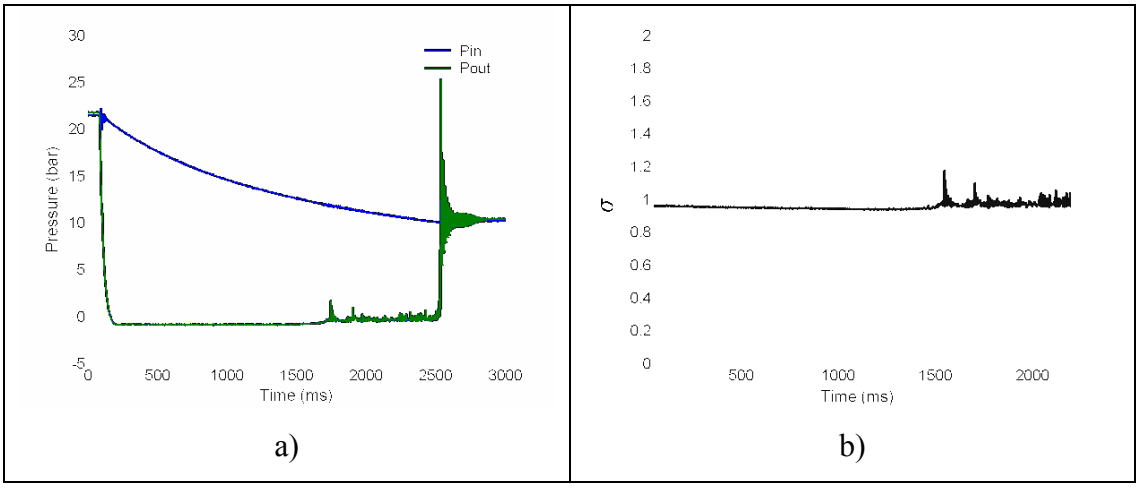

Figure 5-30. a) Pressure vs. Time b) Cavitation Number vs. Time

5.2.2.2 Case 2: $\Phi_1 = 30$ deg, $\Phi_2 = 7$ deg, $\sigma=2$

In case 2, it is observed in high speed camera pictures (Figure 5-31) that the cavitation in the venturi disappears at about t = 1200 ms, which is attributed to the increase in the cavitation number (Figure 5-32(b)). After the cavitation number reaches a value of about 4, the cavitation stops.

The presence of the pressure fluctuations shown in Figure 5-32(a) also indicates the cavitation. The high frequency movement of the bubble in the diffuser part causes the pressure fluctuation at the exit region. It is apparent that the sole source of the pressure fluctuations is the cavitating flow though venturi.

The frequency analysis of the exit pressure variation indicates the significant modes, one is about 400-450 Hz and the other is about150-250 Hz (Figure 5-32(c)).

 t= 215 ms	 t= 1039 ms
 t= 319 ms	 t= 1453 ms
 t= 333 ms	 t=1601 ms

Figure 5-31. High Speed Camera Plots

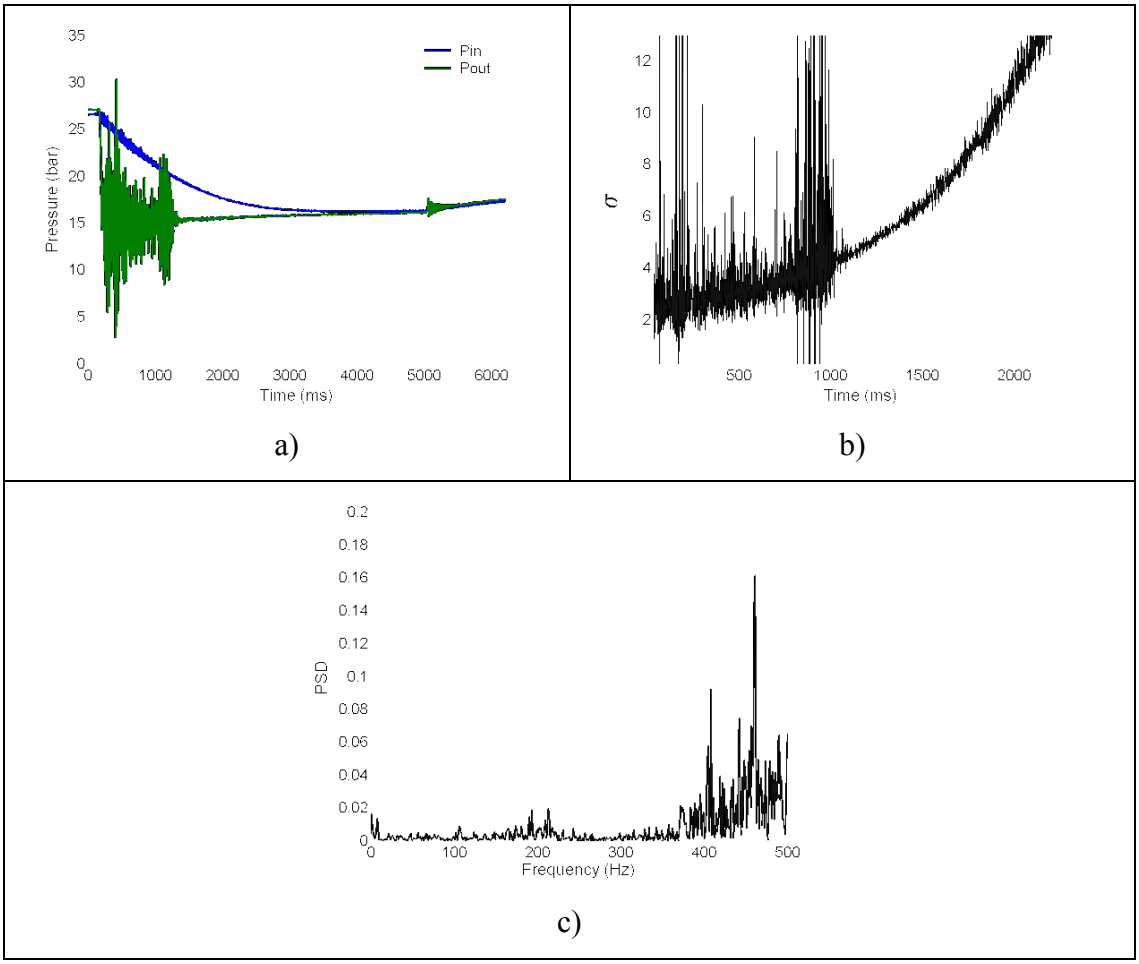

Figure 5-32.a) Pressure vs. Time b) Cavitation Number vs. Time
c) PSD vs. Frequency (Hz)

5.2.2.3 Case 3: Φ_1 = 30 deg, Φ2 = 7 deg, σ=1.2-1.8

In this case the exit pressure is set to P_{out}=12bars and initial inlet pressure is set to P_{in}=34bars. The frequency content of the exit pressure fluctuations changes through the experiment due to the change in the cavitation number (Figure 5-33 (b) & (d)). With the increasing cavitation number, the back pressure pushes the cavitation bubble upward direction through the diffuser and this upstream motion gives less space to the bubble to collapse. Therefore the frequency of the fluctuations increases with the increasing cavitation number. But the amplitude of the fluctuations decreases. In Figure 5-33 (c) the range of fluctuation in the exit pressure are about 100-150 Hz and 400-450 Hz at the beginning of the experiment. Through the experiment with the increasing cavitation number the lower frequency fluctuations tend to be disappearing. Also these low frequency oscillations can be calculated from the high speed camera plots which are given in Figure 5-34. From this figure if the one period of the fluctuations is assumed to be between t=710 to 718 and t=720 to 730 the frequency of this fluctuations can calculated as between 100-125, which can be seen on the waterfall diagram given in Figure 5-33(d).

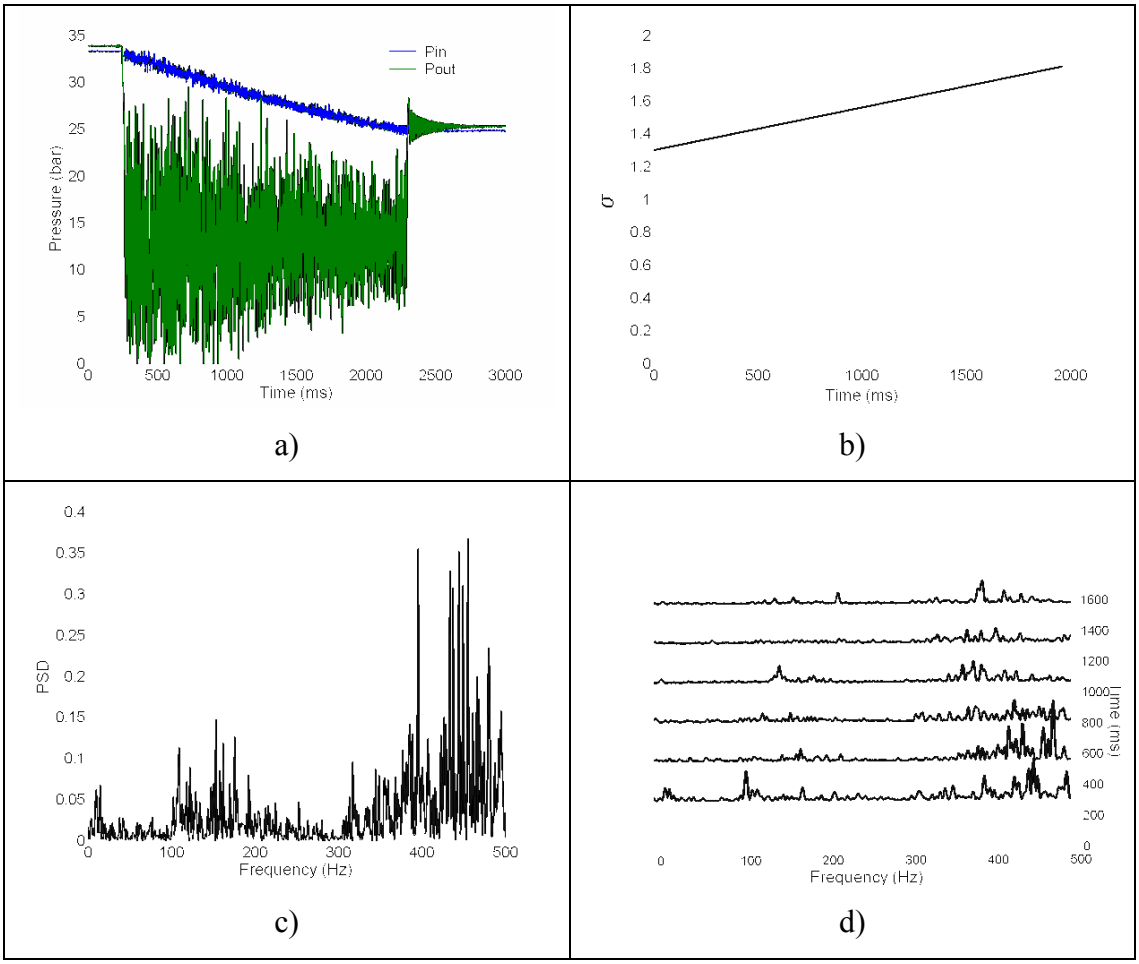

Figure 5-33. a) Pressure vs. Time b) Cavitation Number vs. Time c) PSD vs. Frequency (Hz) d) Waterfall Diagram of Exit Pressure

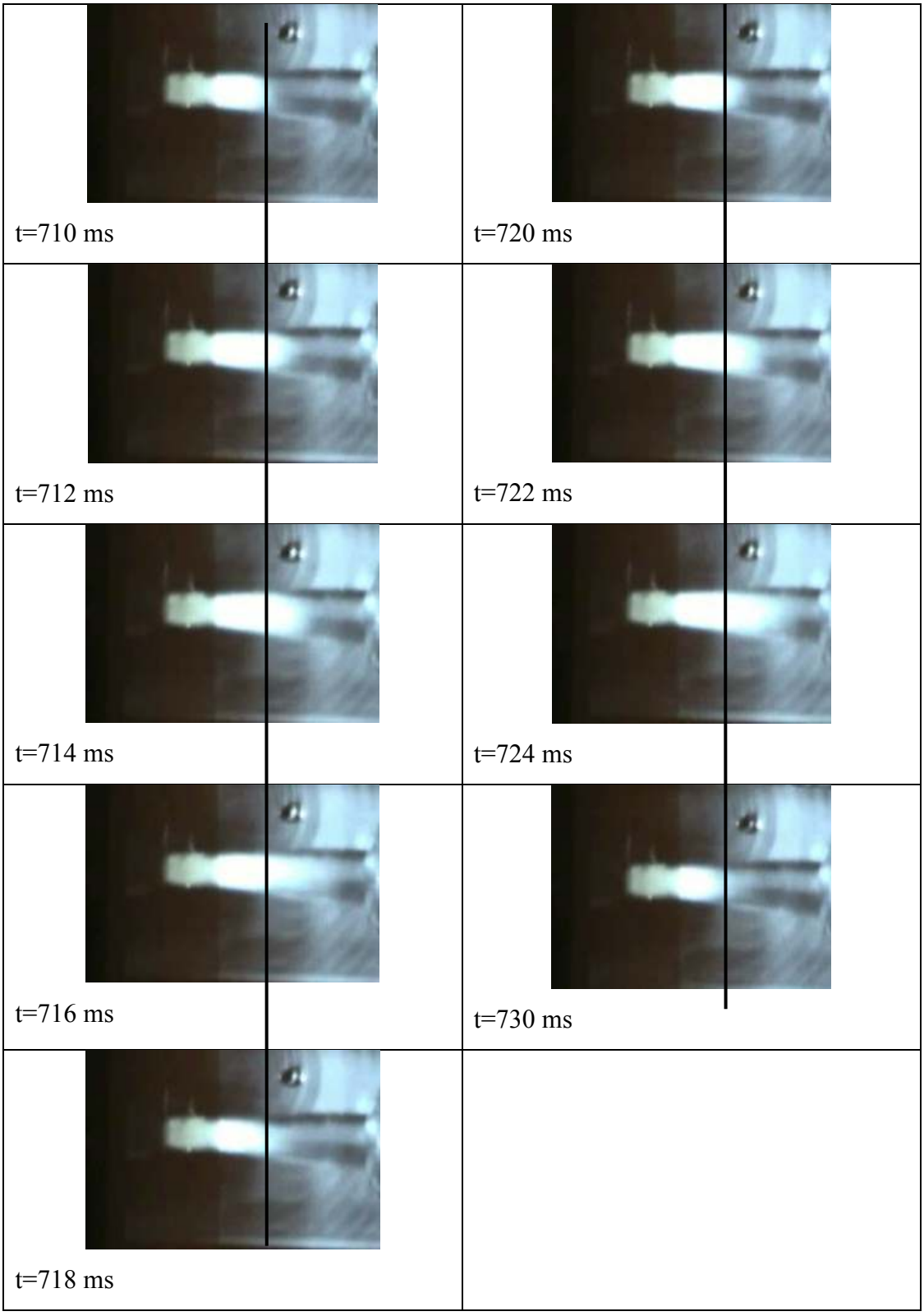

Figure 5-34. High Speed Camera Plots

5.2.2.4 Case 4: Φ_1 = 15 deg, $\Phi 2$ = 15 deg, σ=1.4-1.7

In this case the back pressure is set to P_{out}=8 bars and the inlet pressure is set to P_{in}=30 bars. Through the experiment the cavitation number kept under 2. (Figure 5-35 (b)). The pressure fluctuations at the exit plane are damped out with the increasing cavitation number in this experiment also. The amplitudes of the oscillations in the inlet pressure are more than the previous venturies. This shows that the inflow is not fully uncoupled with the exit pressure for cavitation number which is closer to critical cavitation number. Also in Figure 5-35(c) it can be seen that the oscillations exits in the range 200-275 Hz.

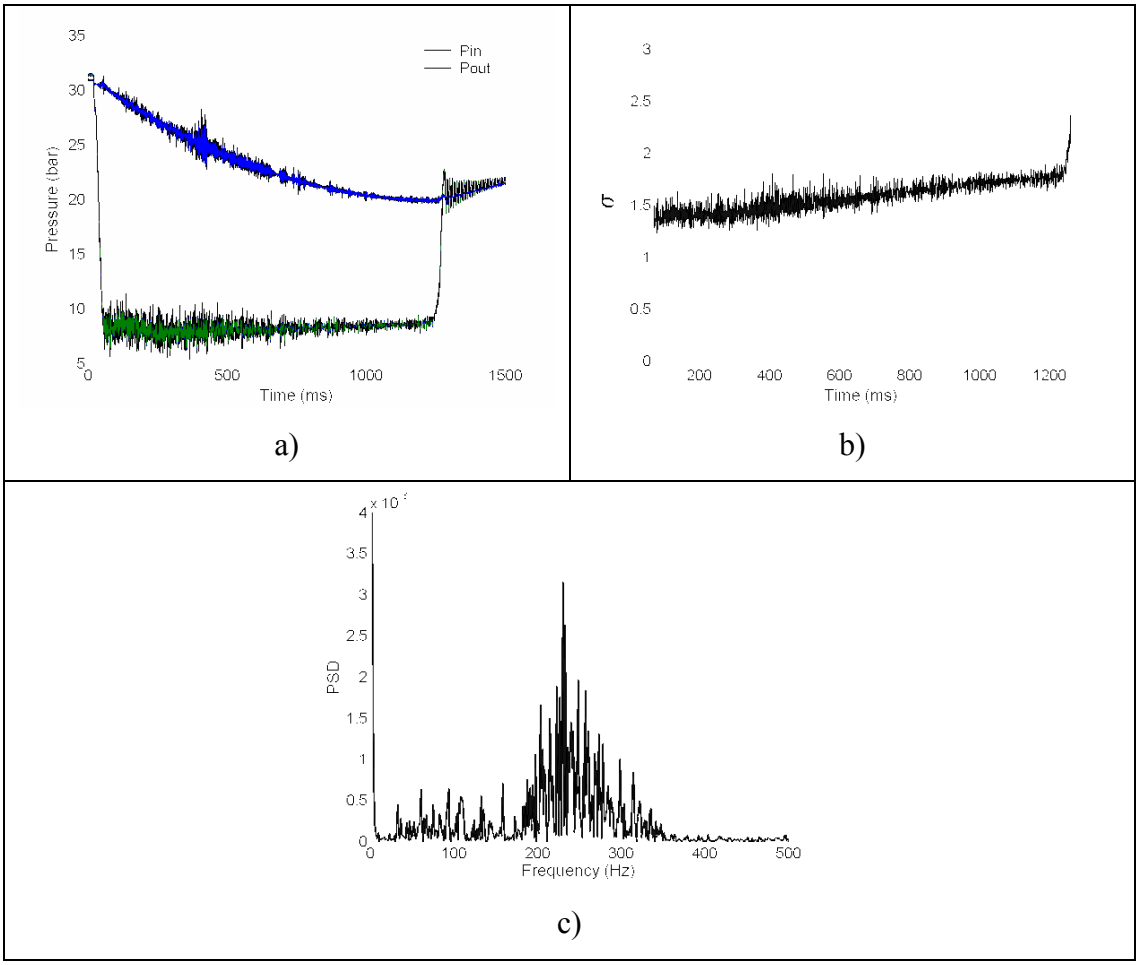

Figure 5-35. a) Pressure vs. Time b) Cavitation Number vs. Time c) PSD vs. Frequency

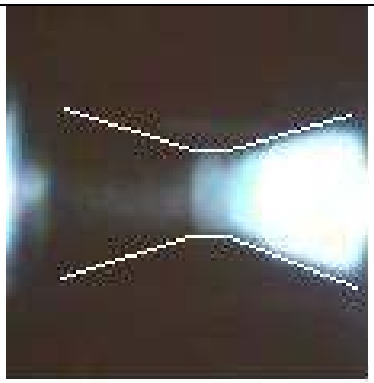

t=244 ms

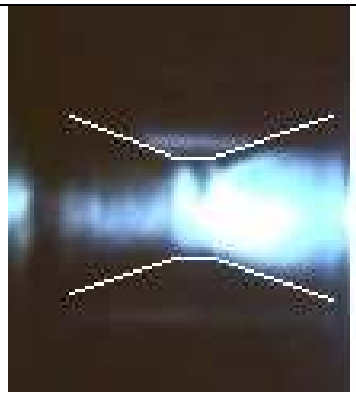

t=900 ms

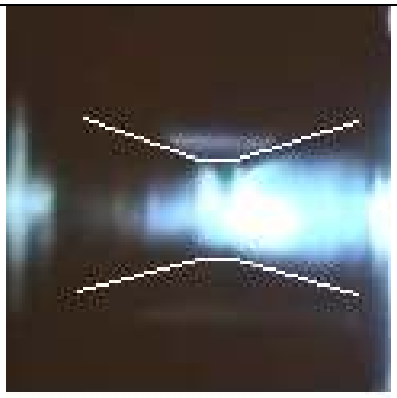

t=1007 ms

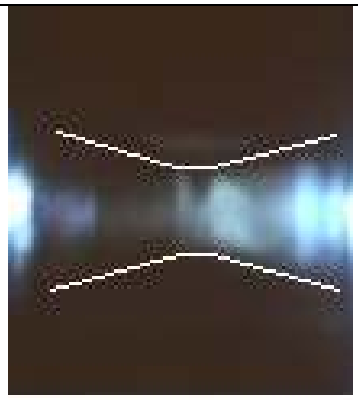

t=1185 ms

Figure 5-36. High Speed Camera Plots

5.2.2.5 Case 5: Φ_1 = 15 deg, Φ2 = 15 deg, σ=1.5-2.0

In case 5, an almost constant cavitation is achieved through the experiment. In figure 5-37 (a), the effect of the exit pressure on the inlet pressure is more visible in this experiment. Through the experiment the cavitation number is kept under 2 so that the cavitation is continuous. Again the power spectrum density plots shows that the oscillations are take place in the range of 200-350Hz. This shows a similarity with the previous experiment for this venturi.

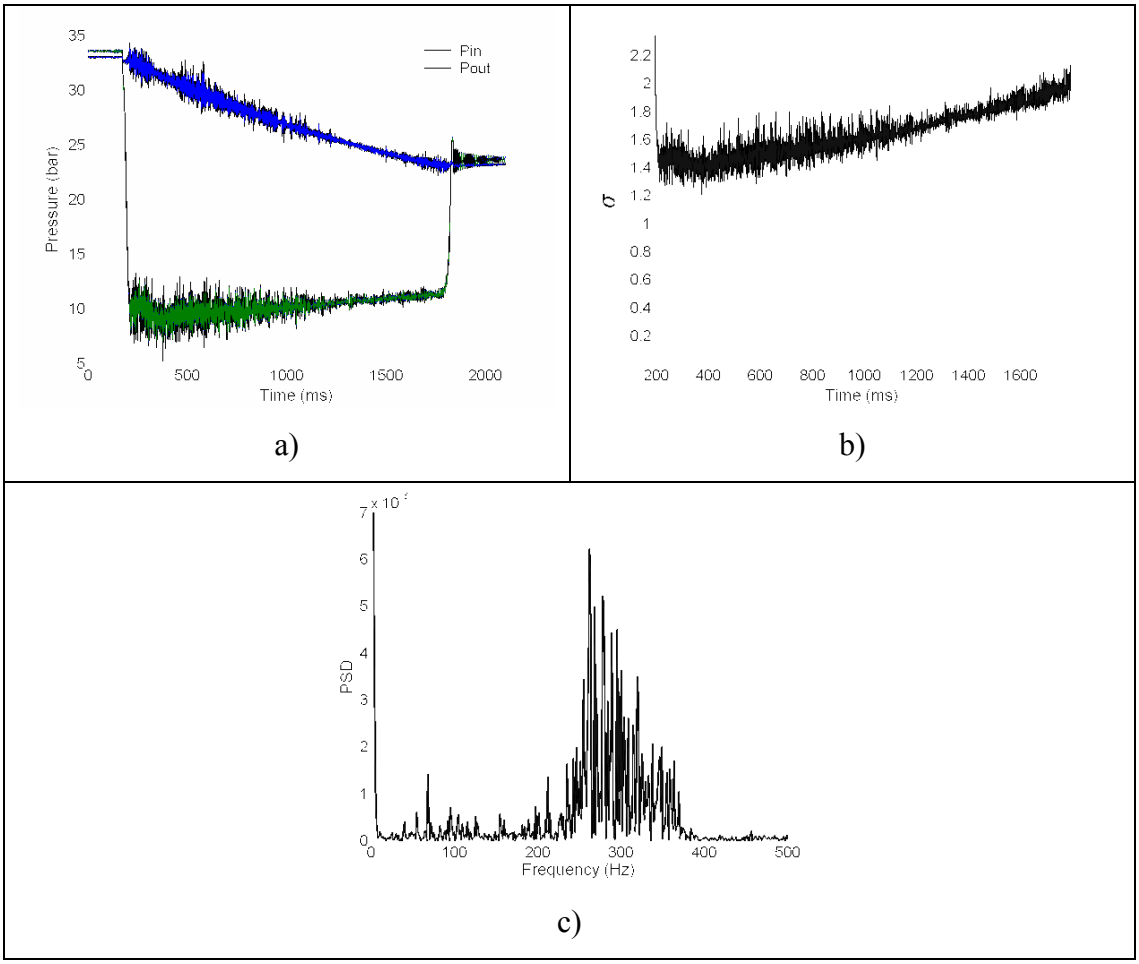

Figure 5-37. Pressure vs. Time b) Cavitation Number vs. Time c) PSD vs. Frequency

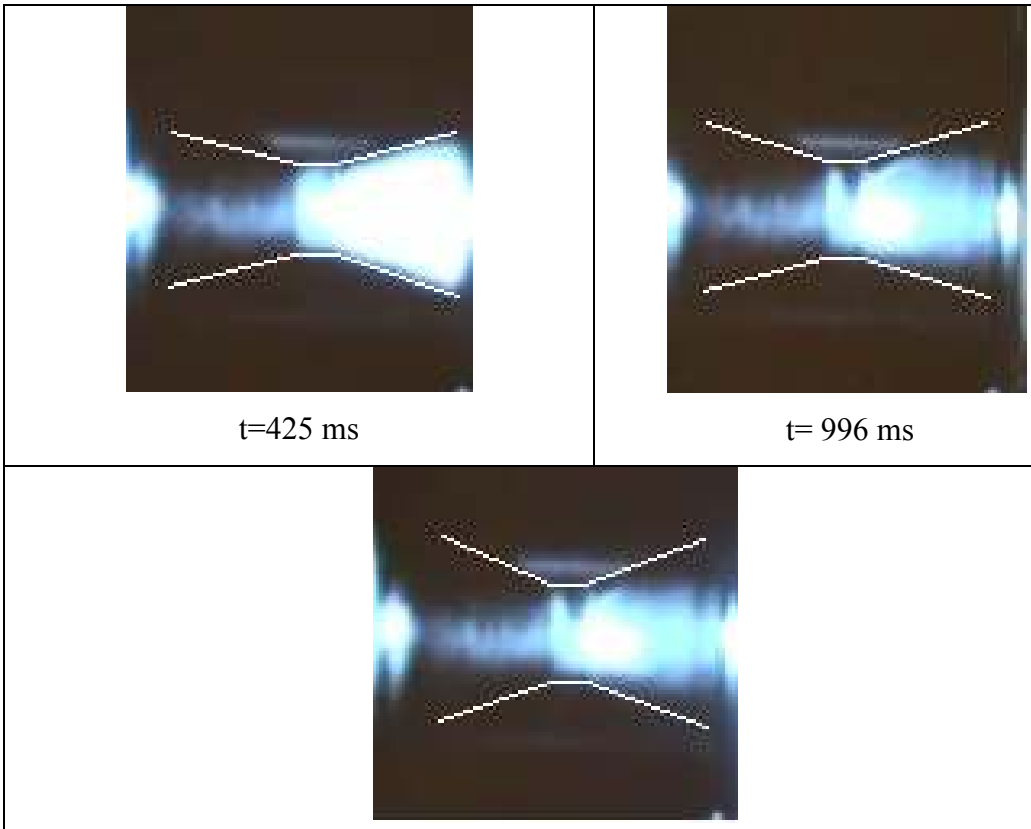

Figure 5-38. High Speed Camera Plots

5.2.2.6 Case 6: $\Phi_1 = 15$ deg, $\Phi_2 = 60$ deg, σ=1.2-1.4

In this case rather interesting results are obtained. In Figure 5-39 (a), the frequency of the oscillations in the exit pressure changes with the rising cavitation number, which is given in Figure 5-39(b). The cavitation number value is about 1.2 at the beginning and increases to 1.4 at the end of the experiment. And with the increasing cavitation number the oscillation frequencies are increased. Due to this low cavitation numbers the effect of exit oscillations on the inlet pressure is minimized.

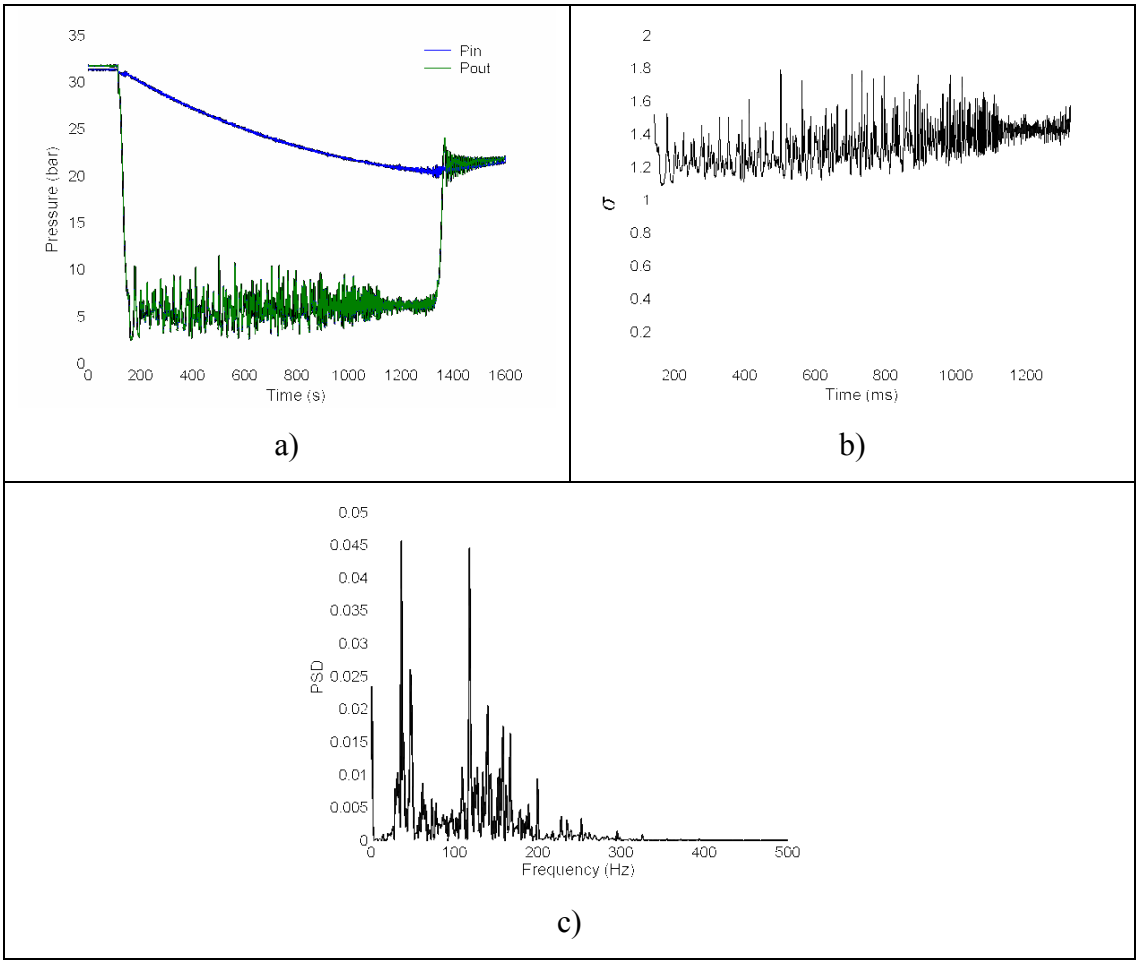

Figure 5-39. a) Pressure vs. Time b) Cavitation Number vs. Time c) PSD vs. Frequency

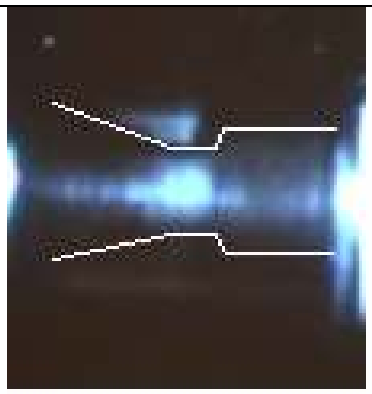

t=203 ms

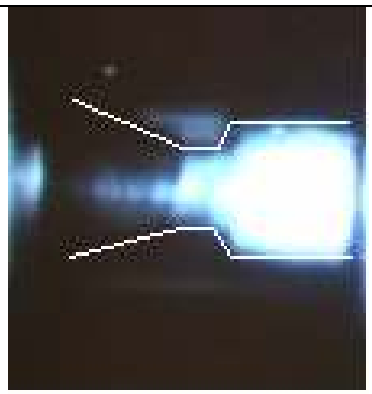

t=224 ms

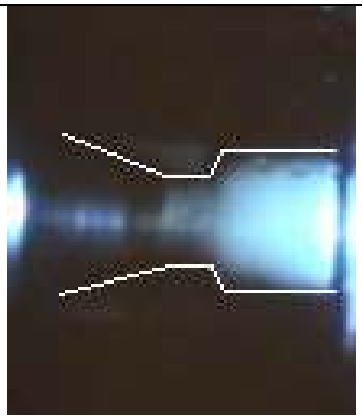

t=1340 ms

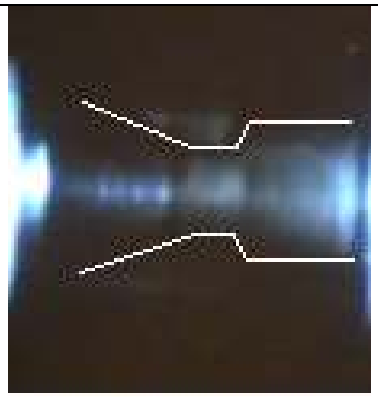

t= 1359 ms

Figure 5-40. High Speed Camera Plots

5.2.2.7 Case 7: Φ_1 = 15 deg, Φ2 = 60 deg, σ=1.4-3.0

In Figure 5-41(a) the pressure variation obtained in case 7 is given. As it is observed the cavitation occurs between t=200-1250 ms where the cavitation number is less than 2. Also in Figure 5-41 (c) the frequency of the fluctuations is seen to be in the range of 200-350 Hz.

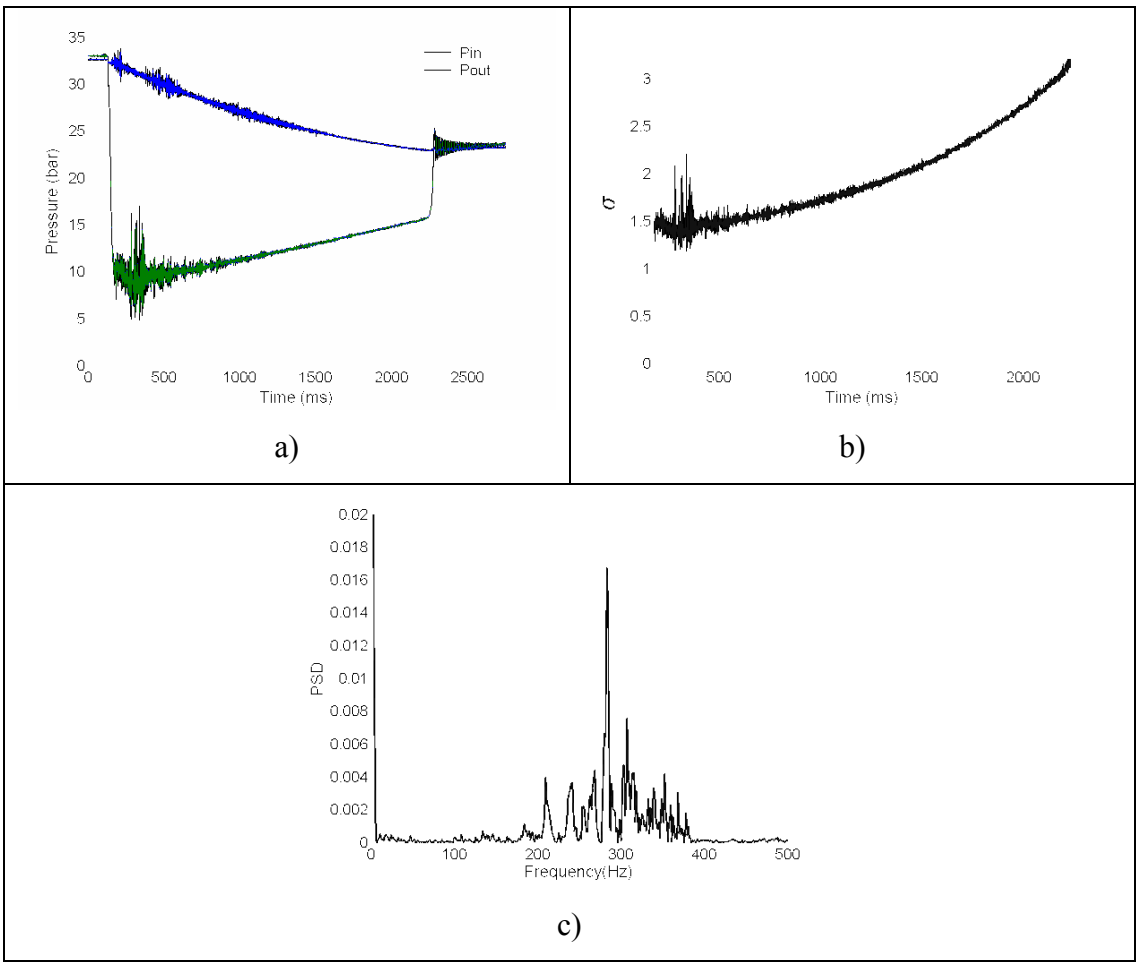

Figure 5-41. a) Pressure vs. Time b) Cavitation Number vs. Time c) PSD vs. Frequency

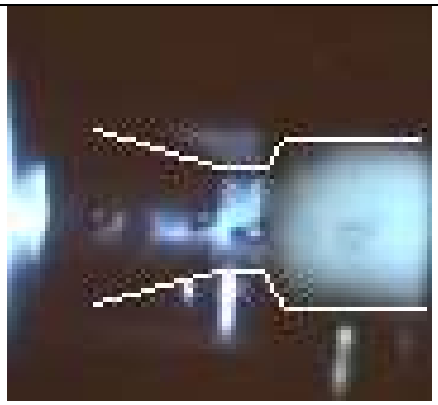

t= 450 ms

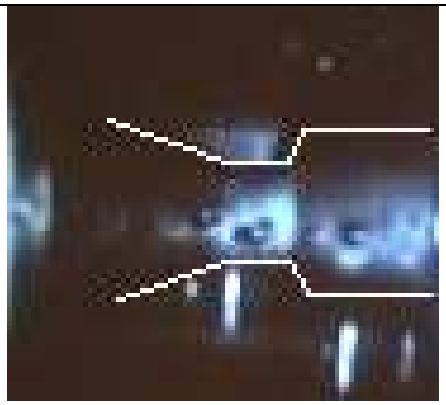

t=1060 ms

t=1400 ms

Figure 5-42. High Speed Camera Plots

5.2.2.8 Case 8: $\Phi_1 = 15$ deg, $\Phi_2 = 60$ deg, σ=1.0

In this case the exit pressure is set to be 0 bars, which sets the cavitation number to 1. As seen in Figure 5-43 (a), pressure fluctuations do not exist anymore, which indicates that the bubble formed in the diffuser is stable and stays stationary. The two-phase flow in the core region is similarly stable. (Figure 5-43 (c)).

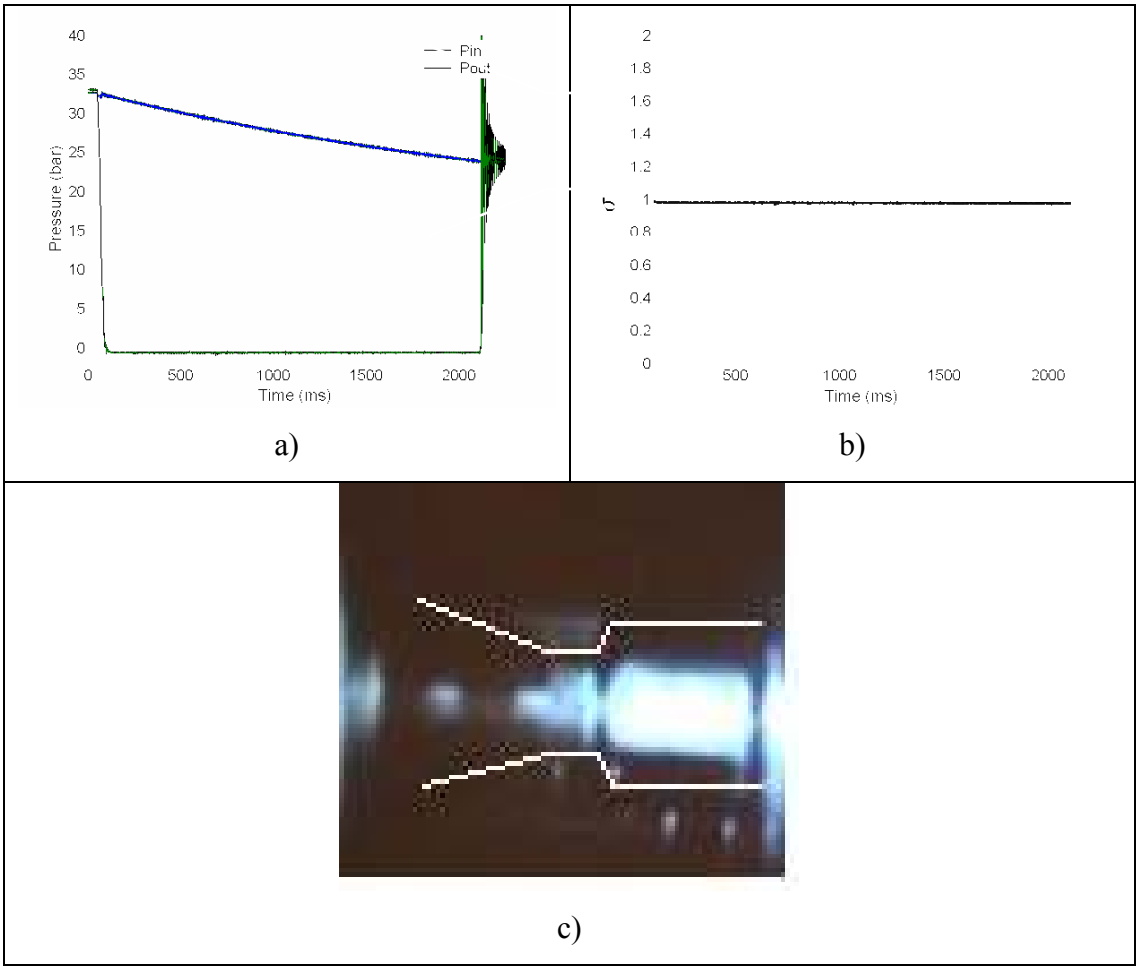

Figure 5-43. a) Pressure vs. Time b) Cavitation Number vs. Time c) High Speed Camera Plot

5.2.3 Previous Engine Tests in TÜBITAK-SAGE

In Figure 5-44. The pressure variation in the combustion chamber obtained from an engine test is given. Based on the results presented above, the high amplitude oscillations at about 250-300 Hz, which could not be explained then, can now be attributed to the cavitating venturi flows.

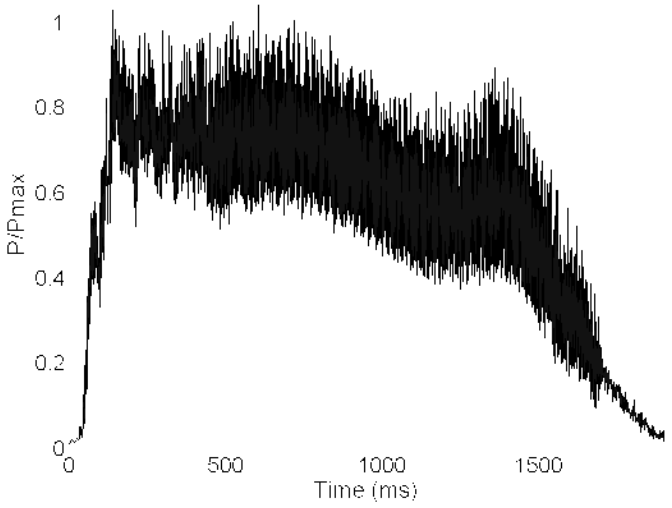

Figure 5-44. Engine Combustion Chamber Pressure Data.

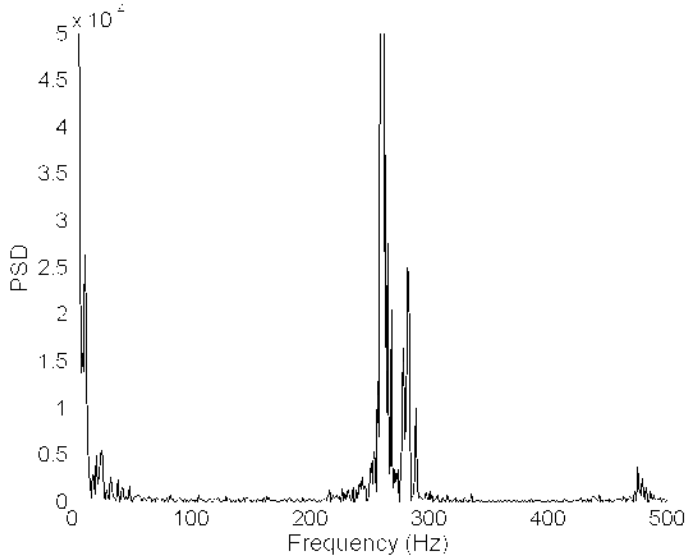

Figure 5-45. Engine Combustion Data Frequency Analysis.

5.2.4 Failure in the Experiments with 3-D Prismatic Venturis

Experiments with 3-D prismatic venturi flows were not successful due to the failure of the test section. The venturi walls made of Plexiglas was broken under the high pressure. Quick modifications to reduce the stress concentration at the corners of the machined parts did not prevent the failure. These experiments were therefore abandoned.

CHAPTER 6

CONCLUSION

In this work, cavitating venturi flows are investigated numerically and experimentally. Some of the important parameters for cavitating venturi flow like inlet, outlet angles, throat to inlet diameter ratio and length of throat to inlet diameter ratio on discharge coefficient and cavitation behavior are investigated also.

Through the numerical simulations 2-D, 2-D Axisymmetric and 3-D prismatic cases are solved for several Reynolds number and cavitation number values. Results shown that the 2-D and 2-D axisymmetric results are almost having the same discharge coefficients but when in case of oscillations the behavior is different from each other.

Through the experiments three different axisymmetric venturi geometries with different inlet and outlet angles are tested for several cavitation numbers. Due to the problems related to the pressure regulators the inlet pressure can not be kept constant in the experiments but this gives us a chance to investigate the flow at different cavitation numbers. Also the flow meter can not be used in the experiments because of the delay in the response of the flow meter. The first set of experiments shows that the cavitating venturi flow is highly turbulent and three-dimensional. These three-dimensional effects change the frequency of the oscillations. In the numerical simulations because the cavitation modeled as an axisymmetric, the frequency range in rather low. But in the real world these high momentum bubbles can not be survive through the end of the diffuser. These bubbles are collapsed and roll over each other and break down in to smaller bubbles. These low momentum bubbles creates a higher frequency oscillation with

a smaller amplitude in the exit pressure. Also in the numerical simulations the static back pressure is fixed at the exit plane therefore the mass flow rate changes during the simulation. But in the experiments the back pressure can not be fixed.

If we compare the result of the numerical simulations and the experiments, in general we can say that the main parameter like discharge coefficient and critical cavitation number can be foreseen with the FLUENT flow solver. But in the case of oscillation frequency prediction, a more complex three-dimensional flow solution is necessary and may be in the future LES turbulence model can be used to simulate this unsteady creation and collapse of the bubbles in the venturies.

REFERENCES

[1] J. FOX, *"Modeling Cavitating venturies*", 1970

[2] J. A. BOURE, A. A. FRITTE, M. M. GIOR and M. L. REOCREUX, "*Highlights of Two-Phase Critical Flow: On the Links Between Maximum Flow Rates, Sonic Velocities, Propagation and Transfer Phenomena in Single and Two-Phase Flows*", Int. J. Multiphase Flow Vol. 3, pp. 1-22, 1974

[3] K.H.ARDRON and R. B. DUFFEY, "*Acoustic Wave Propagation In a Flowing Liquid-Vapour Mixture*", Int. J. Multiphase Flow Vol. 4, pp. 303-322, 1978

[4] K. H. ARDRON, "*A Two-Fluid Model For Critical Vapor-Liquid Flow*", Int. J. Multiphase Flow Vol. 4,pp. 323-337, 1978

[5] N. T. THANG and M.R. DAVIS, "*Pressure Distribution in Bubbly Flow Through Venturis*", Int. J. Multiphase Flow Vol. 7, pp. 191-210, 1981

[6] Guston and Reises

[7] J.D. SHERWOOD, "*Potential Flow Around a Deforming Bubble In a Venturi*", International Journal of Multiphase Flow26, 2000

[8] GUILLERMO PALAU SALVADOR AND STEVEN H. GRANKEL, *"Numerical Modeling of Cavitation Using FLUENT: Validation and Parametric studies"*,34th AIAA Fluid Dynamics Conference and Exhibit 28 June -1 July 2004, Portland, Oregon, AIAA 2004-2642

[9] Changhai XU, Stephen D. HEISTER and Robert FIELD, "*Modeling Cavitating Venturi Flows*",

[10] E. ELIAS and G.S. LELOUCHE, "*Two-Phase Critical Flow*", Int. J. Multiphase Flow Vol. 20, pp. 91-168, 1994

[11] DAVID P. SCHMIDTH, CHRISTOPHER J. RUTLAND, and M. L. CORRADINI, "*A Fully Compressible, Two-Dimensional, Model of Small, High Speed, Cavitating Nozzles*", 1985

[12] Y. YAN AND R. B. THORPE, "*Flow Regime Transition Due to Cavition In The Flow Through An Orifice*", Int. J. Multiphase Flow Vol. 16, No. 6, pp. 1023-1045, 1990

[13] C. E. BRENNEN, *"Cavitation And Bubble Dynamics",* Oxford Engineering Science Series, ISBN 13:978-0-19-509409-1

[14] FLUENT User Manual

APPENDIX A

EXPERIMENTAL SETUP TECHNICAL DRAWINGS & MEASURMENT EQUIPMENT

A.1 Technical drawings of experimental setup

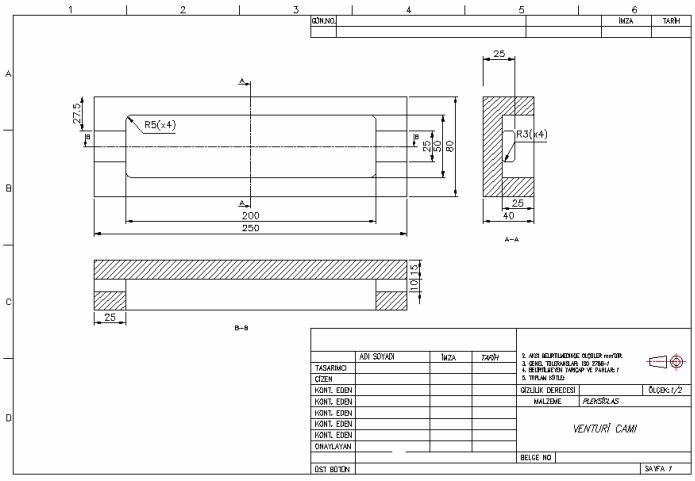

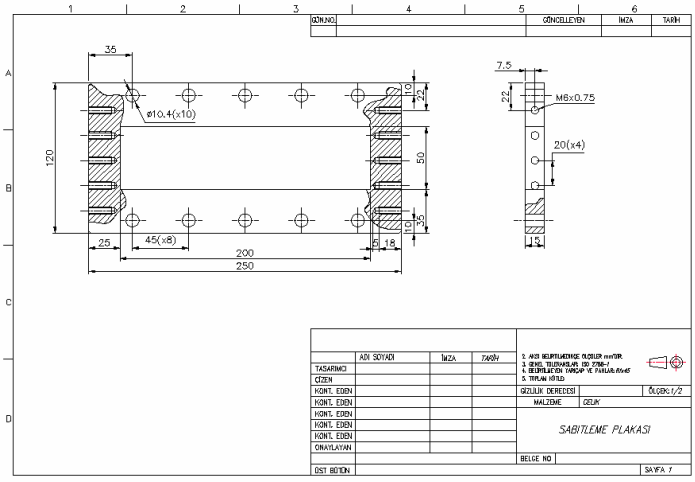

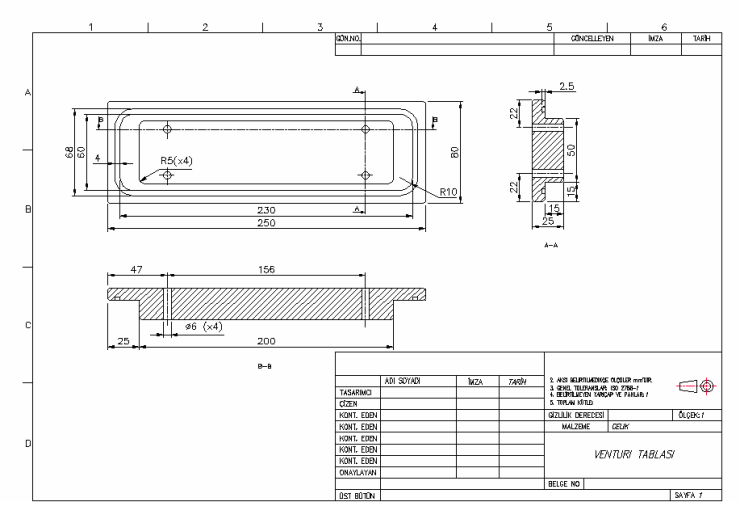
DÖN.NO.
GÜNCELLEYEN
İMZA
TARİH
R5(x4)
R10
2.5
22
50
15
25
A–A
47
156
ø6 (x4)
25
200
B–B
ADI SOYADI
İMZA
TARİH
TASARIMCI
ÇİZEN
KONT. EDEN
ONAYLAYAN
GİZLİLİK DERECESİ
ÖLÇEK:1
MALZEME
ÇELİK
VENTURI TABLASI
BELGE NO
İLK BİTİŞ
SAYFA 1

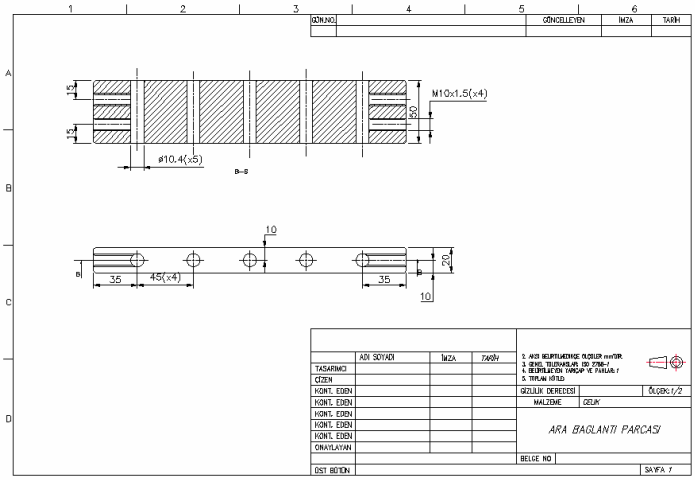
DÖN.NO.
GÜNCELLEYEN
İMZA
TARİH
M10x1.5(x4)
ø10.4(x5)
B–B
10
35
45(x4)
35
10
ADI SOYADI
İMZA
TARİH
TASARIMCI
ÇİZEN
KONT. EDEN
ONAYLAYAN
GİZLİLİK DERECESİ
ÖLÇEK:1/2
MALZEME
ÇELİK
ARA BAĞLANTI PARÇASI
BELGE NO
İLK BİTİŞ
SAYFA 1

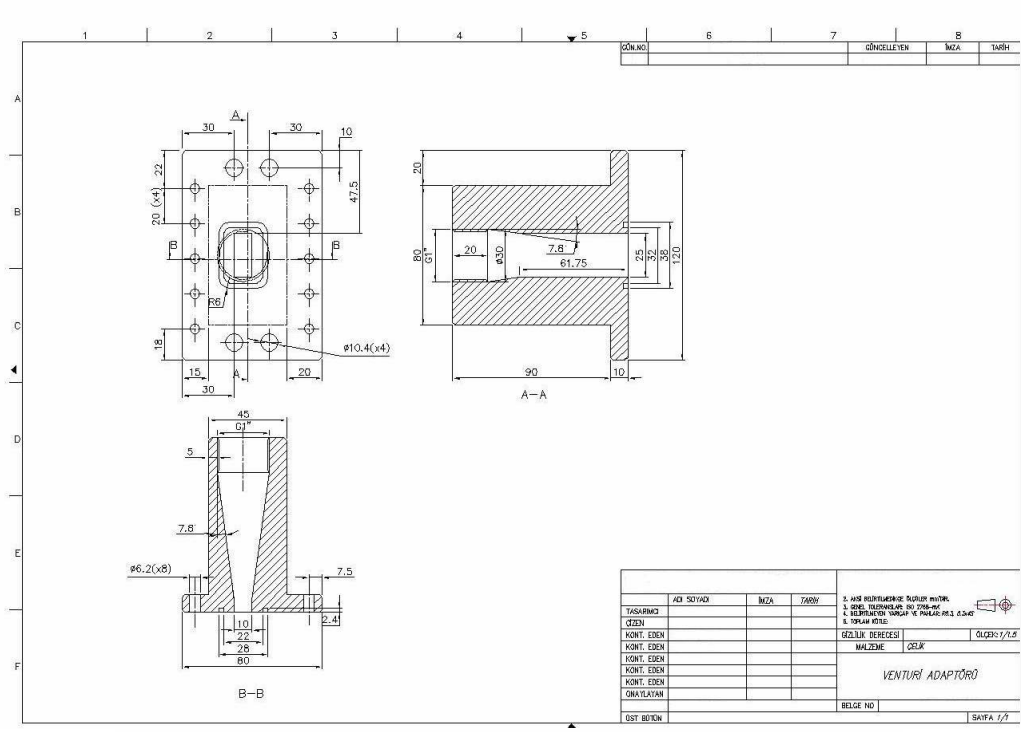
A
30
30
10
22
20 (x4)
47.5
B
B
R6
ø10.4(x4)
18
15
30
20
A–A
20
80
G1"
ø30
20
7.8
61.75
25
32
38
120
90
10
B–B
45
G1"
5
7.8
ø6.2(x8)
7.5
10
22
28
80
2.4
GÖN.NO.
GÜNCELLEYEN
İMZA
TARİH
ADI SOYADI
İMZA
TARİH
TASARIMCI
ÇİZEN
KONT. EDEN
KONT. EDEN
KONT. EDEN
KONT. EDEN
KONT. EDEN
ONAYLAYAN
GST BÖTÜN
ÖLÇEK:1/1.5
MALZEME
ÇELİK
VENTURİ ADAPTÖRÜ
BELGE NO
SAYFA 1/1

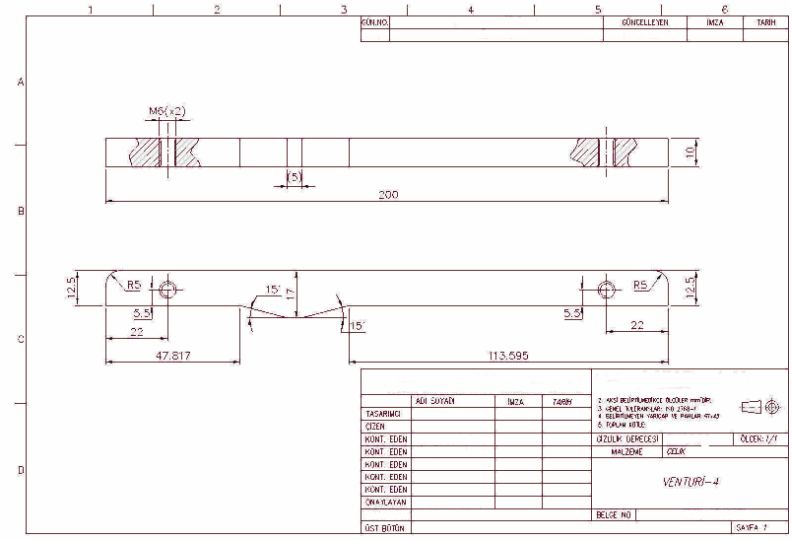
GÖN.NO.
GÜNCELLEYEN
İMZA
TARİH
M6(x2)
10
(5)
200
12.5
R5
15°
17
5.5
22
47.817
15°
R5
5.5
22
113.595
12.5
ADI SOYADI
İMZA
TARİH
TASARIMCI
ÇİZEN
KONT. EDEN
KONT. EDEN
KONT. EDEN
KONT. EDEN
ONAYLAYAN
GST BÖTÜN
ÖLÇEK: 1/1
MALZEME
ÇELİK
VENTURİ-4
BELGE NO
SAYFA 1

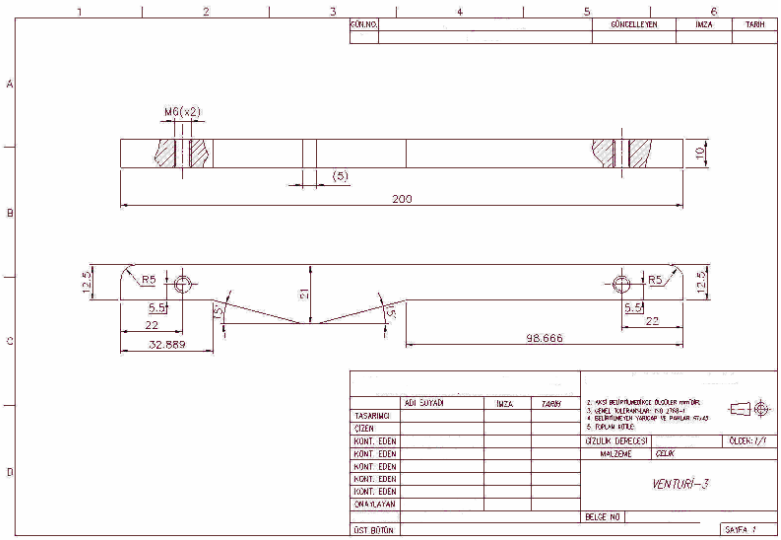
M6(x2)
10
(5)
200
R5
12.5
5.5
22
32.889
21
30°
7°
98.666
VENTURİ-3
ÖLÇEK: 1/1
SAYFA 1

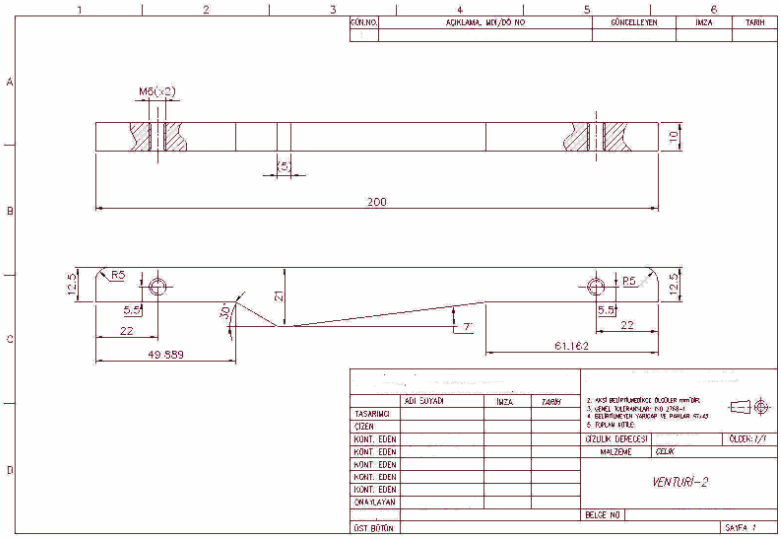
M6(x2)
10
(5)
200
R5
12.5
5.5
22
49.889
21
30°
7°
61.162
VENTURİ-2
ÖLÇEK: 1/1
SAYFA 1

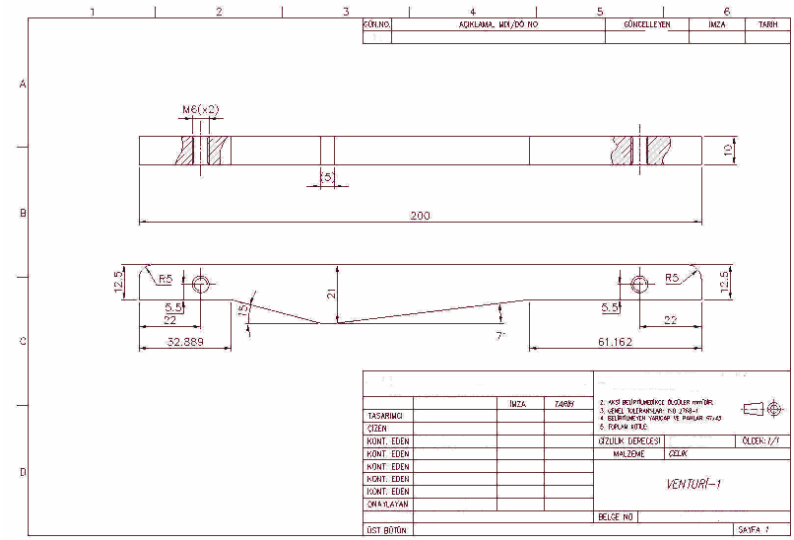
M6(x2)
10
16
200
12.5
R5
5.5
22
32.889
15°
21
7°
61.162
R5
12.5
5.5
22
VENTURİ-1

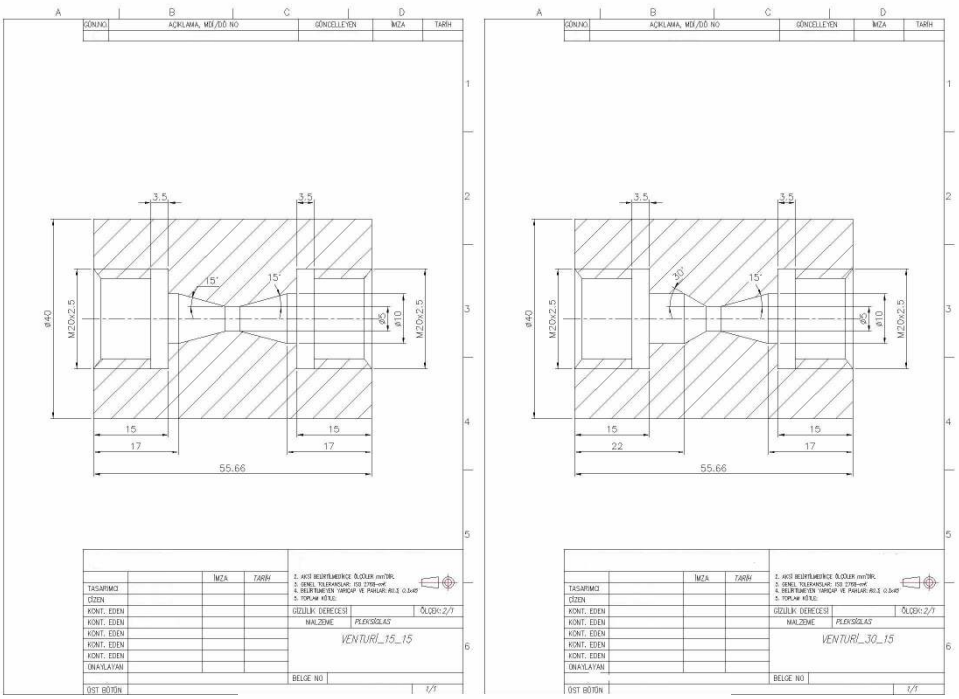
A
B
C
D
GÖNNO
AÇIKLAMA, MDİ/DÖ NO
GÜNCELLEYEN
İMZA
TARİH
3.5
3.5
ø40
M20x2.5
15°
15°
ø5
ø10
M20x2.5
15
17
15
17
55.66
TASARIMCI
ÇİZEN
KONT. EDEN
KONT. EDEN
KONT. EDEN
KONT. EDEN
ONAYLAYAN
ÜST BÖTÜN
İMZA
TARİH
2. AKSİ BELİRTİLMEDİKÇE ÖLÇÜLER mm'DİR.
3. GENEL TOLERANSLAR: ISO 2768-mK
4. BELİRTİLMEDEN YAPILAR KESKİN KENARLAR ALINACAK
5. TOPLAM KÜTLE:
GİZLİLİK DERECESİ
ÖLÇEK:2/1
MALZEME
PLEKSİGLAS
VENTURİ_15_15
BELGE NO
1/1
A
B
C
D
GÖNNO
AÇIKLAMA, MDİ/DÖ NO
GÜNCELLEYEN
İMZA
TARİH
3.5
3.5
ø40
M20x2.5
30°
15°
ø5
ø10
M20x2.5
15
22
15
17
55.66
TASARIMCI
ÇİZEN
KONT. EDEN
KONT. EDEN
KONT. EDEN
KONT. EDEN
ONAYLAYAN
ÜST BÖTÜN
İMZA
TARİH
2. AKSİ BELİRTİLMEDİKÇE ÖLÇÜLER mm'DİR.
3. GENEL TOLERANSLAR: ISO 2768-mK
4. BELİRTİLMEDEN YAPILAR KESKİN KENARLAR ALINACAK
5. TOPLAM KÜTLE:
GİZLİLİK DERECESİ
ÖLÇEK:2/1
MALZEME
PLEKSİGLAS
VENTURİ_30_15
BELGE NO
1/1
A
B
C
D
GÖNNO
AÇIKLAMA, MDİ/DÖ NO
GÜNCELLEYEN
İMZA
TARİH
3.5
3.5
ø40
M20x2.5
60°
15°
ø5
ø10
M20x2.5
15
24.887
15
17
55.66
ADI SOYADI
İMZA
TARİH
TASARIMCI
ÇİZEN
KONT. EDEN
KONT. EDEN
KONT. EDEN
KONT. EDEN
ONAYLAYAN
ÜST BÖTÜN
2. AKSİ BELİRTİLMEDİKÇE ÖLÇÜLER mm'DİR.
3. GENEL TOLERANSLAR: ISO 2768-mK
4. BELİRTİLMEDEN YAPILAR KESKİN KENARLAR ALINACAK
5. TOPLAM KÜTLE:
GİZLİLİK DERECESİ
ÖLÇEK:2/1
MALZEME
PLEKSİGLAS
VENTURİ_60_15
BELGE NO
1/1

A.2 Specifications of transducers, data acquisition system, high speed camera and valves, regulators.

A.2.1 Data Acquisition system

IOTECH Dacbook 2000E

- 16 Channel Analog input
- 200kHz data acquisition capacity from one channel
- 16 Channel Thermocouple extension

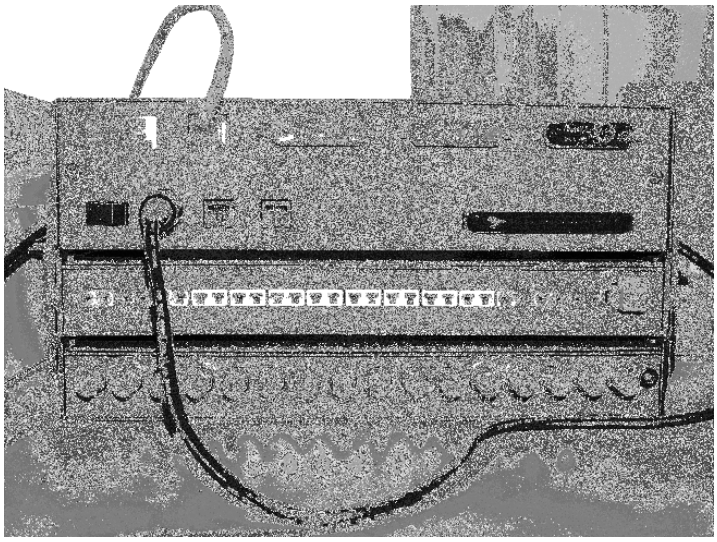

Figure A2-1. Data Acqusition System

A.2.2 Pressure Transducers

Kistler 701 a quartz pressure sensor for measuring dynamic and quasistatic pressures up to 250 bars.

Figure A2-2. Pressure Transducer

A.2.3 Flow Meter

Hoffler turbine type high pressure flow meter.

Figure A2-3.Hoffler Turbine Type Flow Meter

A.2.5 Pressure Regulator

HOKE High pressure (0-400) bars high flow pressure regulator

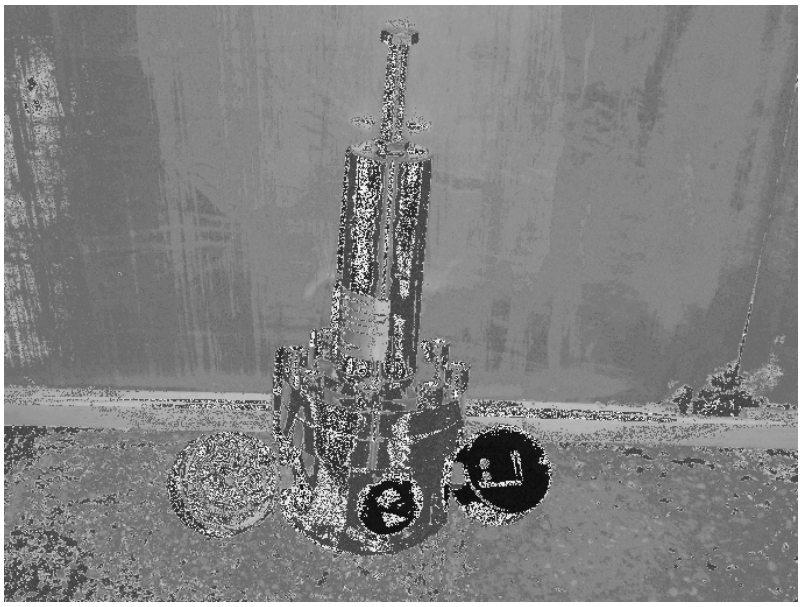

Figure A2-4. Pressure Requlator

APPENDIX B

RESULTS OF NUMERICALS SIMULATIONS

B.1 Temperature vs. Vapor Pressure Table

Taken from the Sonntag, Borgnakke and Van Wylen, "Fundamentals of Thermodynamics", 1998, John Wiley & Sons

Table B-1. Vapor Pressure vs. Temperature.

Temperature C°	Vapor Pressure (Pa)
0,01	611,3
5	872,1
10	1227,6
15	1705
20	2339
25	3169
30	4246
35	5628
40	7384
45	9593
50	12350
55	15758
60	19941
65	25030
70	31190
75	38580
80	47390
85	57830
90	70140
95	84550
100	101300
105	120800
110	143300
115	169100

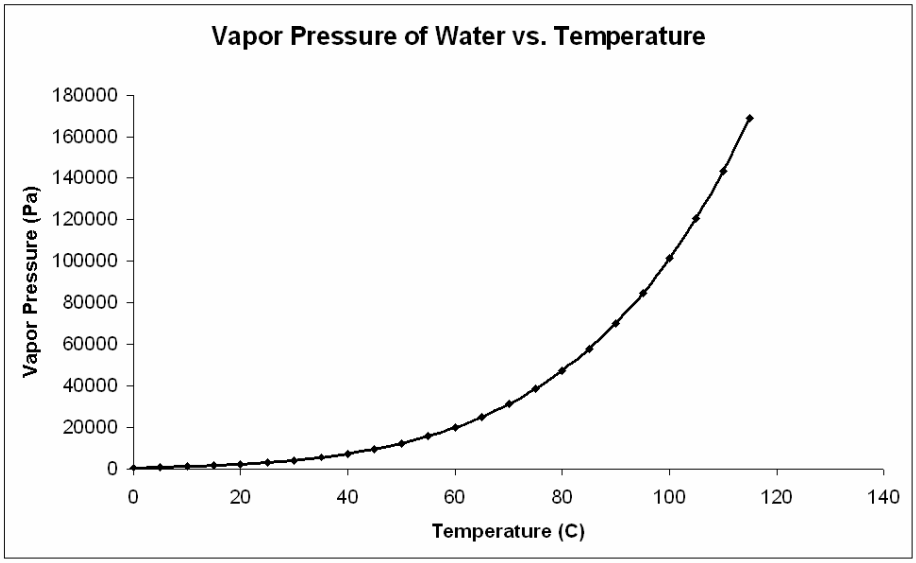

Figure B-1. Vapor Pressure of Water vs. Temperature

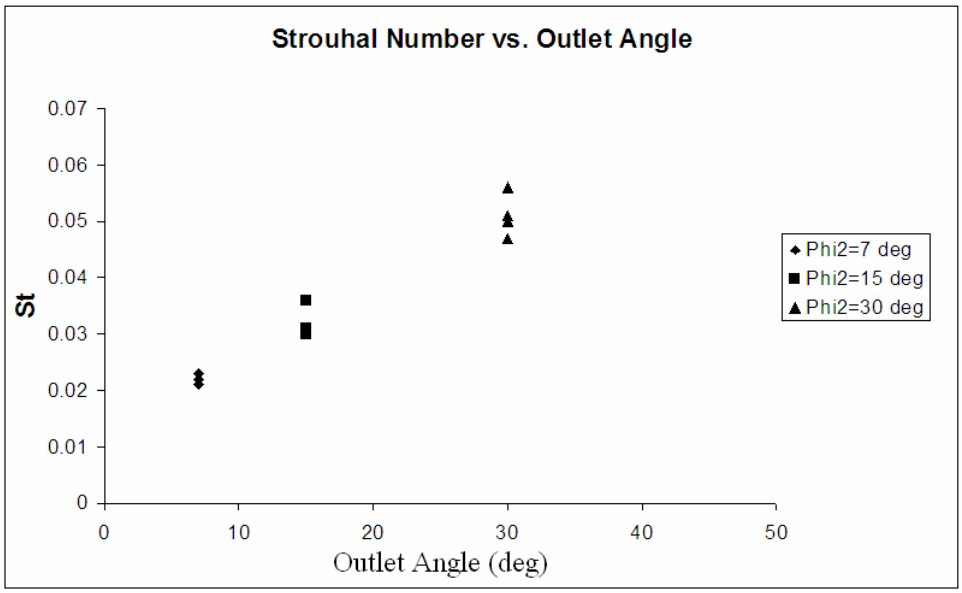

Figure B-2. Strouhal Number vs. Outlet Angle

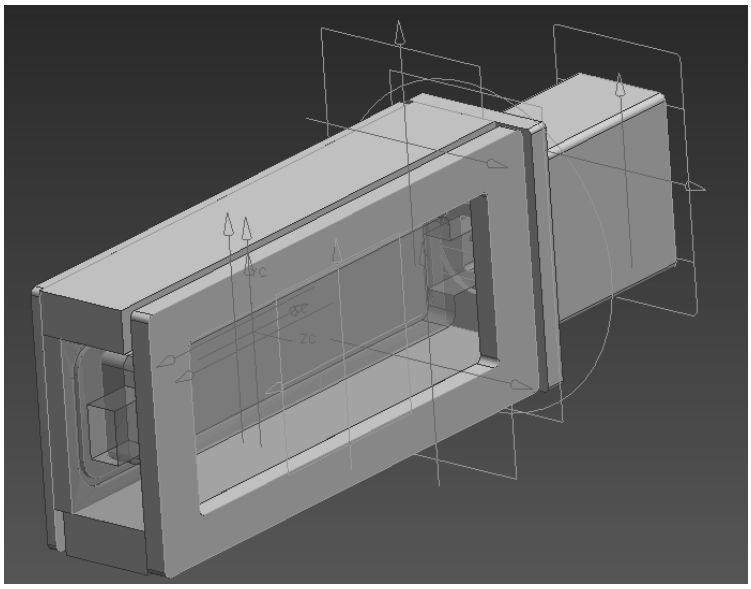

Figure B-3. CAD Drawing of the Test Section and the Adaptors.

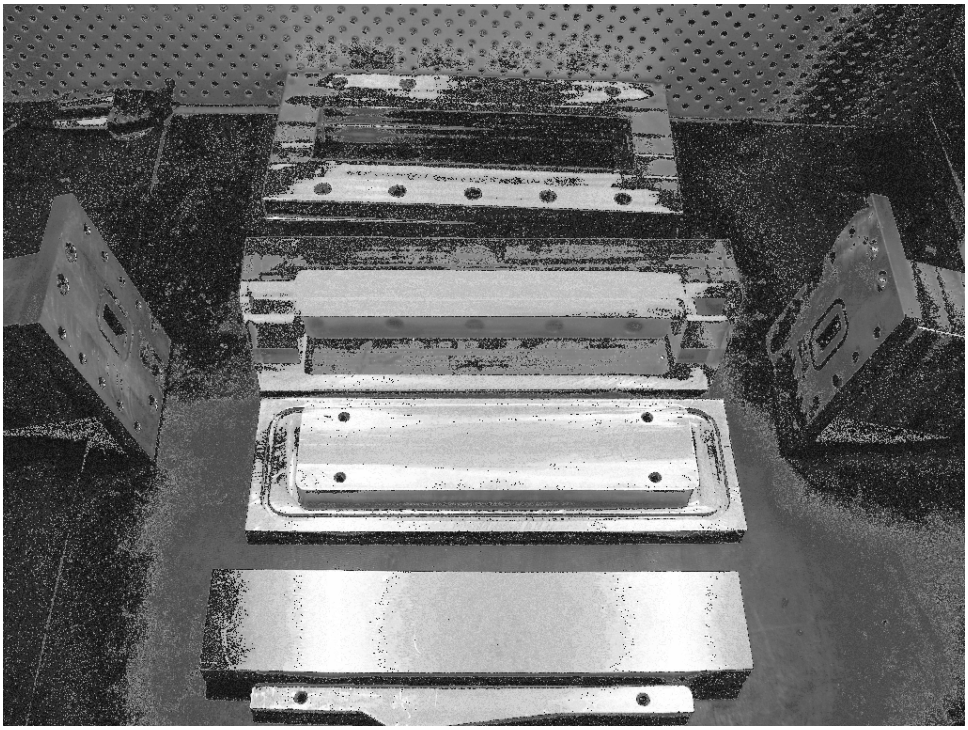

Figure B-4.Parts of the 3-D Prismatic Test Section

Figure B-5. Assembly of the 3-D Prismatic Test Section

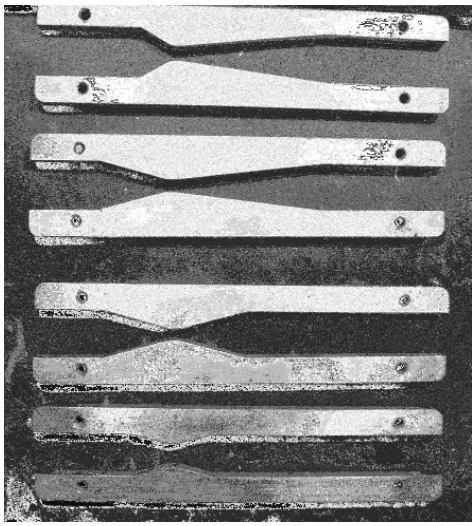

Figure B-6.Four Different Venturi Configuration for 3-D Prismatic Test Section

CAD drawing of the test section is given in Figure B-2. The test section consists of a Plexiglas visual section, a holder for the 3-D prismatic venturi sections at the back of the visual section and two tightening plates and two flow adaptors which are placed at the inlet and the outlet of the test sections. Plexiglas test section is produced with milling method to reduce the leakage from the joints. The technical drawings of the test section are given in Appendix A-1.

Table B-2. Geometric Properties of the Venturies for 3-D Prismatic Test Section

	D_{in}	D_{th}	D_{in}/D_{th}	L_{th}	L_{th}/D_{in}	Φ_1	Φ_2
1	22.4 mm	8 mm	0.357	5 mm	0.223	15 deg	7 deg
2	22.4 mm	8 mm	0.357	5 mm	0.223	30 deg	7 deg
3	22.4 mm	8 mm	0.357	5 mm	0.223	15 deg	15 deg
4	22.4 mm	16 mm	0.714	5 mm	0.223	15 deg	15 deg

B.2 Results of 2-D Axisymmetric Simulations

Table B-3. Results of 2-D Axisymmetric Numerical Simulations

					Re= 6E5									Re=9E5									
	Φ_1	Φ_2	D_{in}/D_{in}	L_{in}/D_{in}	C_d- σ_1	C_d- σ_2	C_d- σ_3			$St_{in}(\sigma_2)$	$St_{in}(\sigma_3)$	$St_{out}(\sigma_2)$	$St_{out}(\sigma_3)$	C_d-σ_1	C_d- σ_2	C_d- σ_3				$St_{in}(\sigma_2)$	$St_{in}(\sigma_3)$	$St_{out}(\sigma_2)$	$St_{out}(\sigma_3)$
1	Curved	7	0.357	0.223	0.9090	0.9090	0.9090	c	c	0.027	0.000	0.027	0.034	0.9132	0.9132	0.9131	c	c	c	0.023	0.025	0.022	0.026
2	7	7	0.357	0.223	0.9259	0.9259	0.9259	c	c	0.028	0.000	0.028	0.035	0.9303	0.9303	0.9303	c	c	c	0.022	0.024	0.023	0.025
3	15	7	0.357	0.223	0.8818	0.8834	0.8834	c	c	0.028	0.000	0.028	0.035	0.8859	0.8859	0.8859	c	c	c	0.023	0.000	0.023	0.025
4	30	7	0.357	0.223	0.8026	0.8026	0.8026	c	c	0.026	0.000	0.026	0.000	0.8036	0.8036	0.8036	c	c	c	0.020	0.021	0.021	0.021
5	90	7	0.357	0.223	0.6223	0.6223	0.6210	c	c	0.030	0.000	0.030	0.000	0.6226	0.6223	0.6212	c	c	c	0.023	0.000	0.023	0.000
6	Curved	15	0.357	0.223	0.9083	0.9080	0.9055	c	c	0.000	0.000	0.044	0.000	0.9126	0.9103	0.9101	c	c	c	0.031	0.038	0.031	0.039
7	7	15	0.357	0.223	0.9259	0.9259	0.9123	c	-	0.046	0.000	0.048	0.000	0.9303	0.9301	0.9188	c	c	-	0.036	0.000	0.036	0.000
8	15	15	0.357	0.223	0.8784	0.8784	0.8794	c	c	0.041	0.000	0.041	0.000	0.8827	0.8827	0.8813	c	c	c	0.030	0.000	0.030	0.000
9	30	15	0.357	0.223	0.8022	0.8007	0.8013	c	c	0.044	0.000	0.044	0.048	0.8032	0.8032	0.8020	c	c	c	0.030	0.032	0.031	0.032
10	90	15	0.357	0.223	0.6235	0.6230	0.5355	c	c	- 0.051	0.000	0.050	0.000	0.6238	0.6237	0.5356	c	c	-	0.036	0.000	0.036	0.000
11	Curved	30	0.357	0.223	0.9056	0.9055	0.7890	c	c	- 0.000	0.000	0.000	0.000	0.9098	0.9086	0.7908	c	c	-	0.051	0.000	0.052	0.000
12	7	30	0.357	0.223	0.9262	0.9262	0.8042	c	c	- 0.000	0.000	0.000	0.000	0.9305	0.9289	0.8088	c	c	-	0.043	0.000	0.046	0.000
13	15	30	0.357	0.223	0.8835	0.8831	0.8030	c	c	- 0.000	0.000	0.000	0.000	0.8859	0.8857	0.8050	c	c	-	0.047	0.000	0.047	0.000
14	30	30	0.357	0.223	0.8041	0.8036	0.7608	c	c	- 0.038	0.000	0.038	0.000	0.8052	0.8040	0.7847	c	c	-	0.063	0.000	0.060	0.000
15	90	30	0.357	0.223	0.6220	0.6200	0.5059	c	c	- 0.032	0.000	0.034	0.000	0.6223	0.6204	0.5059	c	c	-	0.049	0.000	0.051	0.000
16	Curved	60	0.357	0.223	0.9088	0.8917	0.6675	c	c	- 0.000	0.000	0.000	0.000	0.9130	0.8945	0.6692	c	c	-	0.000	0.000	0.000	0.000
17	7	60	0.357	0.223	0.9269	0.9087	0.6841	c	c	- 0.000	0.000	0.000	0.000	0.9121	0.9121	0.6866	c	c	-	0.000	0.000	0.000	0.000
18	15	60	0.357	0.223	0.8823	0.8811	0.6604	c	c	- 0.000	0.000	0.000	0.000	0.8847	0.8830	0.6617	c	c	-	0.000	0.000	0.000	0.000
19	30	60	0.357	0.223	0.8028	0.8013	0.6337	c	c	- 0.000	0.000	0.000	0.000	0.8039	0.8021	0.6344	c	c	-	0.000	0.000	0.000	0.000
20	90	60	0.357	0.223	0.6233	0.6223	0.4771	c	c	- 0.000	0.000	0.000	0.000	0.6236	0.6224	0.4770	c	c	-	0.000	0.000	0.000	0.000
21	Curved	90	0.357	0.223	0.9086	0.8695	0.6153	c	c	- 0.000	0.000	0.000	0.000	0.9132	0.8711	0.6176	c	c	-	0.000	0.000	0.000	0.000
22	7	90	0.357	0.223	0.9195	0.8853	0.6263	c	c	- 0.000	0.000	0.000	0.000	0.9299	0.8875	0.6300	c	c	-	0.000	0.000	0.000	0.000
23	15	90	0.357	0.223	0.8809	0.8860	0.6204	c	c	- 0.000	0.000	0.000	0.000	0.8832	0.8769	0.6217	c	c	-	0.000	0.000	0.000	0.000
24	30	90	0.357	0.223	0.8022	0.8009	0.5918	c	c	- 0.000	0.000	232	0.000	0.8032	0.8018	0.5921	c	c	-	0.000	0.000	0.000	0.000
25	90	90	0.357	0.223	0.6225	0.6215	0.4677	c	c	- 0.000	0.000	0.000	0.000	0.6227	0.6217	0.4674	c	c	-	0.000	0.000	0.000	0.000

Cont'd ...

					Re=6E5										Re=1.2E6									
	Φ_1	Φ_2	D_{th}/D_{in}	L_{th}/D_{in}	C_d-σ_1	C_d- σ_2	C_d- σ_3				$St_{in}(\sigma_2)$	$St_{in}(\sigma_3)$	$St_{out}(\sigma_2)$	$St_{out}(\sigma_3)$	C_d-σ_1	C_d- σ_2	C_d- σ_3				$St_{in}(\sigma_2)$	$St_{in}(\sigma_3)$	$St_{out}(\sigma_2)$	$St_{out}(\sigma_3)$
26	Curved	7	0.714	0.223	0.8822	0.8822	0.8814	c	c	c	0.000	0.000	0.000	0.000	0.8987	0.8987	0.8962	c	c	c	0.000	0.000	0.000	0.000
27	7	7	0.714	0.223	0.9061	0.9061	0.9057	c	c	c	0.000	0.000	0.000	0.000	0.9259	0.9259	0.9238	c	c	c	0.000	0.000	0.000	0.000
28	15	7	0.714	0.223	0.8671	0.8671	0.8660	c	c	c	0.000	0.000	0.000	0.000	0.8805	0.8805	0.8775	c	c	c	0.000	0.000	0.000	0.000
29	30	7	0.714	0.223	0.8154	0.8154	0.8111	c	c	c	0.000	0.000	0.000	0.000	0.8254	0.8254	0.8195	c	c	c	0.000	0.000	0.000	0.000
30	90	7	0.714	0.223	0.6757	0.6757	0.6413	c	c	-	0.000	0.000	0.000	0.000	0.6774	0.6775	0.6406	c	c	-	0.000	0.000	0.000	0.000
31	Curved	15	0.714	0.223	0.8785	0.8785	0.8725	c	c	-	0.000	0.000	0.000	0.000	0.8948	0.8948	0.8853	c	c	-	0.000	0.000	0.000	0.000
32	7	15	0.714	0.223	0.9058	0.9058	0.8851	c	c	-	0.000	0.000	0.000	0.000	0.9256	0.9256	0.8976	c	c	-	0.000	0.000	0.000	0.000
33	15	15	0.714	0.223	0.8702	0.8702	0.8630	c	c	-	0.000	0.000	0.000	0.000	0.8835	0.8835	0.8687	c	c	-	0.000	0.000	0.000	0.000
34	30	15	0.714	0.223	0.8034	0.8034	0.7883	c	c	-	0.000	0.000	0.000	0.000	0.8112	0.8112	0.7951	c	c	-	0.000	0.000	0.000	0.000
35	90	15	0.714	0.223	0.6737	0.6737	0.6043	c	c	-	0.000	0.000	0.000	0.000	0.6756	0.6756	0.6034	c	c	-	0.000	0.000	0.000	0.000
36	Curved	30	0.714	0.223	0.8831	0.8831	0.8182	c	c	-	0.000	0.000	0.000	0.000	0.8997	0.8997	0.8269	c	c	-	0.000	0.000	0.000	0.000
37	7	30	0.714	0.223	0.9061	0.9061	0.8303	c	c	-	0.000	0.000	0.000	0.000	0.9259	0.9259	0.8481	c	c	-	0.000	0.000	0.000	0.000
38	15	30	0.714	0.223	0.8702	0.8702	0.8263	c	c	-	0.000	0.000	0.000	0.000	0.8836	0.8836	0.8420	c	c	-	0.000	0.000	0.000	0.000
39	30	30	0.714	0.223	0.8034	0.8034	0.7852	c	c	-	0.000	0.000	0.000	0.000	0.8113	0.8113	0.7900	c	c	-	0.000	0.000	0.000	0.000
40	90	30	0.714	0.223	0.6659	0.6659	0.5706	c	c	-	0.000	0.000	0.000	0.000	0.6683	0.6683	0.5697	c	c	-	0.000	0.000	0.000	0.000
41	Curved	60	0.714	0.223	0.8820	0.8820	0.7451	c	c	-	0.000	0.000	0.000	0.000	0.8987	0.8987	0.7509	c	c	-	0.000	0.000	0.000	0.000
42	7	60	0.714	0.223	0.9061	0.9061	0.7568	c	c	-	0.000	0.000	0.000	0.000	0.9260	0.9261	0.7568	c	c	-	0.000	0.000	0.000	0.000
43	15	60	0.714	0.223	0.8697	0.8697	0.7554	c	c	-	0.000	0.000	0.000	0.000	0.8833	0.8833	0.7612	c	c	-	0.000	0.000	0.000	0.000
44	30	60	0.714	0.223	0.8041	0.8041	0.7291	c	c	-	0.000	0.000	0.000	0.000	0.8122	0.8122	0.7312	c	c	-	0.000	0.000	0.000	0.000
45	90	60	0.714	0.223	0.6696	0.6696	0.5692	c	c	-	0.000	0.000	0.000	0.000	0.6719	0.6719	0.5680	c	c	-	0.000	0.000	0.000	0.000
46	Curved	90	0.714	0.223	0.8830	0.8830	0.7390	c	c	-	0.000	0.000	0.000	0.000	0.8995	0.8995	0.7418	c	c	-	0.000	0.000	0.000	0.000
47	7	90	0.714	0.223	0.9061	0.9061	0.7512	c	c	-	0.000	0.000	0.000	0.000	0.9258	0.9258	0.7552	c	c	-	0.000	0.000	0.000	0.000
48	15	90	0.714	0.223	0.8700	0.8700	0.7510	c	c	-	0.000	0.000	0.000	0.000	0.8833	0.8833	0.7543	c	c	-	0.000	0.000	0.000	0.000
49	30	90	0.714	0.223	0.8031	0.8031	0.7186	c	c	-	0.000	0.000	0.000	0.000	0.8107	0.8107	0.7209	c	c	-	0.000	0.000	0.000	0.000
50	90	90	0.714	0.223	0.6694	0.6694	0.5690	c	c	-	0.000	0.000	0.000	0.000	0.6713	0.6713	0.5680	c	c	-	0.000	0.000	0.000	0.000

Cont'd ...

					Re=6E5										Re=9E5									
	Φ_1	Φ_2	D_{th}/D_{in}	L_{th}/D_{in}	C_d-σ_1	C_d- σ_2	C_d- σ_3				$St_{in}(\sigma_2)$	$St_{in}(\sigma_3)$	$St_{out}(\sigma_2)$	$St_{out}(\sigma_3)$	C_d-σ_1	C_d- σ_2	C_d- σ_3				$St_{in}(\sigma_2)$	$St_{in}(\sigma_3)$	$St_{out}(\sigma_2)$	$St_{out}(\sigma_3)$
51	Curved	7	0.357	0.446	0.9070	0.9070	0.9070	c	c	c	0.000	0.000	0.030	0.034	0.9108	0.9108	0.9108	c	c	c	0.000	0.000	0.023	0.023
52	7	7	0.357	0.446	0.9270	0.9270	0.9270	c	c	c	0.000	0.000	0.030	0.033	0.9313	0.9313	0.9313	c	c	c	0.000	0.000	0.025	0.024
53	15	7	0.357	0.446	0.8824	0.8824	0.8824	c	c	c	0.000	0.000	0.028	0.032	0.8847	0.8847	0.8847	c	c	c	0.000	0.000	0.022	0.021
54	30	7	0.357	0.446	0.8028	0.8028	0.8028	c	c	c	0.026	0.000	0.026	0.000	0.8038	0.8038	0.8038	c	c	c	0.000	0.000	0.021	0.019
55	90	7	0.357	0.446	0.6216	0.6216	0.6216	c	c	c	0.000	0.000	0.025	0.000	0.6219	0.6219	0.6205	c	c	c	0.000	0.000	0.021	0.000
56	Curved	15	0.357	0.446	0.9069	0.9069	0.8929	c	c	-	0.000	0.000	0.051	0.000	0.9109	0.9109	0.0000	c	c	-	0.000	0.000	0.037	0.000
57	7	15	0.357	0.446	0.9286	0.9286	0.9042	c	c	-	0.000	0.000	0.054	0.000	0.9325	0.9325	0.9086	c	c	-	0.000	0.000	0.038	0.000
58	15	15	0.357	0.446	0.8813	0.8813	0.8813	c	c	c	0.000	0.000	0.047	0.000	0.8836	0.8836	0.8836	c	c	c	0.000	0.000	0.033	0.000
59	30	15	0.357	0.446	0.8017	0.8017	0.8017	c	c	c	0.000	0.000	0.044	0.000	0.8028	0.8028	0.8028	c	c	c	0.000	0.000	0.031	0.000
60	90	15	0.357	0.446	0.6244	0.6244	0.6018	c	c	-	0.000	0.000	0.041	0.000	0.6246	0.6246	0.6013	c	c	-	0.000	0.000	0.030	0.000
61	Curved	30	0.357	0.446	0.9067	0.9067	0.7831	c	c	-	0.000	0.000	0.000	0.000	0.9108	0.9108	0.7834	c	c	-	0.000	0.000	0.000	0.000
62	7	30	0.357	0.446	0.9271	0.9271	0.7938	c	c	-	0.000	0.000	0.000	0.000	0.9313	0.9313	0.7983	c	c	-	0.000	0.000	0.000	0.000
63	15	30	0.357	0.446	0.8812	0.8812	0.7912	c	c	-	0.000	0.000	0.000	0.000	0.8835	0.8835	0.7934	c	c	-	0.000	0.000	0.000	0.000
64	30	30	0.357	0.446	0.8026	0.8026	0.7545	c	c	-	0.000	0.000	0.000	0.000	0.8037	0.8037	0.8025	c	c	-	0.000	0.000	0.000	0.000
65	90	30	0.357	0.446	0.6241	0.6241	0.5404	c	c	-	0.000	0.000	0.026	0.000	0.6243	0.6243	0.5407	c	c	-	0.000	0.000	0.040	0.000
66	Curved	60	0.357	0.446	0.9082	0.8893	0.6445	c	c	-	0.000	0.000	0.000	0.000	0.9121	0.8923	0.6466	c	c	-	0.000	0.000	0.000	0.000
67	7	60	0.357	0.446	0.9271	0.9065	0.6592	c	c	-	0.000	0.000	0.000	0.000	0.9313	0.9102	0.6645	c	c	-	0.000	0.000	0.000	0.000
68	15	60	0.357	0.446	0.8812	0.8812	0.6506	c	c	-	0.000	0.000	0.000	0.000	0.8835	0.8834	0.6528	c	c	-	0.000	0.000	0.000	0.000
69	30	60	0.357	0.446	0.8028	0.8028	0.6141	c	c	-	0.000	0.000	0.000	0.000	0.8038	0.8038	0.6161	c	c	-	0.000	0.000	0.000	0.000
70	90	60	0.357	0.446	0.6233	0.6233	0.4860	c	c	-	0.000	0.000	0.000	0.000	0.6236	0.6236	0.4859	c	c	-	0.000	0.000	0.000	0.000
71	Curved	90	0.357	0.446	0.9070	0.8585	0.6086	c	c	-	0.000	0.000	0.000	0.000	0.9108	0.8622	0.6230	c	c	-	0.000	0.000	0.000	0.000
72	7	90	0.357	0.446	0.9266	0.8775	0.6218	c	c	-	0.000	0.000	0.000	0.000	0.9308	0.8817	0.6430	c	c	-	0.000	0.000	0.000	0.000
73	15	90	0.357	0.446	0.8803	0.8677	0.6143	c	c	-	0.000	0.000	0.000	0.000	0.8825	0.8694	0.6173	c	c	-	0.000	0.000	0.000	0.000
74	30	90	0.357	0.446	0.7999	0.7999	0.5854	c	c	-	0.000	0.000	0.000	0.000	0.8009	0.8008	0.5885	c	c	-	0.000	0.000	0.000	0.000
75	90	90	0.357	0.446	0.6223	0.6223	0.4767	c	c	-	0.000	0.000	0.000	0.000	0.6225	0.6225	0.4765	c	c	-	0.000	0.000	0.000	0.000

Cont'd ...

					Re=6E5										Re=1.2E6									
	Φ_1	Φ_2	D_{th}/D_{in}	L_{th}/D_{in}	C_d-σ_1	C_d- σ_2	C_d- σ_3				$St_{in}(\sigma_2)$	$St_{in}(\sigma_3)$	$St_{out}(\sigma_2)$	$St_{out}(\sigma_3)$	C_d-σ_1	C_d- σ_2	C_d- σ_3				$St_{in}(\sigma_2)$	$St_{in}(\sigma_3)$	$St_{out}(\sigma_2)$	$St_{out}(\sigma_3)$
76	Curved	7	0.714	0.446	0.8787	0.8787	0.8787	c	c	c	0.000	0.000	0.000	0.000	0.8949	0.8949	0.8947	c	c	c	0.000	0.000	0.000	0.000
77	7	7	0.714	0.446	0.9064	0.9064	0.9064	c	c	c	0.000	0.000	0.000	0.000	0.9261	0.9261	0.9260	c	c	c	0.000	0.000	0.000	0.000
78	15	7	0.714	0.446	0.8706	0.8706	0.8706	c	c	c	0.000	0.000	0.000	0.000	0.8836	0.8836	0.8835	c	c	c	0.000	0.000	0.000	0.000
79	30	7	0.714	0.446	0.8036	0.8036	0.8036	c	c	c	0.000	0.000	0.000	0.000	0.8111	0.8111	0.8106	c	c	c	0.000	0.000	0.000	0.000
80	90	7	0.714	0.446	0.6701	0.6701	0.6532	c	c	-	0.000	0.000	0.000	0.000	0.6720	0.6720	0.6528	c	c	-	0.000	0.000	0.000	0.000
81	Curved	15	0.714	0.446	0.8787	0.8787	0.8625	c	c	-	0.000	0.000	0.000	0.000	0.8949	0.8949	0.8742	c	c	-	0.000	0.000	0.000	0.000
82	7	15	0.714	0.446	0.9066	0.9066	0.8856	c	c	-	0.000	0.000	0.000	0.000	0.9262	0.9262	0.8935	c	c	-	0.000	0.000	0.000	0.000
83	15	15	0.714	0.446	0.8684	0.8684	0.8680	c	c	c	0.000	0.000	0.000	0.000	0.8813	0.8813	0.8796	c	c	c	0.000	72	0.000	71
84	30	15	0.714	0.446	0.8036	0.8036	0.8028	c	c	-	0.000	0.000	0.000	0.000	0.8111	0.8111	0.8083	c	c	-	0.000	0.000	0.000	104
85	90	15	0.714	0.446	0.6698	0.6698	0.6272	c	c	-	0.000	0.000	0.000	0.000	0.6717	0.6717	0.6268	c	c	-	0.000	0.000	0.000	0.000
86	Curved	30	0.714	0.446	0.8787	0.8787	0.8139	c	c	-	0.000	0.000	0.000	0.000	0.8949	0.8949	0.8160	c	c	-	0.000	0.000	0.000	0.000
87	7	30	0.714	0.446	0.9064	0.9064	0.8333	c	c	-	0.000	0.000	0.000	0.000	0.9260	0.9260	0.8336	c	c	-	0.000	0.000	0.000	0.000
88	15	30	0.714	0.446	0.8678	0.8678	0.8203	c	c	-	0.000	0.000	0.000	0.000	0.8809	0.8809	0.8272	c	c	-	0.000	0.000	0.000	0.000
89	30	30	0.714	0.446	0.8038	0.8038	0.7910	c	c	-	0.000	0.000	0.000	0.000	0.8112	0.8112	0.7957	c	c	-	0.000	0.000	0.000	0.000
90	90	30	0.714	0.446	0.6722	0.6722	0.6065	c	c	-	0.000	0.000	0.000	0.000	0.6742	0.6742	0.6058	c	c	-	0.000	0.000	0.000	0.000
91	Curved	60	0.714	0.446	0.8835	0.8835	0.7445	c	c	-	0.000	0.000	0.000	0.000	0.9000	0.9000	0.7483	c	c	-	0.000	0.000	0.000	0.000
92	7	60	0.714	0.446	0.9064	0.9064	0.7528	c	c	-	0.000	0.000	0.000	0.000	0.9260	0.9260	0.7559	c	c	-	0.000	0.000	0.000	0.000
93	15	60	0.714	0.446	0.8684	0.8684	0.7509	c	c	-	0.000	0.000	0.000	0.000	0.8813	0.8813	0.7523	c	c	-	0.000	0.000	0.000	0.000
94	30	60	0.714	0.446	0.8038	0.8038	0.7290	c	c	-	0.000	0.000	0.000	0.000	0.8111	0.8111	0.7314	c	c	-	0.000	0.000	0.000	0.000
95	90	60	0.714	0.446	0.6702	0.6702	0.5933	c	c	-	0.000	0.000	0.000	0.000	0.6722	0.6722	0.5925	c	c	-	0.000	0.000	0.000	0.000
96	Curved	90	0.714	0.446	0.8787	0.8787	0.7299	c	c	-	0.000	0.000	0.000	0.000	0.8949	0.8949	0.7326	c	c	-	0.000	0.000	0.000	0.000
97	7	90	0.714	0.446	0.9064	0.9064	0.7475	c	c	-	0.000	0.000	0.000	0.000	0.9261	0.9261	0.7507	c	c	-	0.000	0.000	0.000	0.000
98	15	90	0.714	0.446	0.8677	0.8677	0.7427	c	c	-	0.000	0.000	0.000	0.000	0.8808	0.8808	0.7462	c	c	-	0.000	0.000	0.000	0.000
99	30	90	0.714	0.446	0.8037	0.8037	0.7187	c	c	-	0.000	0.000	0.000	0.000	0.8112	0.8112	0.7212	c	c	-	0.000	0.000	0.000	0.000
100	90	90	0.714	0.446	0.6708	0.6708	0.5889	c	c	-	0.000	0.000	0.000	0.000	0.6728	0.6728	0.5881	c	c	-	0.000	0.000	0.000	0.000

For 2D case

Table B-4. Results of 2-D Numerical Simulations at Re=6E5

	Φ_1	Φ_2	D_{th}/D_{in}	L_{th}/D_{in}	C_d-σ_1	C_d- σ_2	C_d- σ_3				$St_{in}(\sigma_2)$	$St_{in}(\sigma_3)$	$St_{out}(\sigma_2)$	$St_{out}(\sigma_3)$
1	Curved	7	0.357	0.223	0.912	0.912	0.912	c	c	c	0.000	0.000	0.000	0.000
2	7	7	0.357	0.223	0.933	0.933	0.933	c	c	c	0.000	0.000	0.000	0.000
3	15	7	0.357	0.223	0.895	0.895	0.000	c	c	c	0.000	0.000	0.000	0.000
4	30	7	0.357	0.223	0.825	0.825	0.825	c	c	c	0.000	0.000	0.000	0.000
5	90	7	0.357	0.223	0.654	0.654	0.653	c	c	c	0.000	0.000	0.000	0.000
6	Curved	15	0.357	0.223	0.911	0.911	0.910	c	c	c	0.000	0.000	0.000	0.000
7	7	15	0.357	0.223	0.933	0.933	0.931	c	c	c	0.000	0.000	0.000	0.000
8	15	15	0.357	0.223	0.894	0.894	0.891	c	c	c	0.000	0.000	0.000	0.000
9	30	15	0.357	0.223	0.824	0.824	0.820	c	c	c	0.000	0.000	0.000	0.000
10	90	15	0.357	0.223	0.655	0.655	0.611	c	c	-	0.000	0.000	0.000	0.000
11	Curved	30	0.357	0.223	0.909	0.909	0.841	c	c	-	0.000	0.000	0.000	0.000
12	7	30	0.357	0.223	0.933	0.933	0.854	c	c	-	0.000	0.000	0.000	0.000
13	15	30	0.357	0.223	0.895	0.895	0.847	c	c	-	0.000	0.000	0.000	0.000
14	30	30	0.357	0.223	0.825	0.825	0.810	c	c	c	0.000	0.000	0.000	0.000
15	90	30	0.357	0.223	0.654	0.654	0.575	c	c	-	0.000	0.000	0.000	0.000
16	Curved	60	0.357	0.223	0.912	0.912	0.745	c	c	-	0.000	0.000	0.000	0.000
17	7	60	0.357	0.223	0.655	0.655	0.551	c	c	-	0.000	0.000	0.000	0.000
18	15	60	0.357	0.223	0.895	0.895	0.763	c	c	-	0.000	0.000	0.000	0.000
19	30	60	0.357	0.223	0.823	0.823	0.725	c	c	-	0.000	0.000	0.000	0.000
20	90	60	0.357	0.223	0.934	0.934	0.755	c	c	-	0.000	0.000	0.000	0.000
21	Curved	90	0.357	0.223	0.912	0.912	0.721	c	c	-	0.000	0.000	0.000	0.000
22	7	90	0.357	0.223	0.933	0.933	0.729	c	c	-	0.000	0.000	0.000	0.000
23	15	90	0.357	0.223	0.894	0.894	0.729	c	c	-	0.000	0.000	0.000	0.000
24	30	90	0.357	0.223	0.824	0.824	0.707	c	c	-	0.000	0.000	0.000	0.000
25	90	90	0.357	0.223	0.655	0.655	0.545	c	c	-	0.000	0.000	0.000	0.000
26	Curved	7	0.714	0.223	0.900	0.900	0.761	c	c	-	0.000	0.000	0.000	0.000
27	7	7	0.714	0.223	0.934	0.934	0.771	c	c	-	0.000	0.000	0.000	0.000
28	15	7	0.714	0.223	0.894	0.894	0.768	c	c	-	0.000	0.000	0.000	0.000
29	30	7	0.714	0.223	0.842	0.842	0.746	c	c	-	0.000	0.000	0.000	0.000
30	90	7	0.714	0.223	0.729	0.729	0.633	c	c	-	0.000	0.000	0.000	0.000
31	Curved	15	0.714	0.223	0.898	0.898		c	c	-	0.000	0.000	0.000	0.000
32	7	15	0.714	0.223	0.934	0.934	0.769	c	c	-	0.000	0.000	0.000	0.000
33	15	15	0.714	0.223	0.895	0.895	0.768	c	c	-	0.000	0.000	0.000	0.000
34	30	15	0.714	0.223	0.833	0.833	0.740	c	c	-	0.000	0.000	0.000	0.000
35	90	15	0.714	0.223	0.727	0.698	0.613	c	c	-	0.000	0.000	0.000	0.000
36	Curved	30	0.714	0.223	0.901	0.901	0.735	c	c	-	0.000	0.000	0.000	0.000
37	7	30	0.714	0.223	0.934	0.934	0.743	c	c	-	0.000	0.000	0.000	0.000
38	15	30	0.714	0.223	0.896	0.896	0.742	c	c	-	0.000	0.000	0.000	0.000
39	30	30	0.714	0.223	0.834	0.834	0.722	c	c	-	0.000	0.000	0.000	0.000
40	90	30	0.714	0.223	0.720	0.720	0.590	c	c	-	0.000	0.000	0.000	0.000
41	Curved	60	0.714	0.223	0.901	0.901	0.693	c	c	-	0.000	0.000	0.000	0.000
42	7	60	0.714	0.223	0.934	0.934	0.701	c	c	-	0.000	0.000	0.000	0.000
														Cont'd

	Φ_1	Φ_2	D_{th}/D_{in}	L_{th}/D_{in}	C_d-σ_1	C_d- σ_2	C_d- σ_3				$St_{in}(\sigma_2)$	$St_{in}(\sigma_3)$	$St_{out}(\sigma_2)$	$St_{out}(\sigma_3)$
43	15	60	0.714	0.223	0.897	0.897	0.700	c	c	-	0.000	0.000	0.000	0.000
44	30	60	0.714	0.223	0.835	0.835	0.687	c	c	-	0.000	0.000	0.000	0.000
45	90	60	0.714	0.223	0.724	0.724	0.589	c	c	-	0.000	0.000	0.000	0.000
46	Curved	90	0.714	0.223	0.901	0.901	0.704	c	c	-	0.000	0.000	0.000	0.000
47	7	90	0.714	0.223	0.934	0.000	0.713	c	c	-	0.000	0.000	0.000	0.000
48	15	90	0.714	0.223	0.895	0.895	0.712	c	c	-	0.000	0.000	0.000	0.000
49	30	90	0.714	0.223	0.832	0.832	0.693	c	c	-	0.000	0.000	0.000	0.000
50	90	90	0.714	0.223	0.722	0.722	0.593	c	c	-	0.000	0.000	0.000	0.000
51	Curved	7	0.357	0.446	0.913	0.913	0.913	c	c	c	0.000	0.000	0.000	0.000
52	7	7	0.357	0.446	0.934	0.934	0.934	c	c	c	0.000	0.000	0.000	0.000
53	15	7	0.357	0.446	0.895	0.895	0.895	c	c	c	0.000	0.000	0.000	0.000
54	30	7	0.357	0.446	0.824	0.824	0.824	c	c	c	0.000	0.000	0.000	0.000
55	90	7	0.357	0.446	0.654	0.654	0.654	c	c	c	0.000	0.000	0.000	0.000
56	Curved	15	0.357	0.446	0.911	0.911	0.911	c	c	c	0.000	0.000	0.000	0.000
57	7	15	0.357	0.446	0.935	0.935	0.935	c	c	c	0.000	0.000	0.000	0.000
58	15	15	0.357	0.446	0.894	0.894	0.894	c	c	c	0.000	0.000	0.000	0.000
59	30	15	0.357	0.446	0.823	0.823	0.823	c	c	c	0.000	0.000	0.000	0.000
60	90	15	0.357	0.446	0.656	0.656	0.654	c	c	c	0.000	0.000	0.000	0.000
61	Curved	30	0.357	0.446	0.910	0.910	0.834	c	c	-	0.000	0.000	0.000	0.000
62	7	30	0.357	0.446	0.934	0.934	0.843	c	c	-	0.000	0.000	0.000	0.000
63	15	30	0.357	0.446	0.894	0.894	0.847	c	c	-	0.000	0.000	0.000	0.000
64	30	30	0.357	0.446	0.824	0.824	0.813	c	c	c	0.000	0.000	0.000	0.000
65	90	30	0.357	0.446	0.656	0.656	0.615	c	c	-	0.000	0.000	0.000	0.000
66	Curved	60	0.357	0.446	0.913	0.913	0.743	c	c	-	0.000	0.000	0.000	0.000
67	7	60	0.357	0.446	0.934	0.934	0.748	c	c	-	0.000	0.000	0.000	0.000
68	15	60	0.357	0.446	0.894	0.894	0.751	c	c	-	0.000	0.000	0.000	0.000
69	30	60	0.357	0.446	0.824	0.824	0.719	c	c	-	0.000	0.000	0.000	0.000
70	90	60	0.357	0.446	0.655	0.655	0.567	c	c	-	0.000	0.000	0.000	0.000
71	Curved	90	0.357	0.446	0.913	0.913	0.715	c	c	-	0.000	0.000	0.000	0.000
72	7	90	0.357	0.446	0.934	0.000	0.720	c	c	-	0.000	0.000	0.000	0.000
73	15	90	0.357	0.446	0.894	0.894	0.720	c	c	-	0.000	0.000	0.000	0.000
74	30	90	0.357	0.446	0.823	0.823	0.701	c	c	-	0.000	0.000	0.000	0.000
75	90	90	0.357	0.446	0.655	0.655	0.562	c	c	-	0.000	0.000	0.000	0.000
76	Curved	7	0.714	0.446	0.898	0.898	0.756	c	c	-	0.000	0.000	0.000	0.000
77	7	7	0.714	0.446	0.934	0.934	0.770	c	c	-	0.000	0.000	0.000	0.000
78	15	7	0.714	0.446	0.895	0.895	0.770	c	c	-	0.000	0.000	0.000	0.000
79	30	7	0.714	0.446	0.833	0.833	0.744	c	c	-	0.000	0.000	0.000	0.000
80	90	7	0.714	0.446	0.722	0.722	0.639	c	c	-	0.000	0.000	0.000	0.000
81	Curved	15	0.714	0.446	0.898	0.898	0.751	c	c	-	0.000	0.000	0.000	0.000
82	7	15	0.714	0.446	0.934	0.934	0.766	c	c	-	0.000	0.000	0.000	0.000
83	15	15	0.714	0.446	0.894	0.894	0.763	c	c	-	0.000	0.000	0.000	0.000
84	30	15	0.714	0.446	0.833	0.833	0.739	c	c	-	0.000	0.000	0.000	0.000
85	90	15	0.714	0.446	0.723	0.723	0.627	c	c	-	0.000	0.000	0.000	0.000
86	Curved	30	0.714	0.446	0.898	0.898	0.732	c	c	-	0.000	0.000	0.000	0.000
87	7	30	0.714	0.446	0.934	0.934	0.743	c	c	-	0.000	0.000	0.000	0.000
88	15	30	0.714	0.446	0.894	0.894	0.741	c	c	-	0.000	0.000	0.000	0.000
89	30	30	0.714	0.446	0.833	0.833	0.725	c	c	-	0.000	0.000	0.000	0.000
90	90	30	0.714	0.446	0.725	0.725	0.617	c	c	-	0.000	0.000	0.000	0.000
91	Curved	60	0.714	0.446	0.901	0.901	0.695	c	c	-	0.000	0.000	0.000	0.000
														Cont'd

	Φ_1	Φ_2	D_{th}/D_{in}	L_{th}/D_{in}	C_d-σ_1	C_d- σ_2	C_d- σ_3				$St_{in}(\sigma_2)$	$St_{in}(\sigma_3)$	$St_{out}(\sigma_2)$	$St_{out}(\sigma_3)$
92	7	60	0.714	0.446	0.934	0.934	0.700	c	c	-	0.000	0.000	0.000	0.000
93	15	60	0.714	0.446	0.894	0.894	0.699	c	c	-	0.000	0.000	0.000	0.000
94	30	60	0.714	0.446	0.833	0.833	0.689	c	c	-	0.000	0.000	0.000	0.000
95	90	60	0.714	0.446	0.723	0.723	0.610	c	c	-	0.000	0.000	0.000	0.000
96	Curved	90	0.714	0.446	0.898	0.898	0.701	c	c	-	0.000	0.000	0.000	0.000
97	7	90	0.714	0.446	0.934	0.934	0.712	c	c	-	0.000	0.000	0.000	0.000
98	15	90	0.714	0.446	0.894	0.894	0.710	c	c	-	0.000	0.000	0.000	0.000
99	30	90	0.714	0.446	0.833	0.833	0.696	c	c	-	0.000	0.000	0.000	0.000
100	90	90	0.714	0.446	0.723	0.723	0.610	c	c	-	0.000	0.000	0.000	0.000